

**NANYANG
TECHNOLOGICAL
UNIVERSITY
SINGAPORE**

**Minisystem for monitoring water
quality using UV absorption and
fluorescence**

SHEN GUXUAN

SCHOOL OF ELECTRICAL AND ELECTRONIC ENGINEERING

2025

Minisystem for monitoring water quality using UV absorption and fluorescence

SHEN GUXUAN

SCHOOL OF ELECTRICAL AND ELECTRONIC ENGINEERING

**A DISSERTATION SUBMITTED IN PARTIAL FULFILMENT OF
THE REQUIREMENTS FOR THE DEGREE OF
MASTER OF SCIENCE IN COMPUTER CONTROL AND AUTOMATION**

2025

Statement of Originality

I hereby certify that the work embodied in this thesis is the result of original research and has not been submitted for a higher degree to any other University or Institution.

18 April 2025

.....
Date

U NTU NTU NTU NTU NTU NTU N
FU NTU NTU NTU NTU NTU NTU N
IT NTU NTU NTU NTU NTU NTU NTU N
U NTU NTU NTU NTU NTU NTU N

.....
SHEN GUXUAN

Supervisor Declaration Statement

I have reviewed the content and presentation style of this thesis and declare it is free of plagiarism and of sufficient grammatical clarity to be examined. To the best of my knowledge, the research and writing are those of the candidate except as acknowledged in the Author Attribution Statement. I confirm that the investigations were conducted in accord with the ethics policies and integrity standards of Nanyang Technological University and that the research data are presented honestly and without prejudice

18 April 2025

.....
Date

U NTU NTU NTU NTU NTU NTU N
TU NTU NTU NTU NTU NTU NTU NTU I
ITU NTU NTU NTU NTU NTU NTU NTU
U NTU NTU NTU NTU NTU NTU NTU N

.....
A/P Poenar Daniel Puiu

Authorship Attribution Statement

This thesis does not contain any materials from papers published in peer-reviewed journals or from papers accepted at conferences in which I am listed as an author.

18 April 2025

.....
Date

.....
Shen Guxuan
.....

.....
SHEN GUXUAN

Table of Contents

Abstract	iii
Acknowledgement	iv
Acronyms	v
Lists of Figures	vii
Lists of Tables	viii
1 Introduction	1
1.1 Background	1
1.2 Motivation, objectives, novelty and originality	3
1.3 Thesis organization	5
2 Literature review	6
2.1 Introduction	6
2.2 Fluorescence	7
2.2.1 Fluorescence operation principle	7
2.2.2 Fluorescence detection principle	8
2.2.3 UV absorbance measurement principle	10
2.3 Reported examples of fluorescence detection system	12
2.3.1 Dual-path fluorescence detection system	12
2.3.2 Silver mirror detection window - In-capillary fiber optic LED induced fluorescence detection system	14
2.3.3 Time-resolved fluorescence immunoassay	17
2.3.4 Comparison and analysis	20
2.4 Weak signal detection methods	21
2.4.1 Background	21
2.4.2 Lock-in detection	22
2.4.3 Application examples of locked-in detection in optical signals	25
2.4.4 Differential and instrumentation amplifiers	27
2.5 Conclusion	30

3 Our designed optical system	31
3.1 Introduction	31
3.2 Overall optical system design	32
3.3 Evaluation of fluorescence capturing performance of the elliptical cylinder reflective cavity	34
3.4 Design of the emission holder and transmission holder	35
3.5 Design of the fluorescence detection holder	47
3.6 Conclusion	48
4 Design of signal processing and control circuits	50
4.1 Introduction	50
4.2 Overall plan of system hardware design	51
4.3 Microcontroller module	53
4.4 Signal conditioning circuits	54
4.4.1 LED constant current drive circuit design and simulation .	54
4.4.2 TIA circuit design and simulation	59
4.4.3 Differential amplifier circuit design and simulation	64
4.4.4 LIA circuit design and simulation	66
4.5 MCU peripheral module usage	70
4.6 Circuit schematic and PCB drawing	71
4.7 Conclusion	78
5 Key accomplishments	79
5.1 Development of our designed optical system	79
5.2 Design of low-noise hardware circuitry	80
5.3 Cross-disciplinary contributions	81
6 Conclusions and suggestions for future work	82
6.1 Conclusions	82
6.2 Future work	83
References	85

Abstract

This study proposes a modular optoelectronic detection platform for water quality monitoring in the desalination process that integrates UV-visible absorption and fluorescence detection. The system uses a optical cavity optimized by Zemax and modular mechanical components designed in Solidworks, and achieves theoretically simulated light collection efficiency through parametric lens configuration analysis. A hybrid signal conditioning architecture combining differential amplification and lock-in amplifier was developed, and the circuit performance was verified through Multisim simulation. An embedded system built on an ESP32 microcontroller implements multi-channel data acquisition and Bluetooth Low Energy transmission, but complete experimental verification remains to be completed. This work establishes a methodological framework for the integration of low-intensity optical detection systems, laying the foundation for subsequent performance characterization and field deployment.

Keywords: low-intensity light detection, ZEMAX, fluorescence, differential amplifier circuit, lock-in amplifier circuit.

Acknowledgements

I sincerely express my gratitude to my supervisor, Associate Professor Poenar Daniel Puiu. His systematic guidance in research direction selection, theoretical framework refinement, and experimental protocol optimization, particularly the critical suggestions in complex optoelectronic system modeling, laid essential foundations for this study. Also, special thanks go to Mr. Loh Jing Chen for his professional contributions to optical simulations. In addition, grateful acknowledgment is extended to all members of the DIP project team. Their dedicated efforts in mechanical assembly, circuit testing, and system calibration of the experimental platform successfully established an experimental environment meeting precision measurement requirements, ensuring smooth implementation of the research. Finally, heartfelt appreciation goes to my parents. Their consistent respect for my academic choices and steadfast understanding throughout this extended research journey have been vital spiritual sustenance for my perseverance.

SHEN GUXUAN

18 April 2025

Acronyms

FLU	Fluorescence
UVA	Ultraviolet Absorbance
PMT	Photomultiplier
SNR	Signal-to-noise ratio
CMRR	Common-mode rejection ratio
MCU	Microcontroller Unit
TIA	Transimpedance Amplifier
LIA	Locked-in Amplifier
GBW	Gain-bandwidth Product
RMS	Root Mean Square
IIC	Inter-Integrated Circuit

List of Figures

2.1	Jablonski diagram (adapted from [17])	7
2.2	Optical path diagram of dual-path fluorescence intensity method (adapted from [20])	13
2.3	Schematic illustration of the SDW-ICOF-LED-IFD-CE system.(1) LED; (2) double convex lens; (3) bandpass filter 1; (4) 35 μm optical fiber; (5) buffer reservoirs; (6) detection window; (7) 75 μm i.d. capillary; (8) Pt electrodes; (9) organic glass plate; (10) high-voltage power supply; (11) microscope objective (60x); (12) bandpass filter 2; (13) PMT; (14) computer; (15) silver mirror. (adapted from [21])	15
2.4	Time-resolved fluorescence immunoassay system (adapted from [23])	18
2.5	Block diagram of lock-in amplifier (adapted from [26])	23
2.6	Differential Amplifier (adapted from [30])	27
2.7	Schematic diagram of an instrumentation amplifier (adapted from [30])	28
2.8	INA114 instrumentation amplifier schematic (adapted from [31]) .	29
3.1	Schematic representation of our designed optical system	32
3.2	Irradiance map of FLU light arriving at the 2nd focal point of the reflector	34
3.3	ZEMAX detector for FLU light	35
3.4	Top view of Version 1A	36
3.5	Zemax Optics Simulation of Version 1A	37
3.6	Five-position luminous flux of Version 1A	37
3.7	Top view of Version 1B	38
3.8	Zemax Optics Simulation of Version 1B	38
3.9	Five-position luminous flux of Version 1B	39
3.10	Zemax Optics Simulation of Version 2A	39
3.11	Five-position luminous flux of Version 2A	40
3.12	Zemax Optics Simulation of Version 2B	40
3.13	Five-position luminous flux of Version 2B	41
3.14	Zemax Optics sequential mode simulation of Version 3A	42
3.15	Zemax Optics Simulation of Version 3A	43
3.16	Five-position luminous flux of Version 3A	43
3.17	Zemax Optics Simulation of Version 3B	44
3.18	Five-position luminous flux of Version 3B	44
3.19	Further analysis of Version 3B	46

3.20 Five-position luminous flux of Version 4	46
3.21 Zemax sequential mode simulation for Version 4	47
3.22 Zemax sequential mode simulation for fluorescence collimation	48
3.23 Zemax non-sequential mode simulation for fluorescence collimation	48
4.1 Generic simplified diagram of the circuitry for the entire system, with circuits for both the UVA/T and fluorescence (Fl.) photode- tected signals	52
4.2 ESP32-WROOM-32D	53
4.3 ESP32 Pin Function Diagram	54
4.4 (a) LZ1-00UBN0 LED, and (b) the LED driver EUM-075S105Dx	55
4.5 Dimming circuit implementation	56
4.6 Voltage bias and amplifier follower circuit	58
4.7 Voltage bias and amplifier follower circuit input	58
4.8 Voltage bias and amplifier follower circuit output	59
4.9 TIA Schematic diagram	60
4.10 Preamplifier method	62
4.11 Application of the TIA with the photodetectors used in our system	63
4.12 Transmission and reference TIA output	63
4.13 Variable gain amplification and low pass filter output	64
4.14 Differential amplifier	65
4.15 Differential amplifier result	65
4.16 H11462-011 module	66
4.17 Lock-in amplifier	67
4.18 Lock-in amplifier input	68
4.19 Lock-in amplifier output	69
4.20 Low-pass filter	69
4.21 Low-pass filter output	70
4.22 Framework diagram of each module of the microcontroller	71
4.23 Light source ((a)circuit schematic; (b)PCB)	72
4.24 Reference holder LEDs((a)circuit schematic; (b)PCB)	73
4.25 Transmission holder LEDs((a)circuit schematic; (b)PCB)	73
4.26 Reference TIA((a)circuit schematic; (b)PCB)	74
4.27 Transmission TIA((a)circuit schematic; (b)PCB)	75
4.28 Differential amplifier((a)circuit schematic; (b)PCB)	76
4.29 LIA((a)circuit schematic; (b)PCB)	77
4.30 Sine wave voltage amplifier((a)circuit schematic; (b)PCB)	77
5.1 System physical picture	80
5.2 Data acquisition interface design	81

List of Tables

2.1 Comparison of three fluorescence measurement systems	21
4.1 Circuit design target parameters	60

Chapter 1

Introduction

Fluorescence analysis has become a key technique in environmental monitoring, particularly for detecting trace organic pollutants in aquatic systems. Advances in fluorescence detection over the past five decades have revolutionized the study of dissolved organic matter, enabling precise identification of pollutants in complex matrices through their unique excitation and emission spectral signatures [1]. These capabilities are in line with Singapore's strategic goal of developing a sustainable water management system, where real-time, highly sensitive tools are essential for optimizing desalination processes and ensuring water purity [2]. So, we want to develop a platform for low intensity light detection used for optical analysis of water purity [3].

1.1 Background

Fluorescence analysis is a technique that quantifies or qualifies substances based on their emission of longer-wavelength light after absorbing specific incident photons. This phenomenon arises from molecular transitions between electronic states, where energy dissipation during the excited state lifetime (typically 1 ns) generates Stokes-shifted emission [1].

Water quality detection technology based on optical principles can achieve multi-parameter non-destructive and pollution-free detection, and is easy to miniaturize, intelligentize and conduct rapid on-site detection. It is a detection method with great potential. As one of the optical methods, adsorption spectrophotome-

try has great application prospects [4], but it has the following limitations:

1. Insufficient selectivity: UV/visible spectrophotometers cannot distinguish between targets and pollutants with the same wavelength absorption peak (such as various nucleic acids contributing to absorbance at 260 nm) [5].
2. Stray light interference: The detector has a broadband response, and sample reflection impurities are prone to signal distortion and reduce the linear range of absorbance [6].
3. Conditional sensitivity: Temperature, pH, impurities, etc. affect the sample absorption characteristics, resulting in detection deviations.
4. Poor sensitivity at low concentrations: The detection ability is insufficient at low concentrations, and the sample needs to be concentrated, which increases the operation time.

In comparison, fluorescence analysis technology has significant advantages:

1. High sensitivity: The signal intensity is positively correlated with the excitation light, and trace substances can be detected [7].
2. High selectivity: Differentiate fluorescent substances through specific Ex/Em wavelength combinations, and accurately identify targets in complex samples.
3. Real-time detection: No complex pre-processing is required, and the results are quickly fed back, which is suitable for real-time detection scenarios such as biomedicine and environmental monitoring [1].
4. Non-destructive detection: It does not destroy the sample and is suitable for precious samples or living tissue analysis.
5. Multiple detection capabilities: Use different fluorescent probes to detect multiple targets simultaneously, meeting the needs of multi-parameter analysis in biological research.

6. Wide application: It has been deeply applied in biomedicine, environmental science, materials science, food safety and other fields [1].

The non-destructive, real-time and compatibility of fluorescence analysis with multiple detections make it a cornerstone of environmental monitoring, especially for evaluating dissolved organic matter in aquatic systems [8]. Recent advances in micro-optical systems and low-light detection technology have further enhanced its applicability in portable, on-site water quality assessment [4]. Therefore, our project decided to use fluorescence detection methods to detect trace pollutants in water.

1.2 Motivation, objectives, novelty and originality

Traditional UV/Vis spectrophotometry suffers from inherent limitations, including poor selectivity (e.g., overlapping absorption bands of nucleic acids at 260 nm [5]), susceptibility to stray light [6], and inadequate sensitivity for trace contaminants [7]. In contrast, fluorescence analysis overcomes these challenges through wavelength-specific excitation/emission filtering, enabling precise identification of target analytes even at ultralow concentrations [9].

This project aims to develop a dual-mode optical platform integrating fluorescence and absorbance measurements for real-time water purity assessment. Key objectives include:

1. High-Sensitivity Detection: Amplify weak fluorescence signals (e.g., from chlorophyll-a or organic dyes) using advanced photodetectors (e.g., PMTs) and noise-suppression circuits (e.g., lock-in amplifiers) [10].
2. Multidimensional Analysis: Simultaneously quantify absorbance (via differential amplification) and fluorescence to cross-validate results, improving reliability in turbid or heterogeneous samples [11].
3. Miniaturization: Optimize optical geometry (e.g., elliptical cavities) and low-power electronics to enable portable, field-deployable systems for desalination plants and marine environments [12].

The core innovation of this study is to build a modular integrated optoelectronic detection platform, which breaks through the limitations of traditional water quality detection systems in terms of functional integration and flexibility. Different from the independent application mode of single spectral technology (such as relying only on ultraviolet absorption or fluorescence detection) in existing research, this platform realizes the deep integration of FLU and UVA detection for the first time. Through the Zemax optimization design of the confocal optical cavity and the coordination of the modular mechanical structure of SolidWorks, the problem of efficient coupling of multi-modal optical signals in the same physical space is solved. This design not only avoids the defects of the traditional discrete instrument, which is bulky and complex to calibrate, but also strives to maximize the theoretical light collection efficiency through parametric lens configuration analysis, laying a hardware foundation for the accurate detection of low-concentration pollutants.

In terms of signal processing and system architecture, this study proposes a hybrid signal conditioning architecture that innovatively integrates the principles of differential amplification and lock-in amplifier detection. Compared with the single amplification or filtering scheme in traditional detection systems, this architecture can improve noise suppression capabilities through Multisim simulation verification, especially in low signal-to-noise ratio environments (such as trace organic matter detection in seawater desalination processes). In addition, the embedded system design based on the ESP32 microcontroller realizes the integrated integration of multi-channel data acquisition and low-power Bluetooth transmission, which solves the problems of cumbersome wired connections and high power consumption of traditional detection equipment, and provides a feasible solution for rapid on-site deployment and remote monitoring.

In existing literature, water quality detection systems often focus on the performance optimization of a single detection technology (such as improving the quantum efficiency of fluorescence sensors or the stability of ultraviolet light sources), while there are few studies on the system-level integration of multi-modal technologies. This study not only realizes modular design at the hard-

ware level from scratch, but also establishes an integrated methodological framework for low-intensity optical signal detection systems in terms of methodology, including interdisciplinary collaborative strategies for optical design, circuit architecture, and embedded control.

1.3 Thesis organization

This dissertation is organized as follows:

Chapter 1 introduces the background of fluorescence analysis and the motivation for building a water purity analysis platform through fluorescence detection.

Chapter 2 reviews the basics of fluorescence, existing detection systems, and weak signal processing methods.

Chapter 3 focuses on the design and simulation of the optical system. Multiple versions of optical simulation are performed using Zemax software to determine the optical path structure for UVA parameter detection. At the same time, the optical path structure for FLU parameter detection is initially explored, and an improvement plan is proposed based on the simulation results.

Chapter 4 details the hardware circuit design of the system. Multisim is used to simulate the circuits of each part to verify the rationality of the design. The circuit schematic and PCB are drawn using EDA design tools to build a complete and usable hardware platform prototype.

Chapter 5 outlines the main results of the current research work.

Chapter 6 summarizes the interim results of this research and provides prospects for future research content.

Chapter 2

Literature review

2.1 Introduction

As an efficient and sensitive analytical method, fluorescence detection has shown significant potential in the field of water quality monitoring of environmental pollutants in recent years. Its core relies on the specific interaction between fluorescent molecules and targets, and sensitive detection of targets is achieved through quantitative changes in fluorescence signals. However, in practical applications, the fluorescence signals of trace pollutants are often extremely weak and easily interfered by environmental noise, which places strict requirements on the optical design and signal processing of the detection system.

In order to break through this bottleneck, researchers have explored from three levels in recent years: first, in-depth analysis of the physical mechanism and detection principle of fluorescence phenomena to lay a theoretical foundation for system design; second, developing a variety of fluorescence detection system architectures to balance sensitivity, cost and practicality; finally, combining weak signal processing technology to extract effective signals from noise. The coordinated optimization of these three levels constitutes the key path to promote fluorescence detection technology from the laboratory to practical application. This dissertation will review the basic principles, system examples and signal enhancement methods, and systematically sort out the evolution and future direction of fluorescence detection.

2.2 Fluorescence

2.2.1 Fluorescence operation principle

Fluorescence is a physical property in which specific atoms or molecules absorb light at a specific wavelength and then emit a longer wavelength of light. The fluorescence process consists of three important stages: Excited state lifetime (E_x), and fluorescence emission (E_m). The time delay from Ex to fluorescence E_m is of about 1 ns, making fluorescence a good indicator for real-time observation [12].

The fluorescence process initiates with photon energy absorption by a fluorophore, typically facilitated by an external energy source such as an incandescent lamp, UV light, or laser [13]. Upon excitation, the fluorophore undergoes vibrational relaxation (occurring at picosecond timescales) to reach the lowest vibrational level of the first excited singlet state (S_1'). During the excited-state lifetime (nanosecond scale), the molecule may undergo conformational changes or energy dissipation to the surrounding environment. Subsequently, fluorescence emission occurs as the fluorophore returns to the ground state (S_0), releasing a photon with lower energy than the absorbed excitation light ($h\nu_{EX}$), resulting in a longer emission wavelength ($h\nu_{EM}$) [14]. The energy difference between excitation and emission, termed the Stokes shift $h\nu_{EX} - h\nu_{EM}$, is critical for fluorescence detection [15].

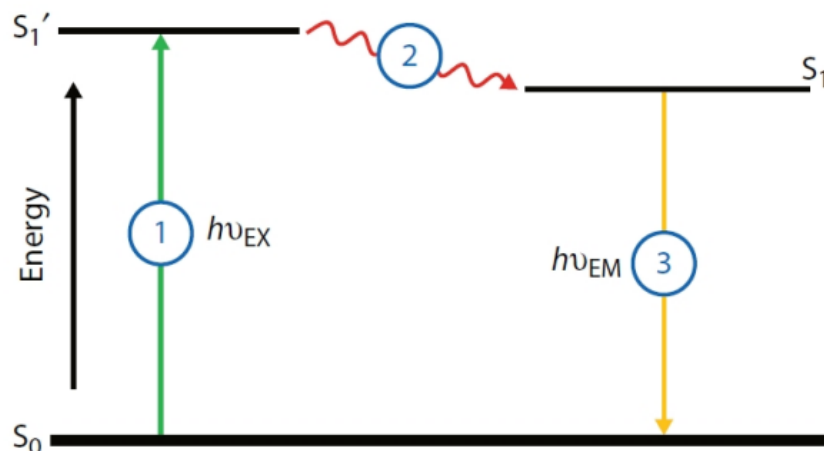


Figure 2.1: Jablonski diagram (adapted from [17])

As the Stokes shift enables spectral separation of the emission signal from excitation interference, thereby enhancing measurement sensitivity [16]. Figure 2.1 below shows a simple electronic state diagram (called a Jablonski diagram) of the fluorescence process [17]. It illustrates the process involved in the creation of an excited electronic singlet state in fluorescence molecules by optical absorption and subsequent fluorescent light E_m .

2.2.2 Fluorescence detection principle

Fluorescent dyes exhibit distinct absorption and emission spectral profiles critical for analytical applications. The absorption spectrum reflects wavelength-dependent light absorption via electronic transitions, enabling qualitative and quantitative identification through substance-specific spectral peaks [12]. The emission spectrum arises from radiative decay from excited to ground states, producing unique fluorescence signatures ideal for high-sensitivity detection [18]. Combined analysis of these spectra provides comprehensive insights into optical properties, facilitating optimized detection strategies for trace substance identification and quantification [19].

Fluorescence intensity (I_f) correlates with dye concentration (c) through the Beer-Lambert law:

$$I_f = \phi I \left(1 - 10^{-abc} \right) \quad (2.1)$$

where I is incident light intensity, ϕ is fluorescence efficiency, ϵ is the molar absorption coefficient, and b is optical path length. Under dilute conditions ($\epsilon bc < 0.05$), higher-order terms in the Taylor expansion are negligible, yielding a linear approximation:

$$I_f = 2.3\phi I \epsilon bc \quad (2.2)$$

When the fluorescent dye solution is very dilute, the fluorescence intensity has a great linear relationship with the concentration of the fluorescent dye, and the fluorescence method has the highest sensitivity.

For increased accuracy, a fluorescence measurement setup should have two sensors, each at the receiving end of a different optical paths: the fluorescence light detection path and reference path, respectively. The latter is necessary because the luminous intensity of the light can be affected by various factors (temperature, drive current fluctuations, aging). It detects a fraction of the light source's intensity which is separated from the main beam that excites the sample's fluorescence, using, e.g. a beam splitter. The measurement of light intensity variations by both detectors enables one to compensate the influence of the light source's intensity fluctuations on the measured fluorescence.

The emitted light intensity is I_0 , and the fluorescence intensity detected by is I_f . The intensity of light used to excite fluorescence is $K_f I_0$, and the intensity of light entering the reference path is $K_r I_0$. Both K_f and K_r are constants and $K_f + K_r < 1$. I_f can be calculated as follows [12]:

$$I_f = 2.3\phi K_f I_0 \varepsilon b c \quad (2.3)$$

while the reference path detects scattered light intensity:

$$I_r = K_r I_0 \quad (2.4)$$

Normalizing $\frac{I_f}{I_r}$ eliminates light source fluctuations (I_0), we can get the relationship between I_f and I_r :

$$\frac{I_f}{I_r} = \frac{2.3\phi K_f I_0 \varepsilon b c}{K_r I_0} = 2.3 \frac{K_f}{K_r} \phi \varepsilon b c \quad (2.5)$$

This ratio ensures concentration-dependent proportionality under dilute conditions, independent of ambient variations. In short, when the solution is very dilute, the ratio of the two light intensities is proportional to the concentration of the fluorescent dye and is not affected by light source fluctuations.

2.2.3 UV absorbance measurement principle

Real-time monitoring of dynamic changes in fluorophore concentration is a key operational requirement in the development of measurement systems for UV absorbance and fluorescence concentration. The detection principle relies on the correlation between fluorophore concentration and the decay in transmitted light intensity, which is quantified by a photodiode sensor. This relationship emphasizes the importance of precision in the design of the detection circuitry, as its performance directly determines the overall accuracy and sensitivity of the measurement system.

The attenuation of light intensity within the system is governed by the fundamental concept of the extinction cross-section (C_{ext}). The differential reduction in transmitted light intensity can be mathematically expressed as:

$$-SdI = IC_{ext}NSdL \quad (2.6)$$

where S denotes the scattering cross-sectional area, C_{ext} represents the extinction cross-section, N is the number density of fluorophores, and L is the optical path length. Integration of equation (2.6) above yields the exponential attenuation law:

$$I = I_0 e^{-NC_{ext}L} \quad (2.7)$$

Here, I_0 corresponds to the incident intensity emitted by the laser source, while I quantifies the transmitted intensity detected by the photodetector. Variations in fluorophore concentration N induce proportional changes in the transmitted light intensity I , thereby enabling concentration-dependent optical signal modulation.

However, traditional single-beam transmission measurement architectures have a key limitation. Instabilities in the laser source, such as fluctuations in the drive current or intensity variations with temperature, directly affect the transmission signal even when the fluorophore concentration is constant. This introduces systematic errors because the photodetector incorrectly interprets intensity

changes caused by source instabilities as changes in fluorophore concentration. Such artifacts affect the measurement fidelity and require the development of robust error mitigation strategies.

To address this challenge, the system uses a dual-beam differential measurement approach. The laser output is split into two different optical paths by a beam splitter:

1. Measurement path: The primary beam passes through the fluorescent medium and the transmitted intensity is detected by the measurement photodetector.
2. Reference path: The secondary beam bypasses the sample and goes directly to the reference photodetector

A differential amplifier processes the outputs of the two photodetectors. In the case of a stable fluorophore concentration, any perturbation (e.g., due to light source instability) will cause changes in and to occur in the same proportion. Therefore, the differential signal is not affected by light source fluctuations because the common-mode noise components are mathematically canceled. This architecture achieves two key goals:

1. Eliminates systematic errors caused by laser intensity instability.
2. Rejects ambient light interference through coherent noise cancellation.

In a traditional single-beam system, calibration establishes a univariate relationship between transmitted intensity and fluorophore concentration, which depends on the stability of the light source. In a dual-beam differential configuration, the system relates fluorophore concentration to a normalized differential signal, which is essentially decoupled from the concentration. This paradigm shift enhances the robustness of the measurement because the calibration scheme can account for dynamic changes in both concentration and environmental perturbations. Therefore, the differential architecture represents a key advancement towards achieving high-precision real-time fluorescence monitoring under non-ideal experimental conditions.

2.3 Reported examples of fluorescence detection system

2.3.1 Dual-path fluorescence detection system

The system adopts a dual-path design to compensate for the influence of light source fluctuation on the measurement results [20]. The structure is shown in Figure 2.2. The main components include:

1. Light source: 430 nm LED (emission angle $\pm 4^\circ$, bandwidth 20 nm), which efficiently excites chlorophyll a fluorescence without the need for an additional focusing lens.
2. Optical path design: divided into fluorescence detection light path and reference light path, sharing the same LED light source. The fluorescence detection light path is perpendicular to the light source direction and includes a quartz window, a 680 nm interference filter (Thorlabs FB680-10) and a plano-convex lens (Daheng Optics $\phi 12.7, F12.7$) to focus the fluorescence signal. The reference light path captures part of the light intensity of the light source through a beam splitter for real-time calibration.
3. Detector: A high-sensitivity photodiode (Hamamatsu S2386-5K) is used to detect fluorescence signals and reference light signals.
4. Signal processing: The phase-locked amplifier circuit (AD630) is combined with a square wave modulated light source (STM32F103 master control) to extract effective signals and suppress background noise through band-pass filtering, multiplier and low-pass filtering.

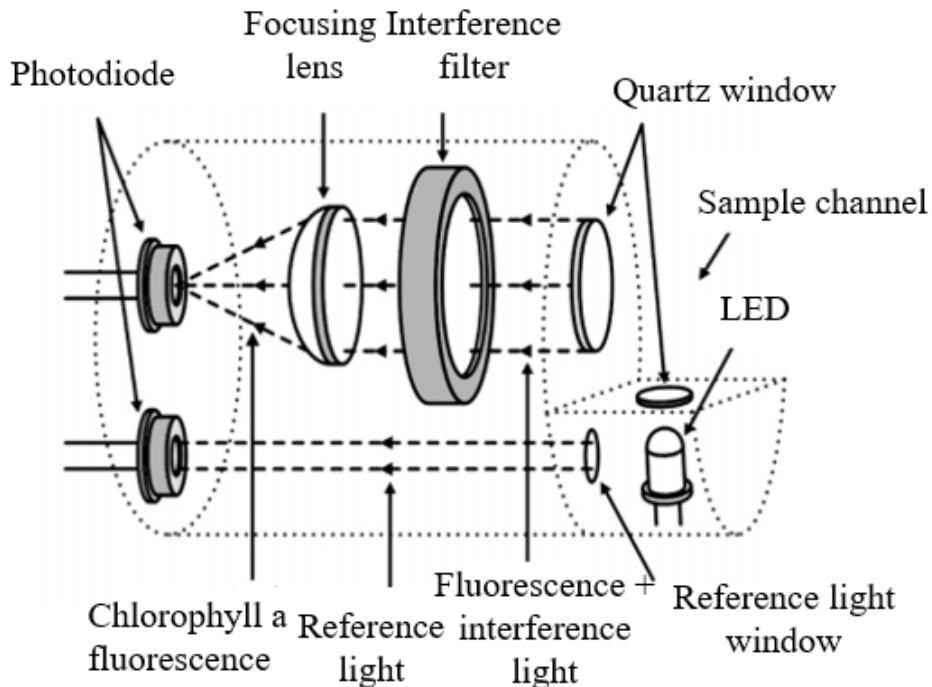


Figure 2.2: Optical path diagram of dual-path fluorescence intensity method (adapted from [20])

It has several obvious advantages:

1. Light source fluctuation compensation: The dual optical path design eliminates the influence of light source intensity changes (such as temperature drift and aging) through the ratio method, and improves long-term stability (linearity $R^2=0.998$).
2. High noise immunity: The phase-locked amplifier circuit significantly suppresses ambient light interference, with a signal-to-noise ratio of 4072 and a minimum resolution of $0.1 \mu\text{g/L}$.
3. Low power consumption design: The low power consumption mode (standby current 0.47 mA) is adopted, combined with lithium battery power supply, and the continuous working time exceeds 5 months.
4. Compact and portable: The cylindrical structure ($137.5 \text{ mm} \times 61 \text{ mm}$) is suitable for in-situ monitoring of marine ranches.

But it also has some shortcomings:

1. Turbidity interference: Suspended particles in high turbidity water may reflect excitation light, which needs to be corrected in combination with turbidity sensors.
2. Calibration dependency: The difference in fluorescence efficiency of different algae requires laboratory calibration to improve accuracy.
3. Dynamic range limit: The upper limit of detection is $200 \mu\text{g/L}$, which is limited by the sensitivity of the filter and photodiode.

The dual-optical path fluorescence measurement system shown in Figure 2.2 shows excellent performance in the detection of chlorophyll a in water: 430 nm LED is used as the excitation light source, the light source fluctuation is compensated by the reference light path, and the anti-interference ability is improved by combining the phase-locked amplifier circuit; the detection range is $0\text{-}200 \mu\text{g/L}$, the linearity $R^2 = 0.998$, the measurement accuracy is $\pm 2 \mu\text{g/L}$, and the resolution is $0.1 \mu\text{g/L}$; the low power consumption design enables it to work continuously for more than 5 months, which is suitable for in-situ real-time monitoring of water environments such as marine ranches.

2.3.2 Silver mirror detection window - In-capillary fiber optic LED induced fluorescence detection system

As shown in Figure 2.3, the system integrates capillary electrophoresis (CE) and fluorescence detection technology. The core structure and key components are as follows [21]:

1. Excitation light source module: A 474 nm blue LED (half-peak width 25 nm) is used as the excitation light source. After collimation by a double convex lens and filtering by a 482 nm bandpass filter, it is introduced into the capillary detection window through a bare optical fiber with an inner diameter of $35 \mu\text{m}$ to directly excite the fluorescent markers in the capillary (such as FITC-derived sulfonamide antibiotics).

2. Detection window and optical path design: Silver mirror detection window: A silver mirror is coated on half of the surface of the capillary detection window to reflect the undetected fluorescence to the photomultiplier tube (PMT), which improves the single-sided fluorescence collection to double-sided reflection collection, significantly enhancing the signal intensity.
3. Optical filtering system: A $60\times$ microscope objective coupled with a 523 nm bandpass filter is used at the emission end to filter out stray light and focus the fluorescence signal to the PMT (Hamamatsu CR 105).
4. Separation and detection unit: Capillary: $75\text{ }\mu\text{m}$ inner diameter fused silica capillary (effective length 45 cm), the inner wall is free of polyimide coating to form a detection window for excitation and collection of fluorescence signals.
5. Signal processing module: After PMT conversion, the analog signal is recorded by the data acquisition card and transmitted to the computer, and quantitative analysis is achieved through peak height integration and standard curve fitting.

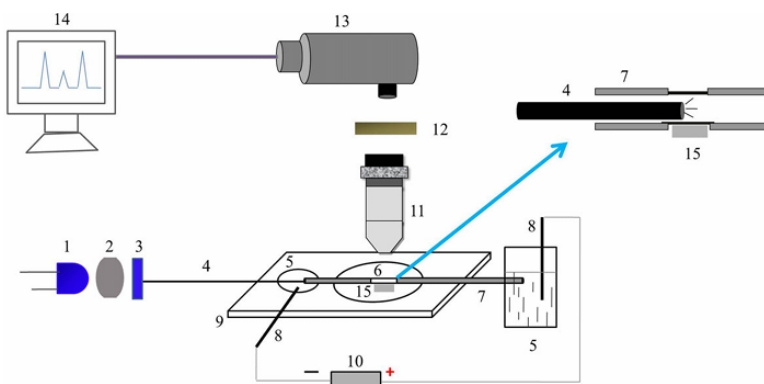


Figure 2.3: Schematic illustration of the SDW-ICOF-LED-IFD-CE system.(1) LED; (2) double convex lens; (3) bandpass filter 1; (4) $35\text{ }\mu\text{m}$ optical fiber; (5) buffer reservoirs; (6) detection window; (7) $75\text{ }\mu\text{m}$ i.d. capillary; (8) Pt electrodes; (9) organic glass plate; (10) high-voltage power supply; (11) microscope objective ($60\times$); (12) bandpass filter 2; (13) PMT; (14) computer; (15) silver mirror. (adapted from [21])

It has many magnificent advantages:

1. High-sensitivity detection: Silver mirror reflection enhancement technology:
The detection sensitivity is increased by nearly 2–4 times by reflecting the uncollected fluorescence with a silver mirror. For example, the detection limit (LOD, $S/N = 3$) of sulfamethoxazole sodium (SMM-Na) is reduced from 3.3 nM in the traditional system to 1.0 nM , which is significantly better than similar LED-induced fluorescence detection technology.
2. Low background noise: The optical fiber directly introduces the excitation light into the capillary to avoid interference from the reflected/scattered light on the outer wall of the capillary. Combined with a narrow-band filter, the background noise is effectively suppressed.
3. Excellent analytical performance: Wide linear range: The linear ranges for sulfadoxine (SDM), sulfamethoxazole (SGD), and SMM-Na are $4.4\text{--}300 \text{ nM}$, $6.7\text{--}600 \text{ nM}$, and $3.4\text{--}200 \text{ nM}$, respectively, and the correlation coefficients are ≥ 0.9995 [21].
4. Low cost and practicality: Advantages of LED light source: Compared with laser induced fluorescence (LIF), LED has the characteristics of small size, low power consumption, long life, and low cost (only $1/10\text{--}1/5$ of LIF light source), which is suitable for on-site detection and miniaturized integration.

However, the system still has some technical limitations:

1. Complexity of detection window preparation: The silver mirror coating needs to be treated with multiple chemical steps such as silicone rubber protection, NaOH activation, and silver ammonia solution reduction. The process is cumbersome and requires high uniformity of the capillary surface, which may affect long-term stability.
2. Label dependence: Depends on fluorescence derivatization (such as FITC labeling), and requires additional derivatization steps for targets without

natural fluorescence, which increases the analysis time (such as 16 h for derivatization reaction).

3. Environmental factors: The detection signal is significantly affected by the pH of the buffer solution (optimized to 9.3) and the ionic strength. Co-existing substances in complex water samples (such as humic acid and protein) may interfere with the fluorescence signal, which needs to be eliminated by optimizing separation conditions or pretreatment.

The silver mirror detection window - intracapillary fiber optic LED induced fluorescence detection system (SDW-ICOF-LED-IFD-CE) shown in Figure 2.3 performs well in the detection of sulfonamide antibiotics in environmental water samples: a 474 nm blue LED is used as the excitation light source, and the undetected fluorescence is reflected by the silver mirror to the photomultiplier tube to improve the detection sensitivity; for FITC-labeled sulfadoxine (SDM), sulfaguanidine (SGD) and sulfamethoxazole sodium (SMM-Na), the detection ranges are 4.4–300 nM, 6.7–600 nM and 3.4–200 nM, respectively, and the detection limit (LOD, S/N=3) is as low as 1.0–2.0 nM, which is significantly better than the traditional intracapillary fiber optic LED induced fluorescence detection system (LOD 2.5–7.7 nM); the intra-day and inter-day precision is good (migration time $RSD < 0.86\%$, peak area $RSD < 3.68\%$), and the spike recovery rate is 92.5%–102.9%; successfully applied to the detection of sulfonamide antibiotics in environmental water samples such as river water and hospital wastewater [21].

2.3.3 Time-resolved fluorescence immunoassay

The time-resolved fluorescence immunoassay system is based on time-resolved fluorescence technology. Its core structure is shown in Figure 2.4, which mainly includes the following components [22]:

1. Excitation light source: pulsed UV LED (340 nm) or nitrogen laser (337 nm) is used to excite the antibody/antigen complex labeled with lanthanide elements (such as europium Eu^{3+} or samarium Sm^{3+}).

2. Spectral separation system: dichroic mirror (DM, reflection wavelength 340 nm, transmission wavelength 615 nm) separates the excitation light and the emission light.
3. Filter: bandpass filter (BP 615 nm \pm 5 nm) filters out non-target fluorescence signals.
4. Delayed detection unit: avoids short-lived background fluorescence (such as solvent or impurity fluorescence, lifetime <10 ns) through time gating circuit (delay time 50–200 μ s).
5. Detector: photomultiplier tube (PMT, Hamamatsu R928) or silicon photodiode array, supporting high-sensitivity time-resolved signal acquisition.
6. Signal processing: FPGA-based pulse counting module combined with time-to-digital converter (TDC) quantifies fluorescence lifetime and intensity.

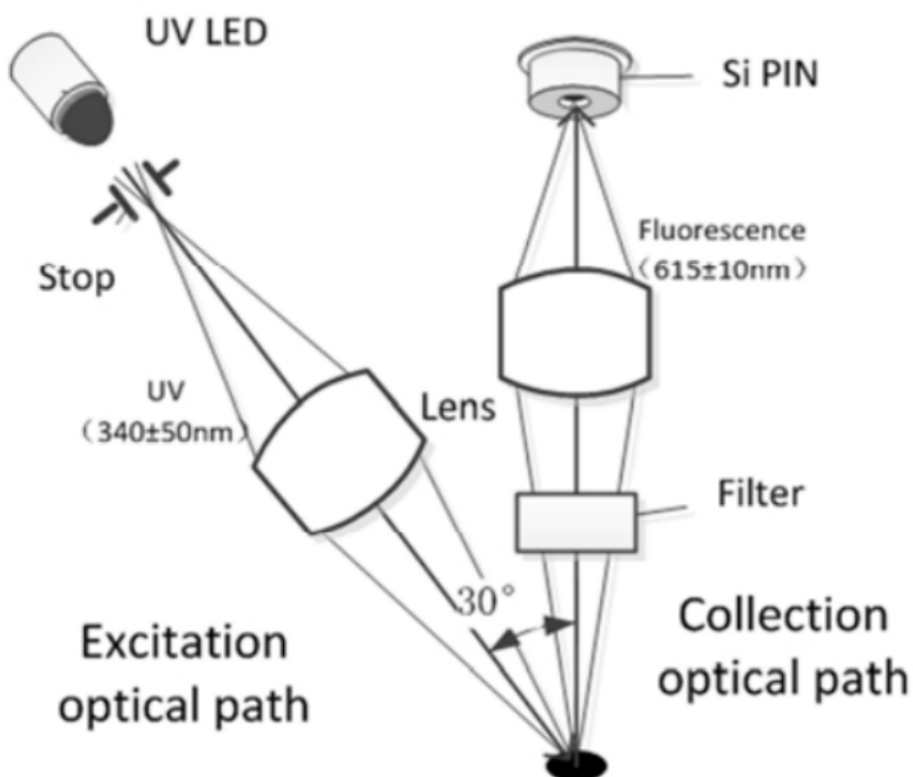


Figure 2.4: Time-resolved fluorescence immunoassay system (adapted from [23])

It has many significant advantages:

1. Ultra-high sensitivity: Lanthanide chelates have long fluorescence lifetimes (100–1000 μs), and time-resolved technology can effectively eliminate background noise, with a detection limit as low as 0.01 ng/mL ($SNR=3$) [23].
2. Multi-label detection: The emission wavelength differences of different lanthanides (such as Eu^{3+} , Tb^{3+}) support simultaneous detection of multiple targets.
3. Wide dynamic range: The linear range covers 3 orders of magnitude, which is suitable for low-abundance biomarker analysis (such as tumor markers, hormones).
4. Strong anti-interference ability: Time gating technology can suppress solvent Raman scattering and impurity fluorescence, improving the signal-to-noise ratio (SNR larger than 1000) [22].

However, this method also has some disadvantages:

1. High system complexity: It requires precise synchronization of pulse light source, delay circuit and detector, and the hardware cost and maintenance difficulty are relatively high.
2. Limited stability of markers: Lanthanide chelates are easily affected by pH and temperature and require strict storage conditions (such as avoiding light and keeping low temperature).
3. Long detection time: A single measurement requires multiple pulse accumulations (typical cycle 1–5 minutes), making it difficult to achieve real-time monitoring.

The light-emitting diode induced fluorescence detector shown in Figure 2.4 exhibits excellent performance: UV-LED (KED365UH) around 340 nm is used as the excitation light source, combined with time-resolved detection technology to suppress autofluorescence interference; the detection range is 1-400 $\mu g/mL$,

and the repeatability is excellent when the concentration is greater than 100 $\mu\text{g/mL}$; fluorescence signal conversion is achieved based on silicon photodiode (Si PIN), combined with mechanical scanning and embedded control, it is suitable for quantitative detection of immunochromatographic test strips in the POCT field. For FITC-labeled phenylalanine, the detection limit (LOD) is 19 $n\text{M}$ without pre-concentration treatment, and the signal-to-noise ratio (SNR) is 3; with the help of pre-concentration technology, the detection limit can be further reduced to below 1 $n\text{M}$. The detector shows good linear response in the concentration range of 10^{-7} M to $2\times10^{-5} \text{ M}$, with a correlation coefficient $R^2 = 0.999$ [22].

2.3.4 Comparison and analysis

A comparative analysis of the three fluorescence measurement systems introduced above is conducted, and the core technical parameters and application characteristics are presented in the following Table 2.1.

The dual-Path fluorescence chlorophyll-a sensor focuses on marine ecological environment monitoring, the silvering detection window-CE fluorescence detector is aimed at the analysis of antibiotic residues in water quality, and the portable time-resolved fluorometer is aimed at biomedical field rapid testing (POCT). The three correspond to the fields of environmental science, analytical chemistry and clinical medicine respectively. They perform well in specific scenarios, but all have problems such as single detection parameters (only for specific analyte) and limited adaptability to multiple scenarios.

Therefore, this passage designs a low-intensity light detection and analysis platform that integrates FLU and UVA parameter measurements. The platform is expected to break through the single parameter limitation of traditional fluorescence detection, provide a universal solution for multi-target analysis in low-intensity light scenarios, and promote the integration and innovation of interdisciplinary detection technologies.

Table 2.1: Comparison of three fluorescence measurement systems

System Type	Excitation Wavelength	Detection Range	Sensitivity	LOD
Dual - Path Fluorescence Chlorophyll - a Sensor [20]	430 nm LED	0–200 $\mu\text{g}/\text{L}$	Linearity:0.998 Accuracy: $\pm 2 \mu\text{g}/\text{L}$	0.1 $\mu\text{g}/\text{L}$
Silvering Detection Window - CE Fluorescence Detector [21]	474 nm LED	SGD: 6.7–600 nM SDM: 4.4–300 nM SMM - Na: 3.4–200 nM	SGD: 2.24 mV/nM SDM: 4.71 mV/nM SMM - Na: 6.82 mV/nM	SGD: 2.0 nM SDM: 1.3 nM SMM - Na: 1.0 nM
Portable Time - Resolved Fluorometer [22]	340 nm UV-LED	0–400 $\mu\text{g}/\text{mL}$	$CV = 2.6\%$, (1 $\mu\text{g}/\text{mL}$)	1 $\mu\text{g}/\text{mL}$

2.4 Weak signal detection methods

2.4.1 Background

In both quotidian environments and specialized fluorescence detection systems, the ubiquitous presence of noise constitutes a fundamental challenge to signal integrity. These extraneous interference signals exhibit spectral overlap with target signals, creating a composite waveform in which discriminative separation of signal and noise components becomes intractable through conventional signal separation techniques. Such interference not only compromises system functionality but also severely degrades signal fidelity, necessitating advanced methodologies for noise suppression or elimination to recover meaningful information from contaminated datasets. This challenge becomes particularly acute in weak signal detection applications, where the inherently low signal-to-noise ratio (SNR) amplifies operational complexity compared to high-amplitude signal regimes [24].

Weak signal detection encompasses the metrological characterization of both physical parameters (e.g. optical intensity, mechanical displacement) and derived electrical analogues. Through transducer-mediated conversion protocols, all physical quantities can be expressed as electrical parameters—including but not limited to voltage potentials, current flows, and capacitive reactance. The opera-

tional domain of weak signal detection is defined by extreme amplitude regimes:

1. Voltage measurement spans $10^{-10} - 10^{-6}$ μV ;
2. Current detection thresholds reach $10^{-5} - 0.1$ nA ;
3. Photometric sensitivity extends to $10^{-17} - 10^{-13}$ W/cm^2 ;
4. Capacitance resolution achieves $10^{-5} - 10^{-1}$ pF in sub-picofarad measurements.

Typically, conventional detection systems achieve SNR values about 10 : 1, fundamentally limited by analog circuit noise floors and environmental interference. In contrast, advanced weak signal detection architectures employing lock-in amplification, stochastic resonance, and coherent averaging techniques demonstrate multiplicative SNR enhancement—reaching over 10⁴ : 1 under optimized conditions [25]. This technological imperative drives innovations in ultra-low-noise amplification, cryogenic signal conditioning, and adaptive digital filtering to resolve signals buried 40–60 dB below the noise floor. The paradigm shift from amplitude-domain detection to phase-sensitive measurement techniques further enables discrimination of weak periodic signals from broadband noise through spectral compression and correlation-based recovery algorithms.

2.4.2 Lock-in detection

The lock-in detection is very common and widely used for weak signal detection, as it can effectively separate useful signals from noise. A sinusoidal signal is used to modulate the Ex light source, thereby modulating the intensity of the fluorescence, which will provide the input signal for the system. At the same time, a sinusoidal reference signal **with the same frequency and phase** as the fluorescence response signal is used to demodulate the weak input signal, and a narrow bandpass filter with an extremely high quality factor is used to filter out only one of the modulation components with high selectivity [26]. The block diagram of the lock-in amplifier is shown in Figure 2.5.

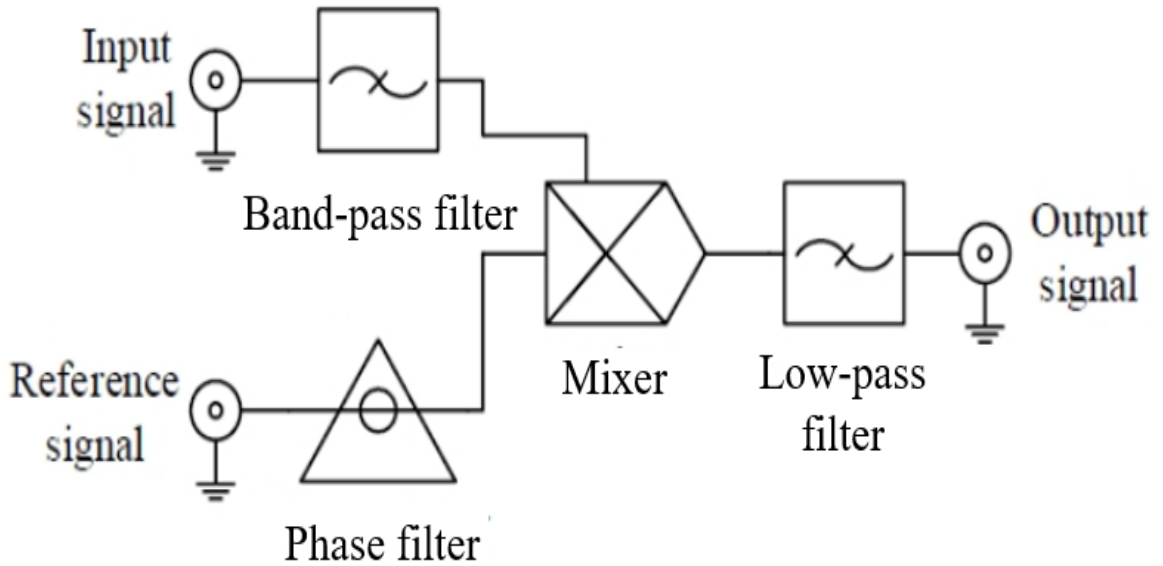


Figure 2.5: Block diagram of lock-in amplifier (adapted from [26])

The following will combine mathematical formulas to specifically introduce how the locked-in amplifier circuit improves the signal-to-noise ratio, thereby ensuring the system's good anti-interference ability.

First, a mathematical model of signal and noise is established. Assume that the weak fluorescence signal to be measured is:

$$S(t) = V_s \sin(\omega t + \phi) \quad (2.8)$$

Where V_s is the signal amplitude, ω is the angular frequency, and ϕ is the initial phase. The noise $N(t)$ is assumed to be Gaussian white noise, with a power spectrum density of N_0 and a bandwidth of Δf . The total input signal is:

$$X(t) = S(t) + N(t) \quad (2.9)$$

After that, it is the phase-sensitive detection process. Assume that the reference signal $R(t)$ with the same frequency as the signal is used by the locked-in amplifier:

$$R(t) = V_r \sin(\omega t + \theta) \quad (2.10)$$

Where θ is the reference signal phase. Multiply the input signal by the reference signal:

$$X(t) \cdot R(t) = [S(t) + N(t)] \cdot V_r \sin(\omega t + \theta) \quad (2.11)$$

After expansion, we get:

$$\begin{aligned} X(t)R(t) &= V_s V_r \sin(\omega t + \phi) \sin(\omega t + \theta) + N(t) V_r \sin(\omega t + \theta) \\ &= \frac{V_s V_r}{2} [\cos(\phi - \theta) - \cos(2\omega t + \phi + \theta)] + N(t) V_r \sin(\omega t + \theta) \end{aligned} \quad (2.12)$$

The high-frequency component (such as the 2ω term) is filtered out by a low-pass filter, and the DC and low-frequency components are retained. The output after filtering is:

$$Y(t) = \frac{V_s V_r}{2} \cos(\phi - \theta) + \tilde{N}(t) \quad (2.13)$$

Where $\tilde{N}(t)$ is the residual component of the noise after filtering. When $\theta = \phi$ (phase locked), the signal component is maximized:

$$Y_{\text{signal}} = \frac{V_s V_r}{2} \quad (2.14)$$

After multiplication, the power spectrum density of the noise term $N(t)V_r \sin(\omega t + \theta)$ becomes:

$$S'_N(f) = N_0 \cdot \frac{V_r^2}{2} \left[\delta(f) + \frac{1}{2} \delta(f - 2\omega) \right] \quad (2.15)$$

The bandwidth of the low-pass filter is B , and only the power of the noise in $[-B, B]$ is retained, so the residual noise power is:

$$P_{\text{noise}} = \int_{-B}^B S'_N(f) df = N_0 \cdot \frac{V_r^2}{2} \cdot 2B = N_0 V_r^2 B \quad (2.16)$$

Therefore, the original signal-to-noise ratio is:

$$SNR_{in} = \frac{P_{signal}}{P_{noise}} = \frac{V_s^2/2}{N_0\Delta f} \quad (2.17)$$

The signal-to-noise ratio after phase-locked amplification (output):

$$SNR_{out} = \frac{(V_s V_r / 2)^2}{N_0 V_r^2 B} = \frac{V_s^2}{4 N_0 B} \quad (2.18)$$

Hence, we can calculate the signal-to-noise ratio improvement multiple:

$$\frac{SNR_{out}}{SNR_{in}} = \frac{\Delta f}{2B} \quad (2.19)$$

We can find that the locked-in amplifier improves the SNR through the following mechanisms:

1. Spectral compression: Concentrate the signal energy near DC (the bandwidth B is much smaller than Δf).
2. Noise suppression: Only the power of the noise in the narrow band B is retained, and the noise power is reduced by $\frac{2B}{\Delta f}$.

This method is particularly suitable for detecting weak fluorescence signals (such as sinusoidal responses), and the SNR can be improved by $10^3 - 10^6$ times, depending on the parameters of the system design B and Δf .

2.4.3 Application examples of locked-in detection in optical signals

Locked-in detection technology has important applications in optical signal processing in environmental monitoring, biomedicine, precision measurement and other fields through phase-sensitive detection and noise suppression of weak optical signals.

In high-speed coherent optical communication, Liu et al. (2018) [27] proposed an optical phase-locked loop based on a delayed XOR phase detector to solve the phase noise problem through phase-locked detection technology. The system achieves an optical signal sensitivity of -40.4 dBm at a rate of 5 Gbps , and a bit error rate as low as 1.55×10^{-8} . Its core is to use a phase-locked

loop to track the phase difference between the reference light and the received light in real time, and control the phase detection error within 0.07 V through multi-level loop control, which is suitable for high-noise environments such as space optical communication.

In chlorophyll-a fluorescence detection, locked-in amplification technology is often used to separate weak fluorescence signals from strong background light. For example, the LED-based fluorescence sensor designed by Jacob J Lamb et al. (2012) [28] achieves high-sensitivity detection in the concentration range of 0-5 $\mu\text{mol/L}$ by frequency modulation and phase-locked demodulation of the excitation light source, effectively suppressing the interference of scattered light and ambient light in the water body, and proving the reliability of phase-locked detection in fluorescence quantitative analysis.

In the field of precision measurement, Li et al. (2022) [29] used phase-locked detection combined with IQ demodulation technology to improve the signal-to-noise ratio in the phase-sensitive optical time-domain reflectometer (ϕ -OTDR). By phase modulating the optical carrier and using the phase-locked loop to track the phase change in real time, the signal-to-noise ratio is increased by 12.5 dB in the frequency range of 80-3400 Hz, and the phase demodulation distortion suppression rate reaches 95%, realizing high-precision detection of vibration signals in long-distance (such as 100 km) optical fiber links.

The core advantage of locked-in detection technology in optical signal processing is to achieve high-sensitivity extraction and noise suppression of weak signals through frequency modulation, phase locking and phase-sensitive demodulation. The above cases cover the fields of environmental monitoring, biomedicine, precision measurement, quantum communication, etc., indicating that it has wide applicability in practical engineering and scientific research. Therefore, this dissertation plans to use phase-locked amplification detection technology to extract weak optical signals from a large amount of background light noise.

2.4.4 Differential and instrumentation amplifiers

The differential amplifier circuit has a strong ability to suppress common-mode signals. It is very effective in reducing the dark current of components in photoelectric detection systems and the impact of ambient temperature changes on circuits. The differential amplifier circuit is shown in Figure 2.6.

In the circuit, the main function of the bypass capacitor C is to prevent oscillation and reduce the ripple of the output DC level [30].

It can be seen from the circuit that the relationship between the output V_O of the differential amplifier circuit and the inverting input terminals V_1 and V_2 is:

$$V_O = -\frac{R_f}{R_1}V_1 + \left(\frac{R_3}{R_2 + R_3} \right) \left(1 + \frac{R_f}{R_1} \right) V_2 \quad (2.20)$$

When $R_1 = R_2$ and $R_3 = R_f$, we can get:

$$V_O = -\frac{R_f}{R_1}V_1 + \frac{R_f}{R_1}V_2 = \frac{R_f}{R_1}(V_2 - V_1) \quad (2.21)$$

The three-op-amp high CMRR instrument amplifier circuit is a typical circuit in the differential amplifier. It has a high common-mode rejection ratio (CMRR), low noise performance and high input impedance.

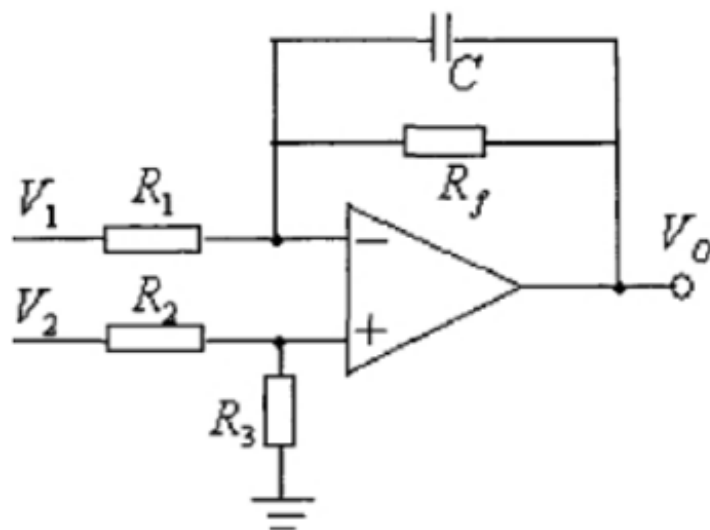


Figure 2.6: Differential Amplifier (adapted from [30])

As an amplifier with differential input and single-ended output, the basic working principle of the instrument amplifier is similar to that of the differential amplifier, but the performance is better. The main problem of the traditional differential amplifier is the precise matching of resistors, while the instrument amplifier can complete the amplification of the differential signal under better conditions and has a strong common-mode suppression capability. This is very useful in the weak light signal detection circuit.

The classic architecture of the general instrument amplifier is a three-op-amp structure (as shown in Figure 2.7), which consists of two differential input buffer stages (N_1 , N_2) and a differential output stage (N_3).

The current I_R flowing through R_1 , R_0 and R_2 can be written from the input stage current as:

$$I_R = \frac{u_{o2} - u_{i2}}{R_2} = \frac{u_{i1} - u_{ol}}{R_1} = \frac{u_{i2} - u_{i1}}{R_0} \quad (2.22)$$

From this we can get:

$$u_{ol1} = \left(1 + \frac{R_1}{R_0}\right) u_{i1} - \frac{R_1}{R_0} u_{i2} \quad (2.23)$$

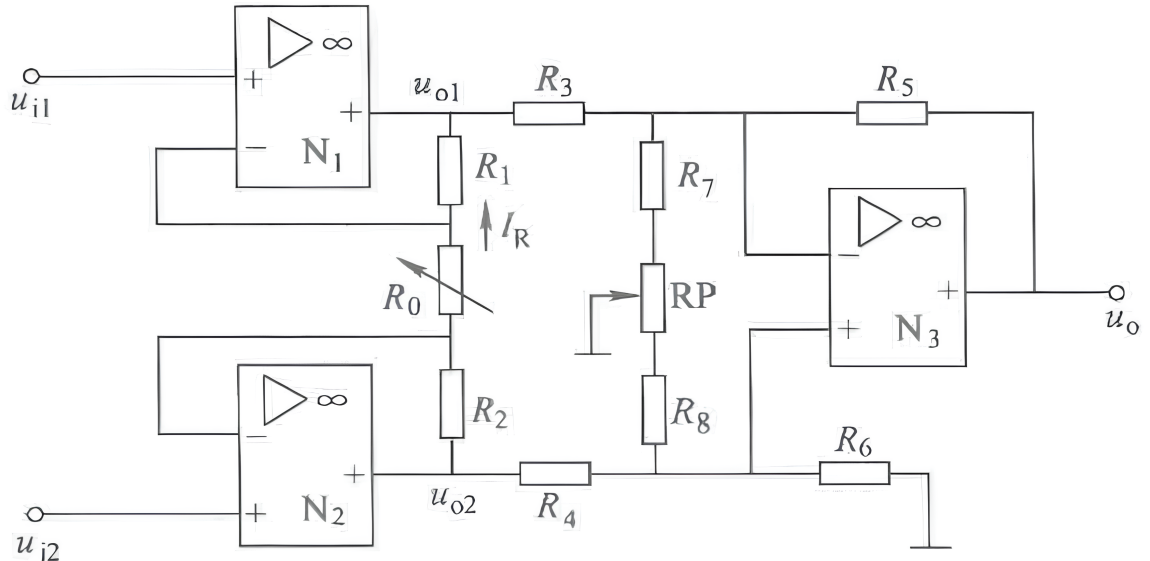


Figure 2.7: Schematic diagram of an instrumentation amplifier (adapted from [30])

Also we can get:

$$u_{o2} = \left(1 + \frac{R_2}{R_0} \right) u_{i2} - \frac{R_2}{R_0} u_{i1} \quad (2.24)$$

So, the output voltage of the input stage, that is, the difference between the outputs of the operational amplifiers $N2$ and $N1$:

$$u_{o2} - u_{ol} = \left(1 + \frac{R_1 + R_2}{R_0} \right) (u_{i2} - u_{i1}) \quad (2.25)$$

Its differential mode gain K_d :

$$K_d = \frac{u_{o2} - u_{ol}}{u_{i2} - u_{i1}} = 1 + \frac{R_1 + R_2}{R_0} \quad (2.26)$$

The core of general instrument amplifier lies in high common mode rejection ratio (CMRR), high input impedance and low noise characteristics. However, the actual discrete circuit design is limited by component matching. Integrated chips have broken through the bottleneck of discrete solutions through laser trimming and internal resistance matching, becoming the first choice in the field of high-precision data acquisition.

Therefore, this article plans to use INA114 integrated chip as the instrument amplifier.

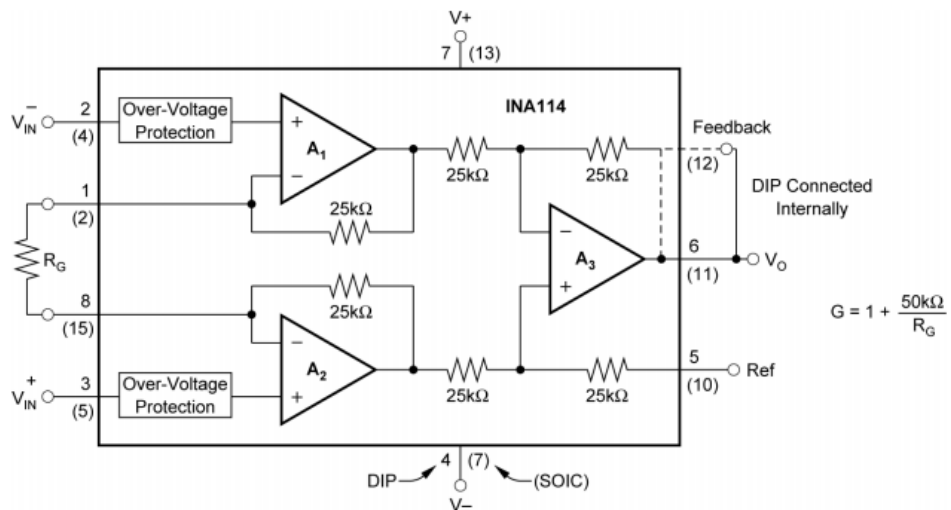


Figure 2.8: INA114 instrumentation amplifier schematic (adapted from [31])

As shown in Figure 2.8 is the schematic diagram of the INA114 precision instrument amplifier produced by Texas Instruments. The INA114 is a low-cost, general-purpose instrumentation amplifier offering excellent accuracy [31]. The versatile three-op-amp design and small size make this device an excellent choice for a wide range of applications. As an integrated module, it can achieve high-precision differential amplification at a low cost. Therefore, this product will also be used as part of the differential amplifier circuit used in this dissertation.

2.5 Conclusion

This chapter systematically sorts out the theoretical basis of fluorescence detection technology, existing system architecture and weak signal processing strategy. The high sensitivity and wavelength selectivity of fluorescence phenomena provide a physical basis for trace analysis of water quality. Although the existing detection system performs well in specific scenarios, it still faces challenges such as insufficient miniaturization, high cost and complex optical alignment. In addition, although weak signal processing technology (such as phase-locked amplification) can effectively improve the signal-to-noise ratio, its implementation complexity may limit the system integration.

Therefore, the core contradiction of the current research lies in how to achieve the compactness and scalability of the system while ensuring the detection sensitivity. To meet this challenge, the subsequent chapters will focus on optical system design and circuit design, optimize fluorescence collection efficiency, and realize multi-modal (UVA and FLU) synchronous detection. By integrating the coordinated optimization of optical and electrical systems, this study aims to break through the limitations of existing technologies and provide innovative solutions for real-time and portable water quality monitoring.

Chapter 3

Our designed optical system

3.1 Introduction

In this dissertation, the main objective is to design and implement a system for analyzing water quality using both UV absorbance (UVA) and fluorescence (FLU). Hence, the system consists of two parts: optical and electrical. The optical system design focused on developing an elliptically cylindrical reflector that enhances the capture of low-intensity FLU light emitted from the UV-illuminated water sample while enabling UVA detection. It involves the integration of beam splitter, long-pass filter, UV LEDs, UV photodiodes, cylindrical lenses and photomultiplier modules (PMT). The electrical system deals with the elements related to powering up the light emission source as well as the circuits for light detection and signal processing. Through systematic iterative simulations, this chapter evaluated various optical assemblies and designed an optimized system that focuses on deployable and practical applications.

For optical system design, we utilized two main software:

1. 3D Design and Modeling – SolidWorks, Autodesk Fusion 360 To create different 3D models with accurate dimensions before importing them into optical simulation software to perform subsequent simulations. After the final specifications and placement location of the necessary optical components are determined, we create the prototype with accurate dimensions to be 3D-printed for prototype testing.

2. Optical Simulation and Raytracing – Zemax OpticStudio To perform iterative simulation to evaluate the performance of the optical assemblies and determine the optimal specifications of the necessary optical components such as cylindrical lenses, etc. Raytracing function in non-sequential mode is used to simulate the light propagation through optical components in any order and plot the irradiance maps to visualize the light distribution at a virtual detector placed at a specific location. Sequential mode is also used to visualize and verify the ray path of lens assembly before they are implemented in the simulation of non-sequential mode.

3.2 Overall optical system design

The proposed optical system can be divided into 5 parts, as shown in Figure 3.1.

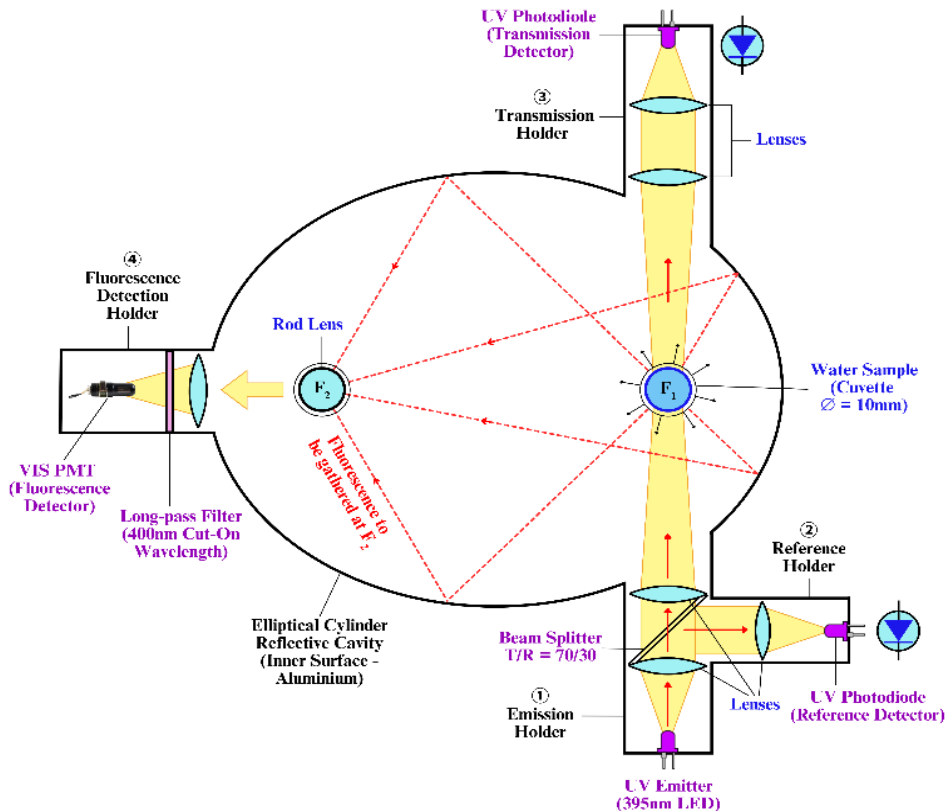


Figure 3.1: Schematic representation of our designed optical system

The five specific parts are:

1. Elliptical cylinder reflective cavity
2. Emission holder
3. Reference holder
4. Transmission/Absorption holder
5. Fluorescence detection holder (PMT holder)

The reflective property of an ellipse states that when a ray leaves one of the foci and meets a point on that ellipse, it will reflect off of the ellipse and pass through the other focus. Based on this property, the UV-illuminated water sample (cuvette) is placed at the first focal point of the elliptical cylinder cavity, and its isotropically emitted FLU light is (ideally) all concentrated at the second focal point of the reflector. The internal surface of the reflector will be coated with reflective aluminium materials to enhance reflection.

At the emission holder, UV LEDs (LZ1-00UBN0) with typical emission peak wavelength of 395 nm are setup at the end of the holder to emit ultraviolet light to excite fluorescence. Cylindrical lenses are placed in the holder to collimate and focus the UV beam onto the water sample. Beam splitter (70T/30R) splits a portion of the excitation UV beam to the reference holder.

At the reference holder, a cylindrical lens is placed to focus the portion of the excitation UV beam onto the reference photodiodes (PDs), which are the same models of the UV LEDs (LZ1-00UBN0).

At the transmission holder, another set of cylindrical lenses are used to focus the UV light onto PDs (LZ1-00UBN0) at the end of the transmission holder. PDs detect the UV light transmitted through the sample. The detected signal is subsequently processed together with the reference signal to determine UVA parameter.

At the fluorescence detection holder (PMT holder), a long-pass filter with 400 nm cut-on wavelength will blocks excitation (ultraviolet wavelength range), allowing only FLU light (visible light wavelength range) to be detected by a

photomultiplier tube (PMT) (Hamamatsu H11642-011) after being transmitted from the second focal point of the elliptical reflector. The detected signal will be used to determine FLU parameter.

3.3 Evaluation of fluorescence capturing performance of the elliptical cylinder reflective cavity

In Zemax OpticStudio software, Ray Trace and Irradiance Maps were used to simulate and visualize the light distribution.

After placing a cylindrical light source that emits light rays isotropically at the first focal point (F_1) of the ellipse, and a detector ($70\text{ mm} \times 110\text{ mm}$) at the second focal point (F_2), we perform Zemax simulation and obtain the irradiance map. The specific Zemax simulation effect is shown in Figure 3.2. The prominent strip in the center of the image shown in Figure 3.3 proves that FLU light is gathered effectively at the second focal point of the elliptical reflector. This proves that the fluorescence capturing performance is excellent and this elliptical cylinder model is ideal to be used in our design.

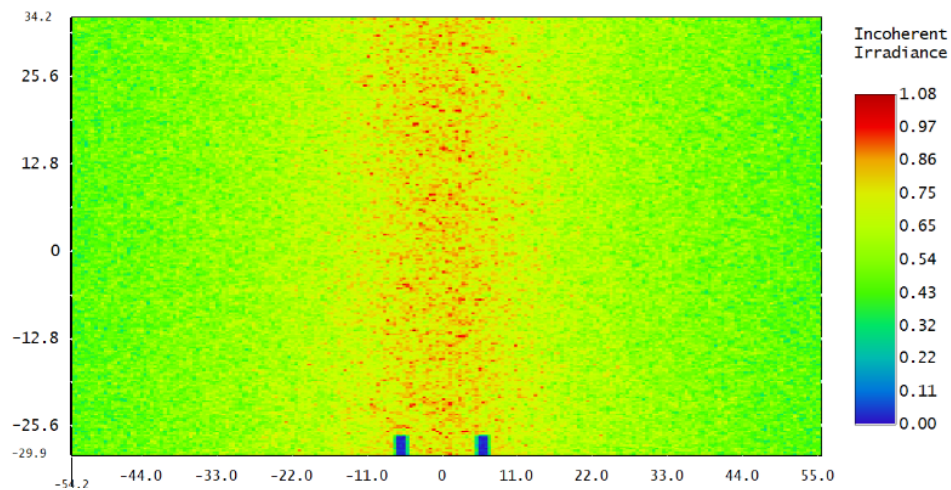


Figure 3.2: Irradiance map of FLU light arriving at the 2nd focal point of the reflector

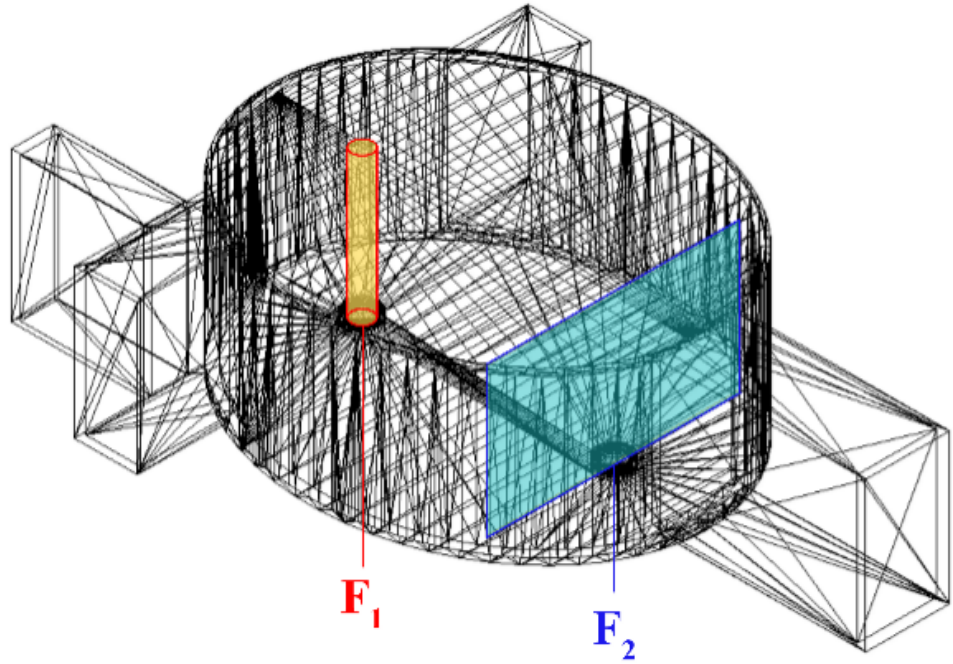


Figure 3.3: ZEMAX detector for FLU light

3.4 Design of the emission holder and transmission holder

At emission and transmission holder, the optimal two-lens combination was determined by using the first lens to collimate the UV beam and the second lens to focus it, thereby illuminating the largest cross-sectional area of the water sample to maximize FLU excitation in the sample. The cuvette's cross-sectional diameter is 10 mm. We propose three types of lens combinations and perform iterative optics simulations:

1. Version 1A: 1 Rod Lens with 2 rows of 5 LEDs
2. Version 1B: 1 Rod Lens with 1 row of 10 LEDs
3. Version 2A: 2 Rod Lenses with 2 rows of 5 LEDs
4. Version 2B: 2 Rod Lenses with 1 row of 10 LEDs
5. Version 3A: 2 Cylindrical Convex Lenses with 2 rows of 5 LEDs
6. Version 3B: 2 Cylindrical Convex Lenses with 1 row of 10 LEDs

7. Version 4: 2 Cylindrical Convex Lenses with 1 row of 10 LEDs (final optimized version)

All simulation versions are done with 395 nm LEDs light sources, beam splitter ($25\text{ mm} \times 25\text{ mm}$), 5 detectors ($12\text{ mm} \times 70\text{ mm}$) at different locations:

1. Detector 1 – LEDs
2. Detector 2 – Emission Holder Slit
3. Detector 3 – Water Sample
4. Detector 4 – Transmission Holder Slit
5. Detector 5 – Photodiodes

According to the top view of version 1A (as shown in Figure 3.4), the cavity optical path is constructed using Zemax non-sequential mode as shown in Figure 3.5, and the luminous flux corresponding to the five detectors is shown in Figure 3.6.

According to the top view of version 1B (as shown in Figure 3.7), the cavity optical path is constructed using Zemax non-sequential mode as shown in Figure 3.8, and the luminous flux corresponding to the five detectors is shown in Figure 3.9.

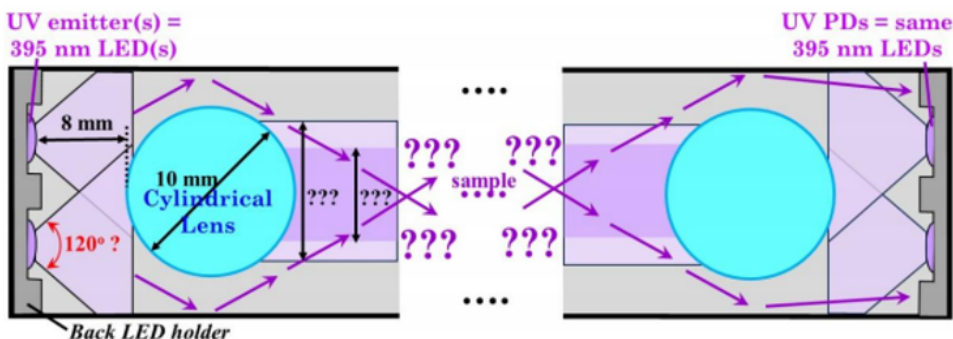


Figure 3.4: Top view of Version 1A

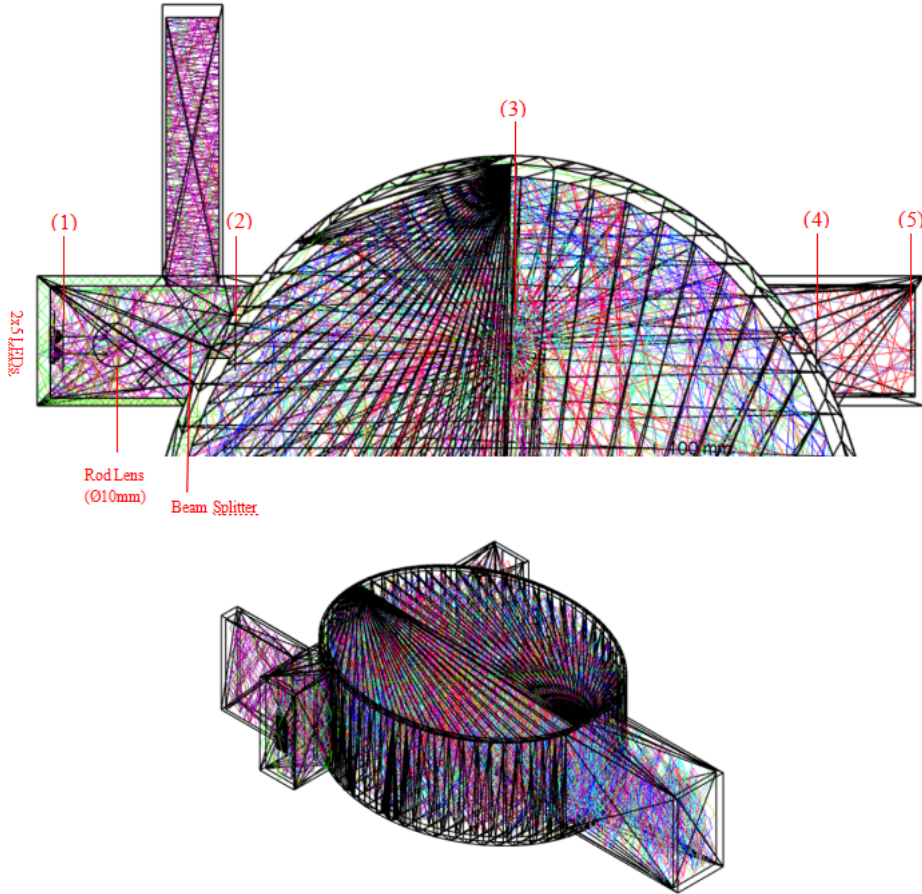


Figure 3.5: Zemax Optics Simulation of Version 1A

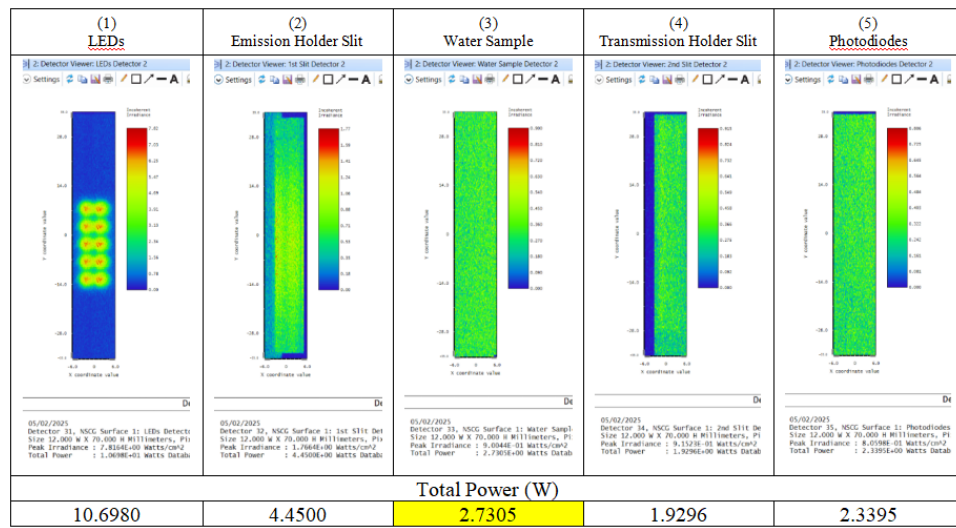


Figure 3.6: Five-position luminous flux of Version 1A

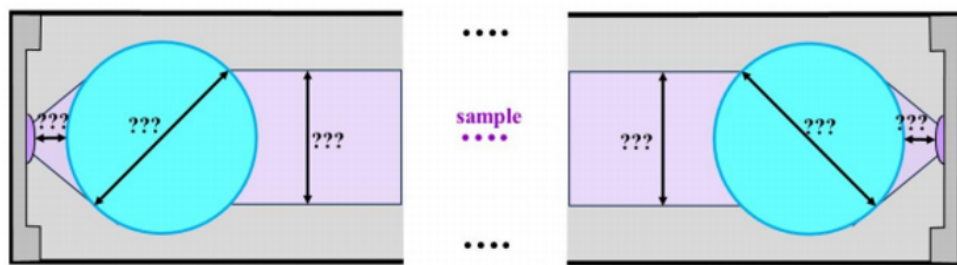


Figure 3.7: Top view of Version 1B

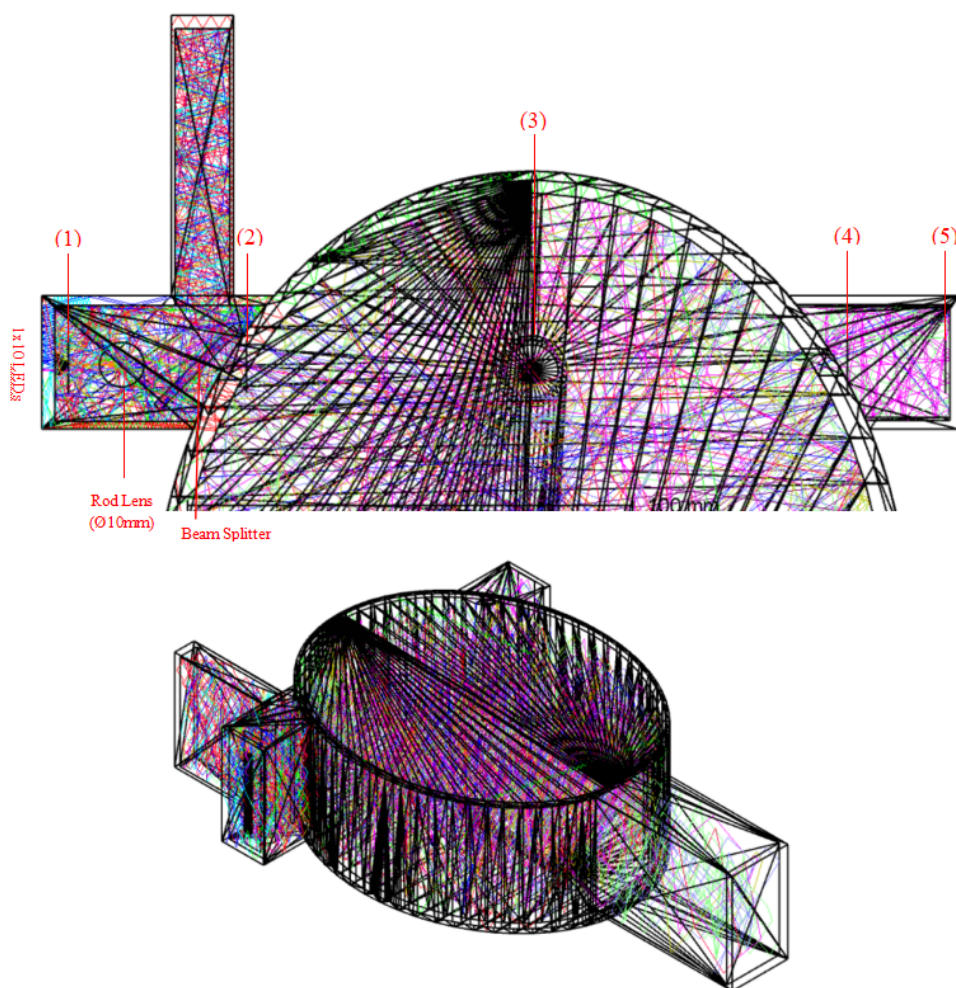


Figure 3.8: Zemax Optics Simulation of Version 1B

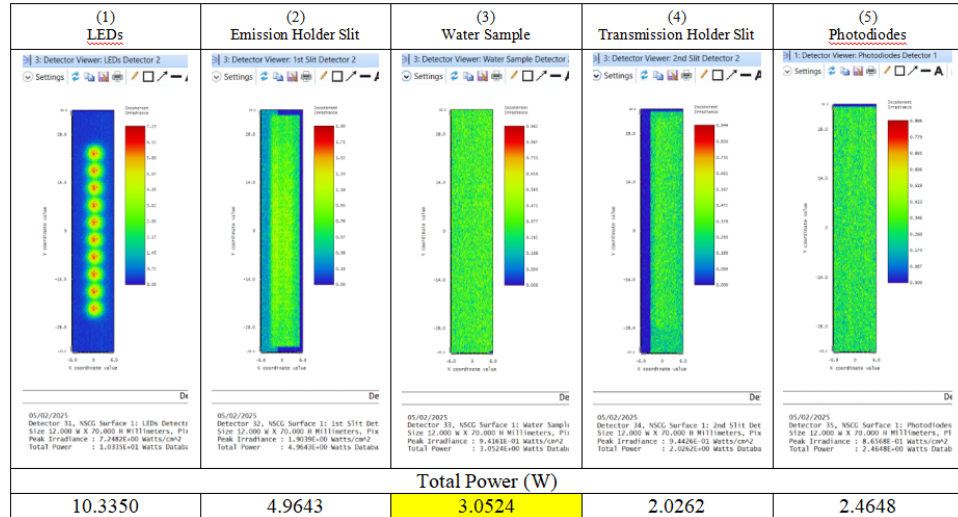


Figure 3.9: Five-position luminous flux of Version 1B

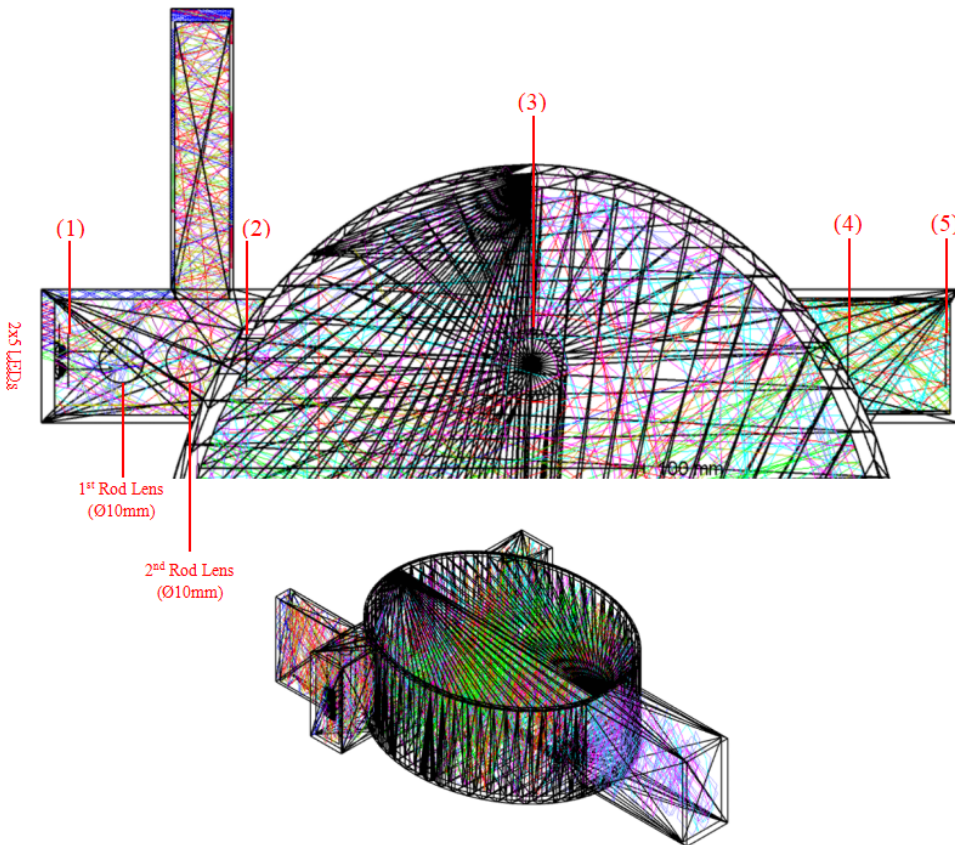


Figure 3.10: Zemax Optics Simulation of Version 2A

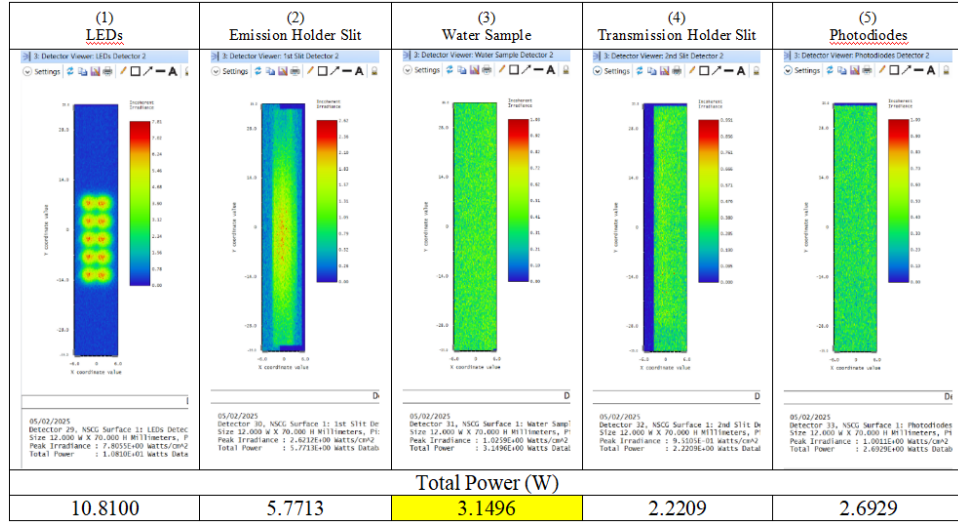


Figure 3.11: Five-position luminous flux of Version 2A

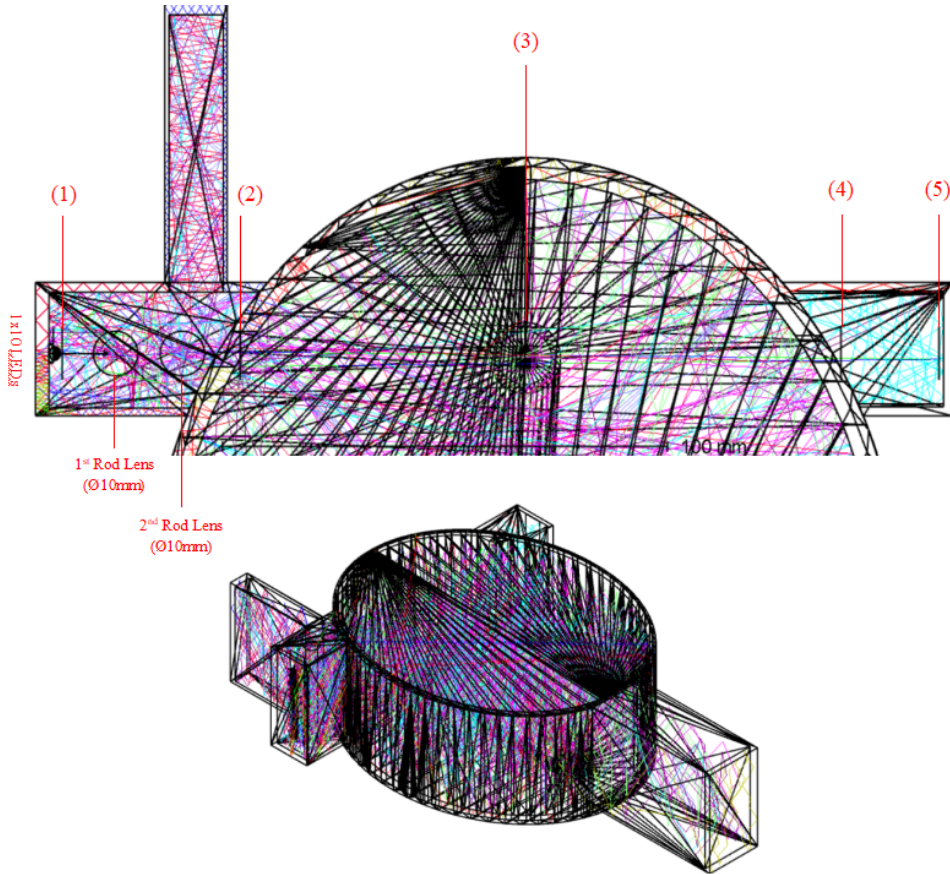


Figure 3.12: Zemax Optics Simulation of Version 2B

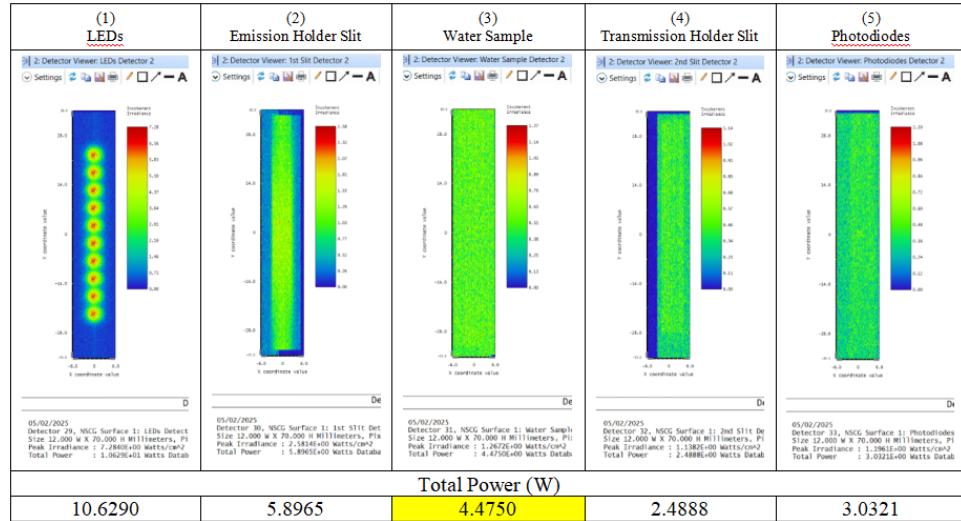


Figure 3.13: Five-position luminous flux of Version 2B

When we use the Version 2A method and utilize the Zemax non-sequential mode to construct the cavity optical path as shown in Figure 3.10, the luminous flux corresponding to the five detectors is shown in Figure 3.11.

When we use the Version 2B method and utilize the Zemax non-sequential mode to construct the cavity optical path as shown in Figure 3.12, the luminous flux corresponding to the five detectors is shown in Figure 3.13.

For the simulation of version 3A, we first simulated in sequential mode as shown in Figure 3.14 to determine the lens specifications and evaluate the focusing performance. Then we imported the lens into non-sequential mode and performed further ray tracing in the reflective cavity.

We modelled a light source (OBJECT) with 80° opening angle. By using Merit Function Editor in the Optimize function and applied constraint setting of ‘RANG’ parameter to 0, the system successfully determined the radius of curvature of the first convex lens to collimate the diverging rays. We then set the second convex lens at 25 mm from the back surface of the first convex lens to allocate the placement of the beam splitter. After that, we use Merit Function Editor in the Optimize function so that the system can determine the radius of curvature of the second convex lens to focus the beam to a spot. We then set a 10 mm frame (IMAGE) to represent the cross-section of the water sample. After some minor adjustments and finetuning of the radius of

curvature of the second convex lens, we set the IMAGE frame to be located at a distance of 64 mm which is the distance from the emission holder opening to the first focal point of the ellipse while ensuring that the cross-section receives the maximum UV illumination.

At the same time, the existing holder design was also modified: on the one hand, the slits on the two holders were removed to improve the focusing performance; on the other hand, the emission holder length was shortened to reduce the light waste in the holder. The cavity optical path shown in Figure 3.15 is constructed using Zemax non-sequential mode, and the luminous flux corresponding to the five detectors is shown in Figure 3.16.

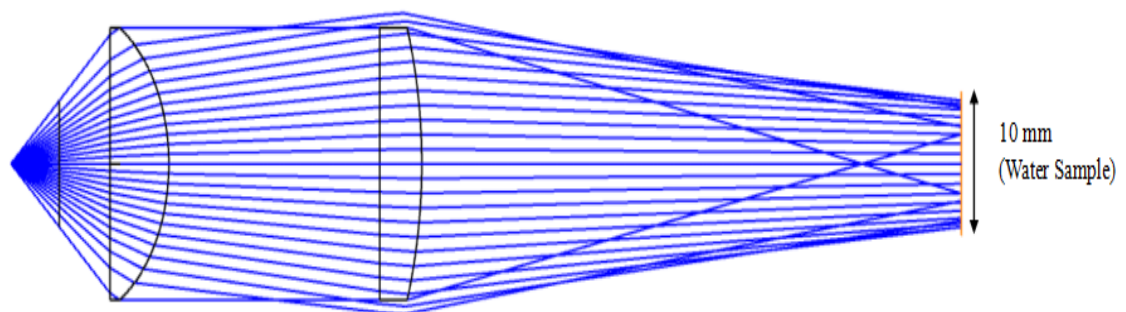
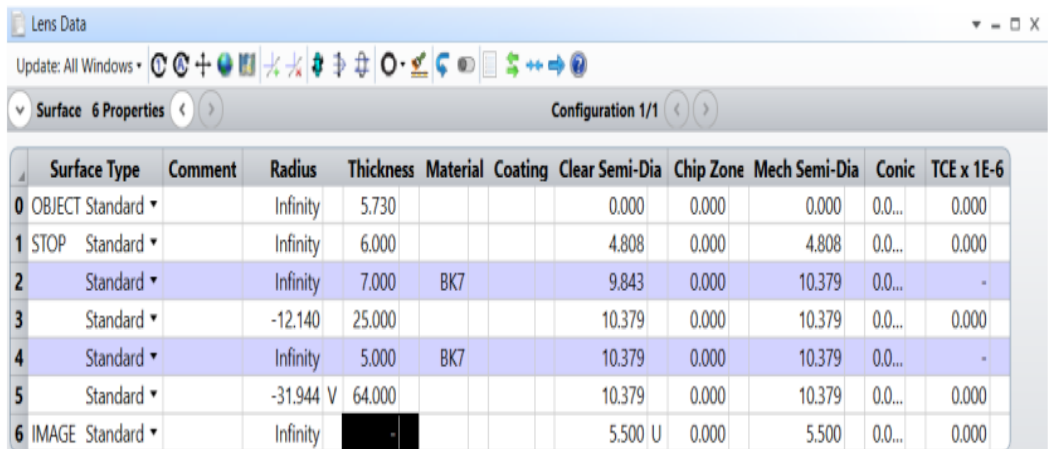


Figure 3.14: Zemax Optics sequential mode simulation of Version 3A

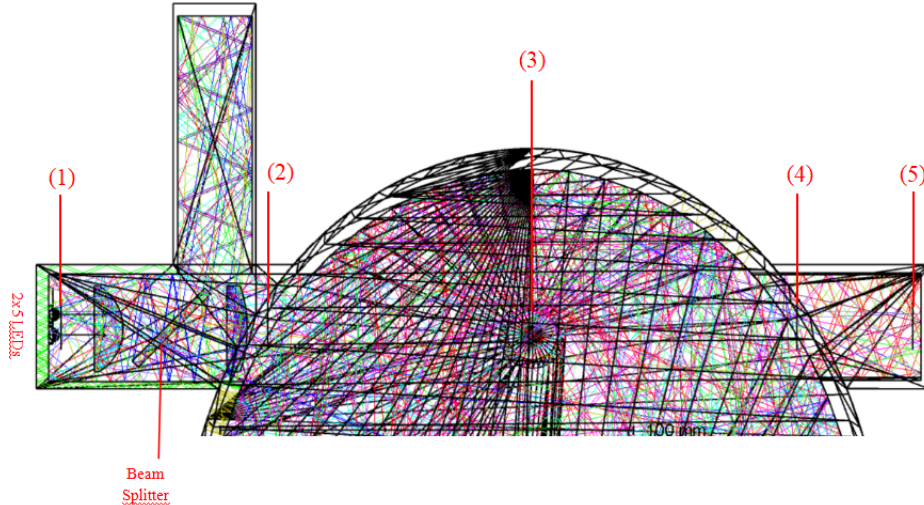


Figure 3.15: Zemax Optics Simulation of Version 3A

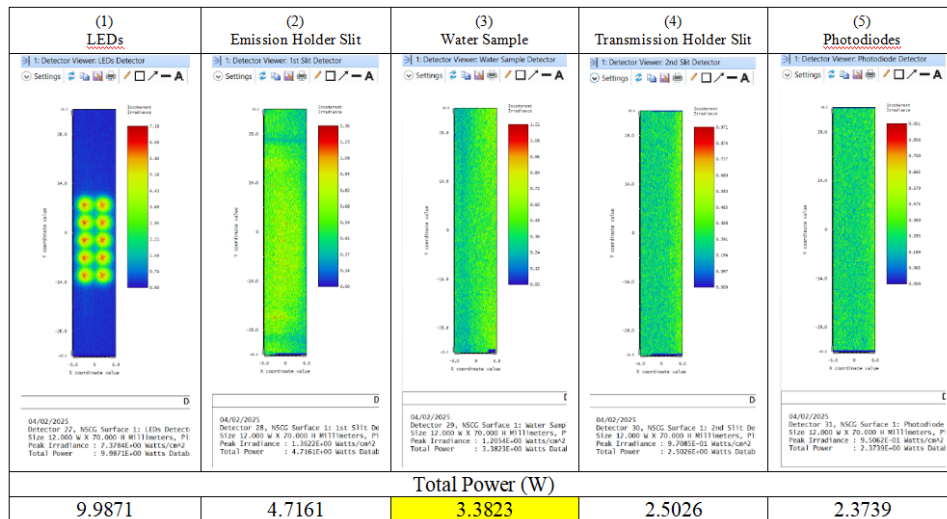


Figure 3.16: Five-position luminous flux of Version 3A

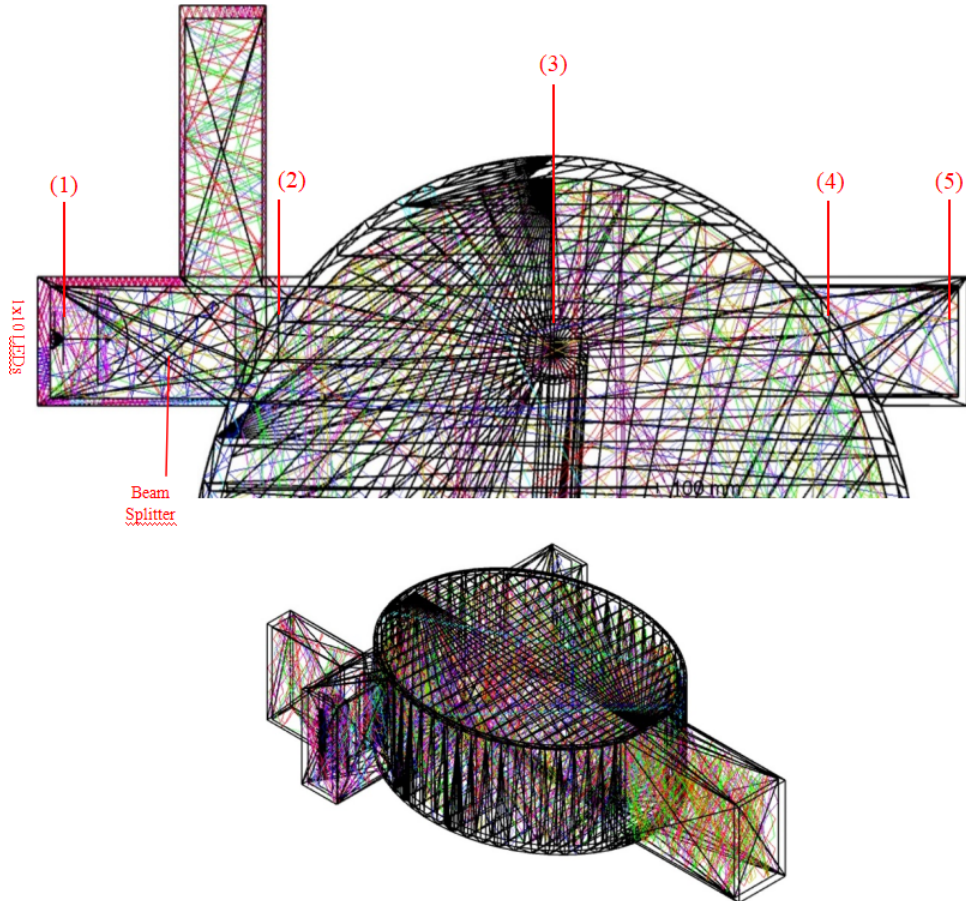


Figure 3.17: Zemax Optics Simulation of Version 3B

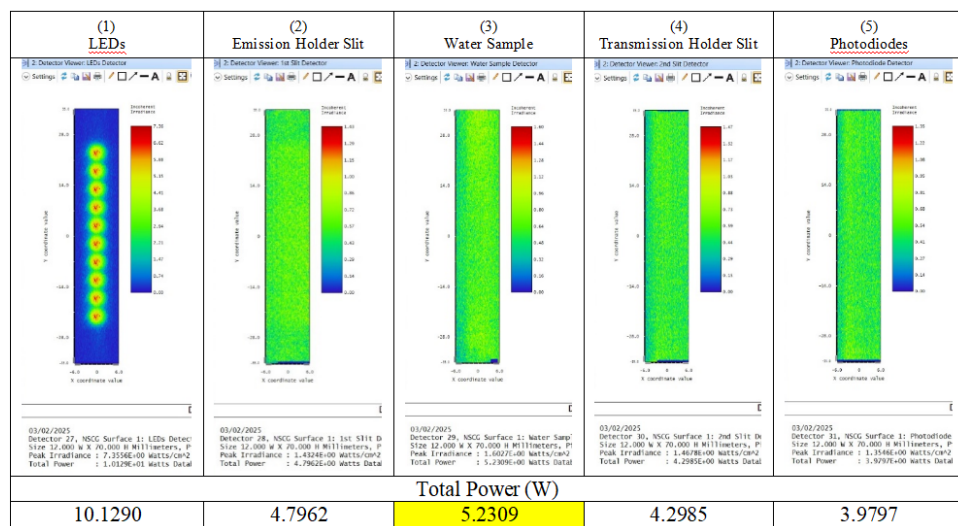


Figure 3.18: Five-position luminous flux of Version 3B

There is a vertical line at the middle of detector 3 showing lower irradiance value, indicating that the light is not focusing and illuminating the water

sample ideally as simulated in the sequential mode. This might be caused by the usage of 2 rows of 5 LEDs which are misaligned at the principal axis. Hence, we consider Version 3B with 1 row of 10 LEDs.

When we use the Version 3B method and utilize the Zemax non-sequential mode to construct the cavity optical path as shown in Figure 3.17, the luminous flux corresponding to the five detectors is shown in Figure 3.18.

It shows that the focusing performance is improved significantly after changing to 1 row of 10 LEDs because of the alignment in principal axis which follows the sequential mode simulation. Therefore, version 3B is chosen for further analysis.

Further analysis of the focusing performance of Version 3B is performed in non-sequential mode but without the reflective cavity. We placed a large detector(35 mm x 35 mm) at the water sample location and perform a ray tracing.

We observed an effective focusing performance done by Version 3B as shown in Figure 3.19. Considering the cuvette's diameter of 10 mm, most of the UV light effectively illuminates the cross-sectional of the water sample. However, there is still a portion of the light that does not illuminate the water sample (outside the white frame). Hence, we did further optimization by increasing the second convex lens's radius of curvature so that the prominent strip of UV light distribution can have an exact width of 10 mm. We optimize the lens parameters and find that the final method is version 4.

This project was finally optimized based on version 3B to obtain version 4. Similar to the previous simulation operation, we first simulated in the sequential mode as shown in Figure 3.21 to determine the lens specifications and evaluate the focusing performance, and then imported the lens into the non-sequential mode, and further ray tracing was performed in the reflection cavity to obtain the luminous flux corresponding to the five detectors as shown in Figure 3.20.

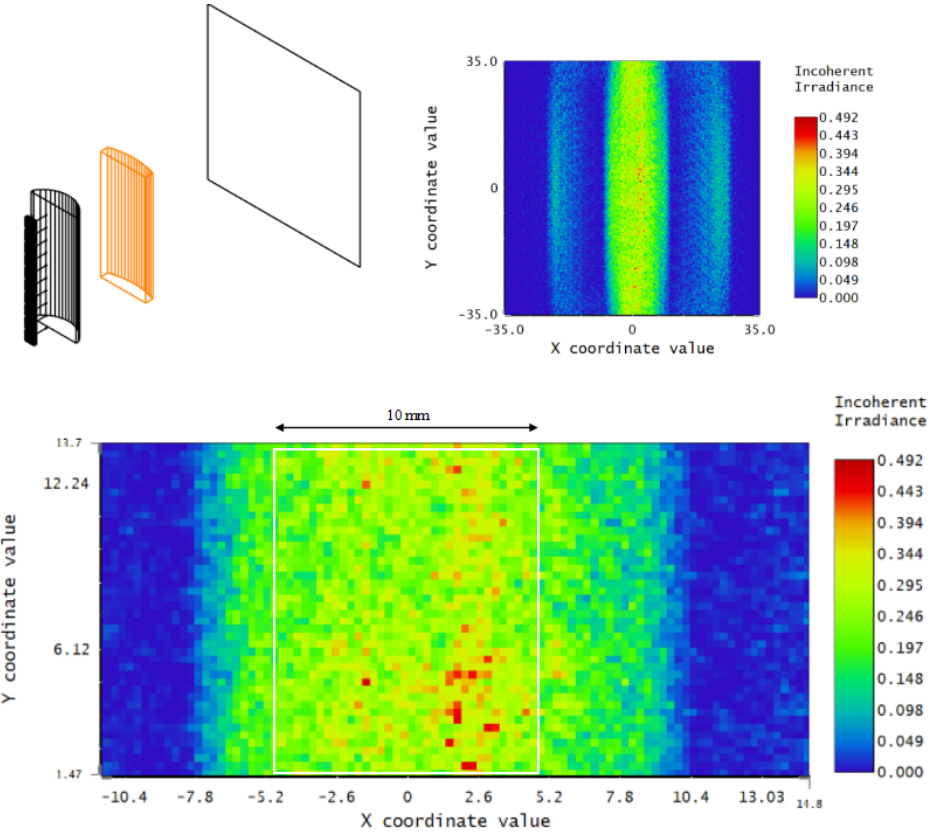


Figure 3.19: Further analysis of Version 3B

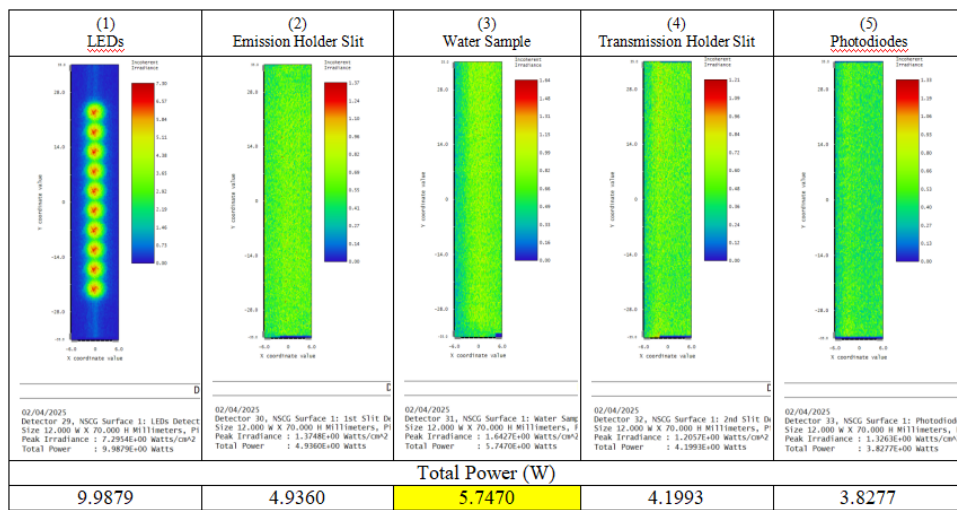


Figure 3.20: Five-position luminous flux of Version 4

It can be found that the luminous flux of the detector located at the water sample is 5.7470 W, which is the best solution among many historical versions.

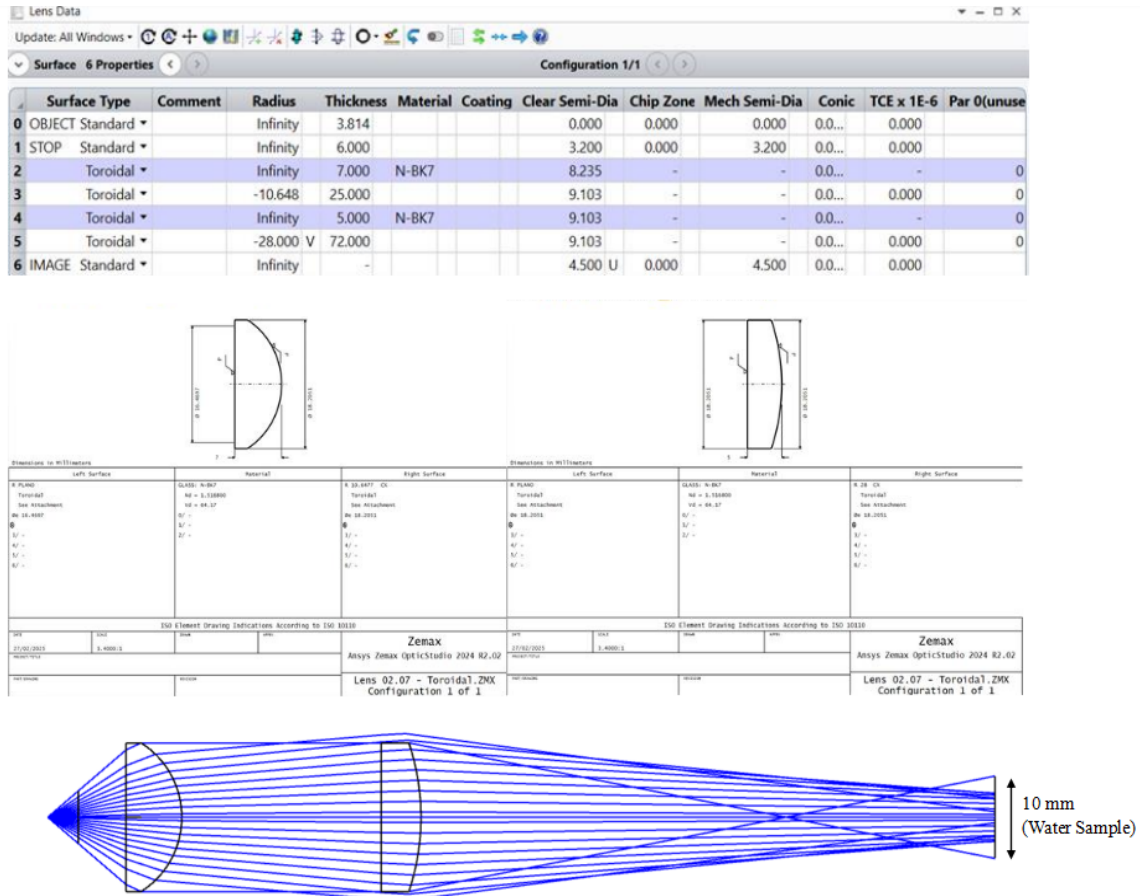


Figure 3.21: Zemax sequential mode simulation for Version 4

3.5 Design of the fluorescence detection holder

In this dissertation, we proposed the use of a rod lens at the second focal point of the elliptical reflective cavity to collimate the fluorescence light reflected from the surface after it was emitted from the UV-illuminated water sample at the first focal point.

Below Figure 3.22 is the simulation done in Zemax sequential mode, showing that fluorescence light can be channeled to the fluorescence detection holder with a rod lens placed at the second focal point, by accepting the fluorescence light that arrives at second focal point with incidence angle.

In Zemax non-sequential mode which as shown in Figure 3.23, we performed ray tracing simulation with the rod lens placed inside the reflective cavity.

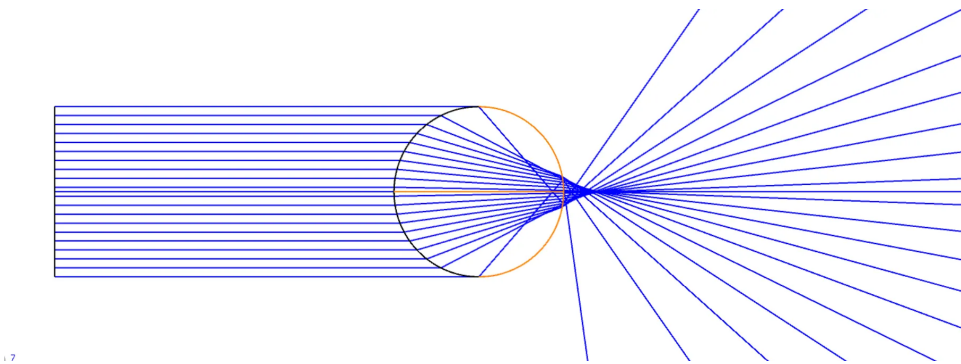


Figure 3.22: Zemax sequential mode simulation for fluorescence collimation

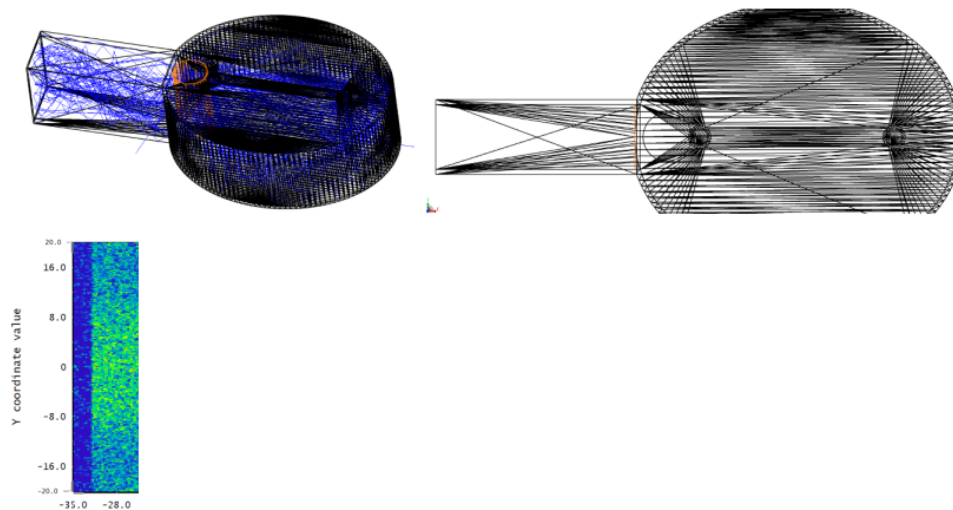


Figure 3.23: Zemax non-sequential mode simulation for fluorescence collimation

We can observe that the fluorescence light emitted from the water sample at the first focal point, is focused and collimated accordingly to pass through the central portion of the detector (dimension is equal to the cross-section of the holder – 40 mm x 70 mm).

3.6 Conclusion

This chapter focuses on the design and simulation of the optical system for low-intensity light detection and analysis platform systems. First, the optical components of the entire system are clearly introduced. Then, the optical path structure for UVA parameter detection is determined through multiple versions

of optical simulation in Zemax. The lens parameters at the emssion holder and transmission holder are specifically confirmed based on the optimization results. At the same time, a preliminary exploration of the optical path structure for FLU parameter detection is also conducted, and an improvement plan is proposed based on the simulation results.

Chapter 4

Design of signal processing and control circuits

4.1 Introduction

The topic studied in this paper is to build a measurement and control system for detecting weak fluorescence (FLU) and UV absorbance (UVA). This chapter mainly introduces the hardware circuit design. Specifically, it is divided into two parts: signal conditioning circuit design and the use of various peripheral modules of the single-chip microcomputer. We need to complete the conversion, amplification and filtering of tiny signals so that they can be converted into readable voltage signals and input into the single-chip microcomputer for subsequent software program design.

The design of the signal conditioning circuit mainly consists of three parts. The first is to design the constant current drive circuit of the LED light source, the second is to design the differential amplifier circuit for UVA detection, and finally the phase-locked amplifier circuit for weak FLU detection.

Based on the output experimental parameters of LED used as a photodetector, we design a circuit to realize the conversion of optical signals to readable electrical signals. At the same time, we will also determine the main control chip model of the system and study the modules required for data acquisition and display. According to the actual size requirements of the mechanical mechanism, the PCB size is reasonably adjusted to optimize the overall circuit layout.

Since the detector outputs a tiny current signal, the following article mainly studies the problem of amplifying the tiny current signal, thereby exploring the solution to the related circuit for processing the weak signal, and uses the simulation software Multisim to verify the rationality of the circuit design and the EDA software to produce the PCB.

4.2 Overall plan of system hardware design

The hardware part of the measurement and control system consists of a microcontroller and a series of circuits. The microcontroller needs to implement two functions. One is to output a given sinusoidal modulation signal through D/A conversion, and the other is to perform A/D conversion and data processing on the analog signal to be collected. The microcontroller will generate a sinusoidal signal through D/A conversion, and then output it to the LED of the emission holder through the PCB, thereby realizing the sinusoidal modulation of the brightness of the LED. In this process, two parameters are measured. First, when the brightness of the LED changes according to the sinusoidal law, the LED used as a detector will convert the detected light signal into a current signal output. At this time, the corresponding system UVA can be obtained by measuring and comparing the changes in the current values in the transmission holder and reference holder circuits; second, when the brightness of the LED changes according to the sinusoidal law, the FLU signal generated by the excitation of the water sample will also change sinusoidally. At this time, by measuring the voltage signal output value in the PMT module, the concentration of trace pollutants in the water body can be analyzed. The specific circuit design scheme for FLU and UVA detection is shown in Figure 4.1.

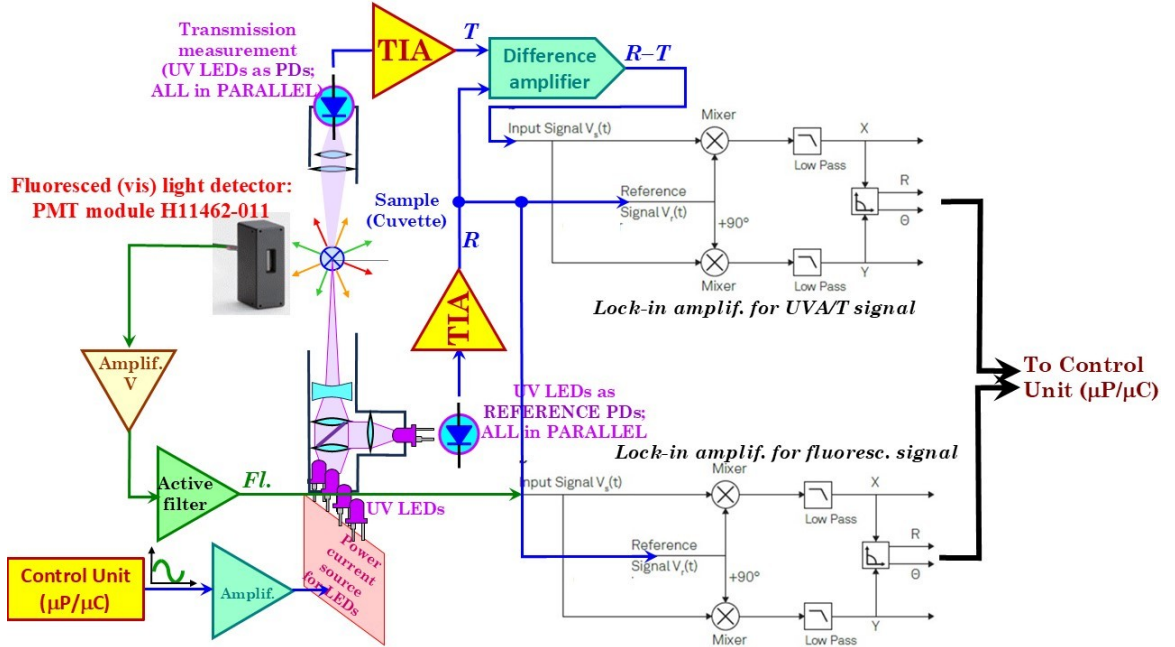


Figure 4.1: Generic simplified diagram of the circuitry for the entire system, with circuits for both the UVA/T and fluorescence (Fl.) photodetected signals

First, the MCU generates a sinusoidal modulation signal and provides it to the LED driver. The fluorescence of the water sample is stimulated to generate a corresponding sinusoidal signal response. The tiny sinusoidal current signal is detected by the PMT module, and its built-in circuit converts the current signal into a voltage signal. The LIA circuit is designed to separate the fluorescence signal from a large amount of background light noise, and then the gain-adjustable amplifier circuit and low-pass filter circuit are designed to achieve distortion-free signal extraction. At the same time, the LED used as a detector in the transmission holder and reference holder will generate two weak current signals. The TIA circuit is designed to convert the tiny current signal into a 0-0.5 V voltage signal. Then, the gain-adjustable amplifier circuit and low-pass filter circuit are used to complete the signal conditioning as needed. After that, the two signals are input into the differential amplifier circuit to convert them into voltage signals readable by the MCU for subsequent data collection and analysis. Finally, the three voltage signals are converted into digital signals through A/D conversion, and data analysis methods are used to process the data through a microcontroller. Bluetooth communication is then achieved

between the MCU and the host computer. Finally, the digital signals are converted into concentration parameters of UVA and trace pollutants and displayed on the host computer to achieve real-time measurement.

4.3 Microcontroller module

The control unit of this system selects ESP32-WROOM-32D as the microcontroller of the system. The peripheral circuit of the chip is mainly composed of crystal oscillator circuit, reset circuit, a debug interface circuit and other circuits. It is designed for more complex IoT development projects. It has a built-in powerful general Wi-Fi+BT+BLE MCU module, which is suitable for low-power detection and compact design scenarios, and can achieve wireless transparent transmission without an external antenna. Therefore, this system plans to choose ESP32 as the main control of the entire system, which can easily perform real-time measurement and data upload. The ESP32 microcontroller diagram is shown in Figure 4.2.



Figure 4.2: ESP32-WROOM-32D

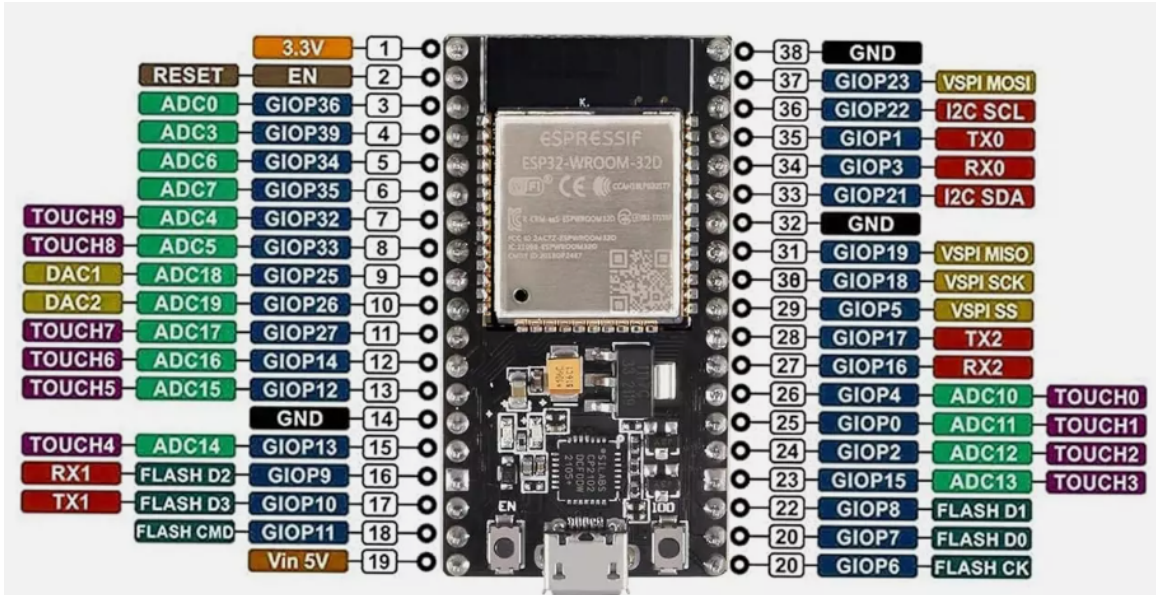


Figure 4.3: ESP32 Pin Function Diagram

The development environment of ESP32-WROOM-32D is compatible with Arduino and MicroPython ecosystems, with a main frequency of up to 240 MHz and rich GPIO resources [32]. It can be seen that it has a built-in DAC output pin and can communicate well with IIC devices. Its deep sleep current is very small, which is suitable for battery-powered scenarios. Through the simple development of Bluetooth app, a closed-loop real-time measurement system can be realized. The specific pin function diagram of ESP32 is shown in Figure 4.3.

This dissertation plans to develop ESP32 based on the Arduino environment to enable it to complete two basic functions: sine wave generation and data acquisition and display.

4.4 Signal conditioning circuits

4.4.1 LED constant current drive circuit design and simulation

In this dissertation, the purpose of the study is to use the LED model shown in Figure 4.4 as the light source of the entire system. OSRAM LZ1-00UBN0 is a high-power UV LED launched by ams-OSRAM AG [33]. It

adopts ceramic packaging and integrated glass lens design, which is optimized for harsh industrial environments and high-performance application scenarios. Its core features include high radiation efficiency, wide temperature adaptability and long life, and it is suitable for light curing, industrial sensing, horticultural lighting and medical phototherapy. In terms of technical parameters, the peak wavelength λ_{peak} is 395 nm (belonging to purple light), the viewing angle is 70 degrees, the maximum forward current is 700 mA, and the typical total radiation flux is 1450 mW (under conditions of 700 mA), which is very suitable for the use scenario of this project. In addition, its package design is suitable for high temperature environment, with a maximum junction temperature and high heat dissipation performance. At the same time, the LED can also be used as a photodetector. After experimental testing, the photocurrent value it generates is about 0.1 μ A.

EUM-075S105Dx is a 75 W constant-current programmable LED driver launched by Inventronics, designed for industrial and commercial lighting applications, shown in Figure 4.4. Its core features include a wide input voltage range (90–305 VAC/127–300 VDC), high energy efficiency, and IP66/IP67 protection level, suitable for harsh environments [34]. It has a very reliable protection mechanism, including overtemperature protection, short circuit protection, and surge protection.



Figure 4.4: (a) LZ1-00UBN0 LED, and (b) the LED driver EUM-075S105Dx

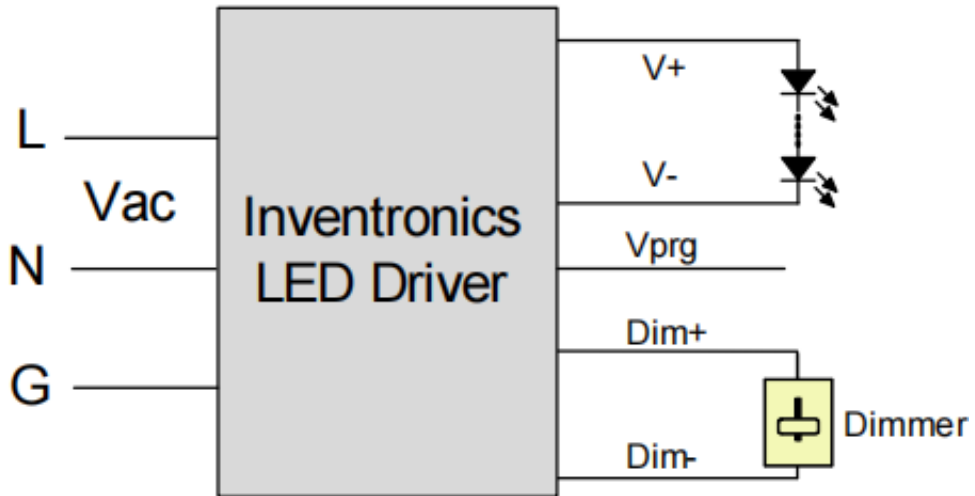


Figure 4.5: Dimming circuit implementation

It has a dimming function and can support three different dimming modes: analog dimming 1–5 V, analog dimming 1–10 V, and PWM dimming. The circuit diagram of analog dimming is shown in Figure 4.5. Therefore, we plan to generate a sinusoidal modulation signal within the input range through ESP32 and input it into the LED driver to achieve sinusoidal modulation of the LED brightness.

ESP32 has two DAC channels (GPIO 25 and GPIO 26) that can output analog voltages of 0-3.3 V. However, the resolution of the DAC is 8 bits [32], which may limit the accuracy of the waveform. However, the application scenario of this system belongs to a low-frequency scenario, and the required frequency of 241 Hz is not high, so the DAC should be able to handle it. The programming idea is not complicated. First, configure the DAC channel, then pre-calculate the sampling points of the sine wave and store them in an array, then set the timer interrupt, and output these points through the DAC loop. After that, connect the DAC output to the first-order RC low-pass filter circuit to filter out high-frequency noise and reduce errors.

After realizing the generation of 0-3.3 V sinusoidal analog voltage, we need to consider the input range of the dimming signal of the LED driver. We noticed that 1 V corresponds to the output relationship of dimming brightness of 0, so it is necessary to bias the sinusoidal analog voltage and realize

the subsequent gain-adjustable amplification, so that the amplitude range of the modified sinusoidal voltage varies within 1-10 V, which is convenient for subsequent experimental test adjustments.

Multisim is used to design and simulate the voltage bias and follower amplifier circuit. The design principle is as follows: This project uses the addition circuit of the operational amplifier to achieve voltage boost. Unlike using the bias voltage directly, this method has better simulation effect. First, set the input signal parameters (amplitude is 2.4 V, bias is 1.7 V), add the 3.3 V bias voltage to the circuit through an inverting addition circuit with a gain of -1, and then use a variable gain low-pass amplifier circuit to amplify the amplitude of our signal. Finally, add a voltage follower as a buffer to avoid signal attenuation and eliminate the load effect. However, in the actual circuit, there will be some input and stray capacitance values on the input pins of the amplifier, which will cause ringing oscillation and output drift, making the entire amplifier circuit unstable.

To overcome this problem, two passive components are required instead of single components such as resistors and capacitors to make the transimpedance circuit work properly. These two components are simply connected in parallel between the in-phase terminal and the output of the amplifier. This project filters out the high-frequency noise of the power supply by connecting a small-capacitance coupling capacitor in parallel to the power supply pin of the amplifier. This design has also been considered in other circuits in the future and will not be described in detail. The specific simulation circuit diagram is shown in Figure 4.6.

The input and output waveforms of the circuit can be observed intuitively using the oscilloscope function of Multisim. Figure 4.7 shows the input signal waveform, and Figure 4.6 shows the output signal waveform. By adjusting the value of the potentiometer R_3 , the voltage bias can be achieved while achieving amplification with different amplitude gains.

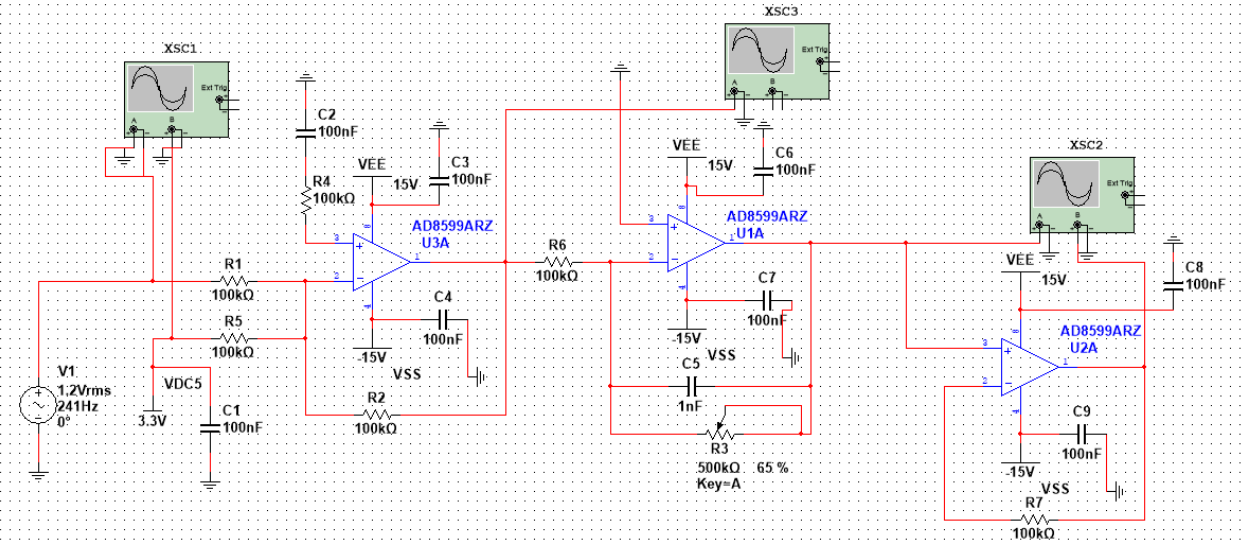


Figure 4.6: Voltage bias and amplifier follower circuit

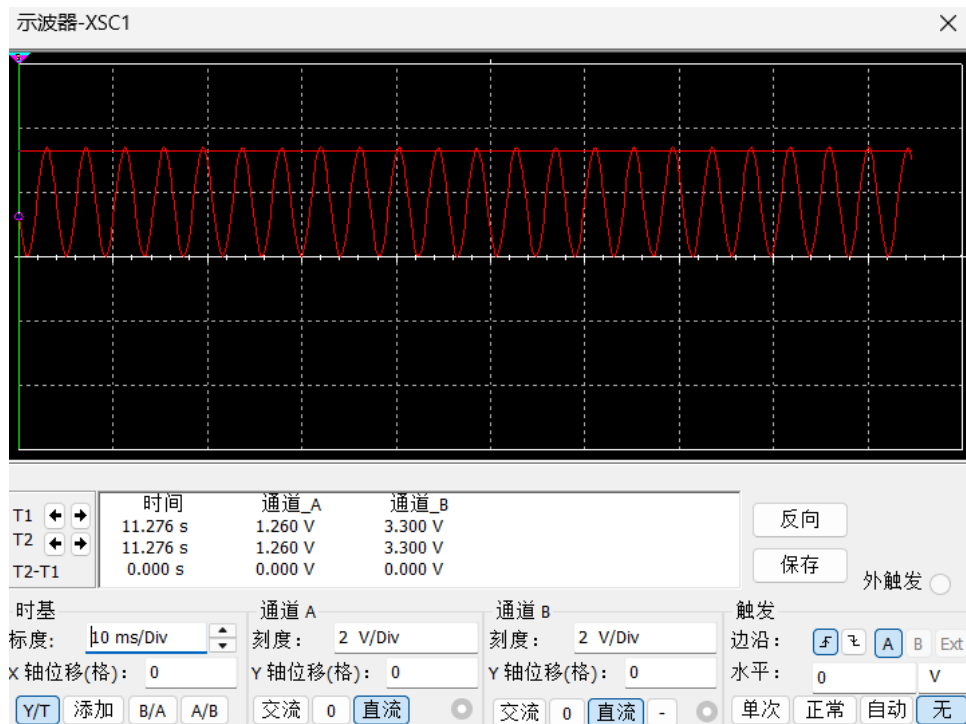


Figure 4.7: Voltage bias and amplifier follower circuit input

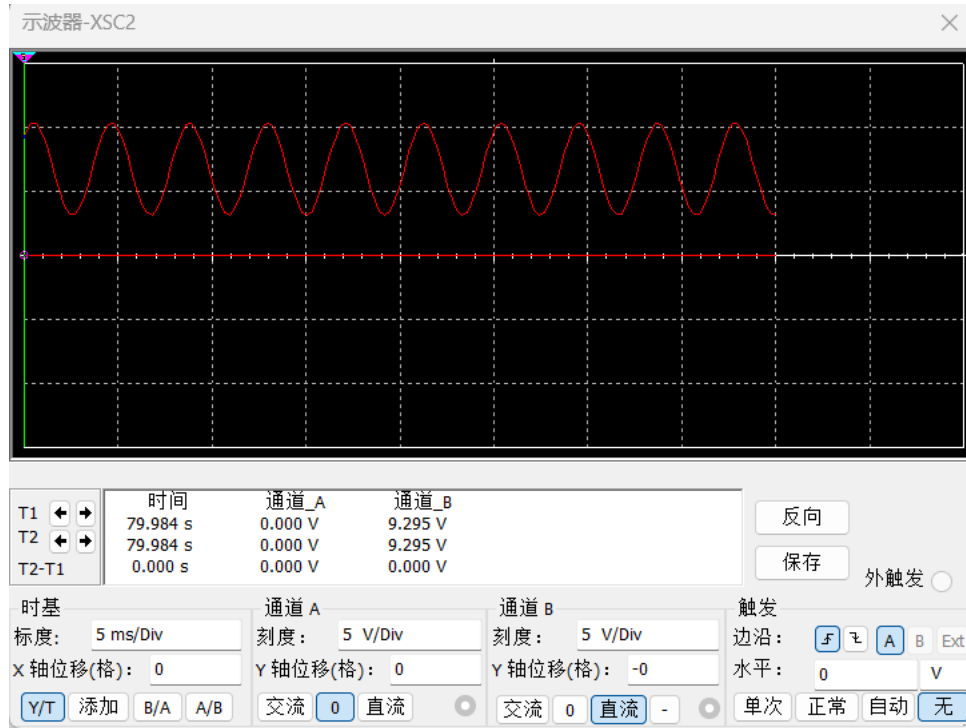


Figure 4.8: Voltage bias and amplifier follower circuit output

4.4.2 TIA circuit design and simulation

TIA, amplifies the current with a set gain into a voltage. The function of the transimpedance amplifier is to convert and amplify the input current signal into a voltage signal. The transimpedance amplifier circuit is actually a very simple inverting amplifier, including negative feedback. The specific schematic diagram is shown in Figure 4.9.

According to the experimental parameters of the LED above, the photocurrent value generated by a single LED as a photodetector is about $0.1\mu A$. This dissertation plans to deliver the photocurrent generated by ten LEDs to a single TIA circuit, so the actual maximum input current of the TIA circuit is about $1\mu A$. Therefore, the design requirements of the target parameter for the circuit in Table 4.1 below can be sorted out, and the specific calculation steps will be introduced below.

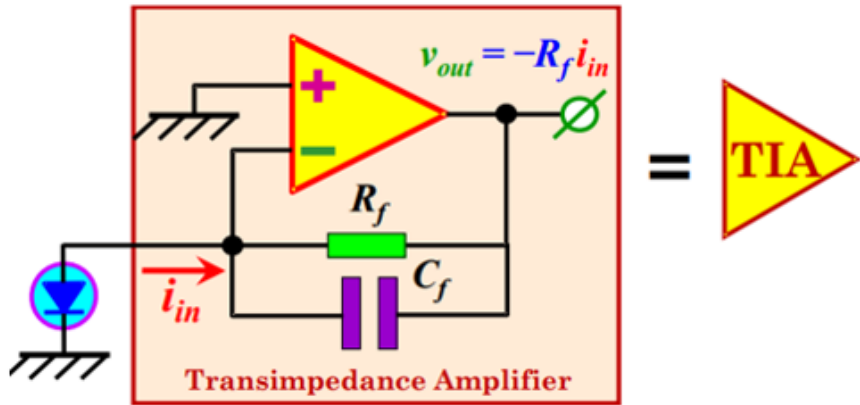


Figure 4.9: TIA Schematic diagram

Table 4.1: Circuit design target parameters

Input Current(μA)	Output Voltage(V)	Bandwidth(kHz)
0–1	0–0.5	3

The specific calculation steps are as follows:

1. Select the gain resistor:

$$R_f = \frac{V_{o\max} - V_{o\min}}{I_{imax}} = \frac{0.5V - 0V}{1\mu A} = 500k\Omega \quad (4.1)$$

2. Select the feedback capacitor that meets the circuit bandwidth requirements:

$$C_1 \leq \frac{1}{2\pi R_f f_p} \leq \frac{1}{2\pi \times 500k\Omega \times 3\text{kHz}} \leq 106.103\text{ pF} \approx 100\text{ pF} \quad (4.2)$$

3. Calculate the op amp bandwidth(GBW) required to keep the circuit stable:

$$\text{GBW} > \frac{C_l + C_i}{2\pi R_1 C_1^2} > \frac{200\text{ pF} + 100\text{ pF}}{2 \times \pi \times 500k\Omega \times (100\text{ pF})^2} > 9.55\text{ kHz} \quad (4.3)$$

$$C_i = C_s + C_d + C_{cm} = 0\text{ pF} + 100\text{ pF} + 100\text{ pF} = 200\text{ pF} \quad (4.4)$$

Where: C_i : Input source capacitance; C_d : Differential input capacitance of the amplifier; C_{cm} : Common-mode input capacitance of the inverting input.

According to the bandwidth requirements of the operational amplifier, AD8599 is selected as the operational amplifier of the transimpedance amplifier. AD8599 is a high-performance dual-channel operational amplifier launched by Analog Devices, designed for low-noise and low-distortion applications [35]. The GBW of AD8599 is 10 MHz, which meets the design index requirements. As a low-noise operational amplifier, AD8599 has ultra-low noise performance and is very suitable for the application scenarios of precision measurement systems.

The design method of the preamplifier is shown in Figure 4.10. The reason for choosing this solution is that the photocurrent value output by each detector is different. If it is connected in series, only the weakest current value among the ten LEDs will be output, which undoubtedly increases the difficulty of extracting the signal. Therefore, using parallel connection can avoid this situation. The photocurrent value generated by each LED detector is different and does not affect each other, which can maximize the signal extraction efficiency. At the same time, the current values of multiple LEDs are transmitted to the same amplifier, which can effectively save actual costs, reduce the actual size of the PCB, and optimize heat dissipation.

This dissertation requires placing photodetectors consisting of 10 LEDs at the transmission holder and reference holder, respectively. The transmission holder has a row of 10 photodetectors, while the reference holder has two rows of 5 photodetectors. The reason for this design is that the optical paths in the emission holder and the transmission holder are similar to mirror structures, so the one-row LED layout at the transmission holder can achieve the maximum light signal collection efficiency, while the two-row LED layout at the reference holder can increase the effective light detection area, also in order to detect as many light signals as possible.

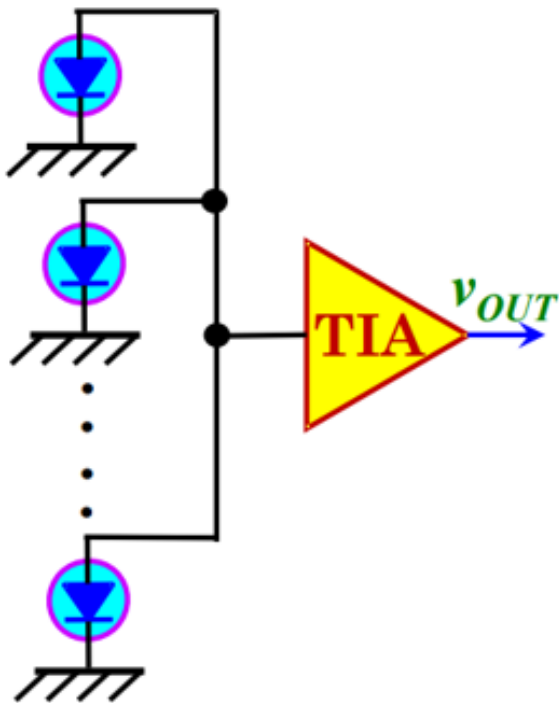


Figure 4.10: Preamplifier method

In this project, Multisim software is used to complete the design and simulation of the two-part TIA circuit at the transmission holder and the reference holder as shown in Figure 4.11.

Set the input at the transmission holder to $0.7 \mu\text{A}$ and the input at the reference holder to $0.3 \mu\text{A}$. After passing through the TIA circuit, the output waveform is shown in Figure 4.12. After that, the two signals will pass through the adjustable gain inverting amplifier circuit and low-pass filter circuit. Set the gain adjustment range to 1-5 and the cutoff frequency of the low-pass filter to 1 kHz . The output waveform is shown in Figure 4.13.

The reason for adding the design of an adjustable gain circuit is mainly because we are uncertain about how much current the detector can generate during actual experiments. In this way, through the potentiometer in the designed adjustable gain circuit, we can appropriately amplify or reduce the detection current value, thereby avoiding the subsequent modification of circuit component values and redrawing of the PCB.

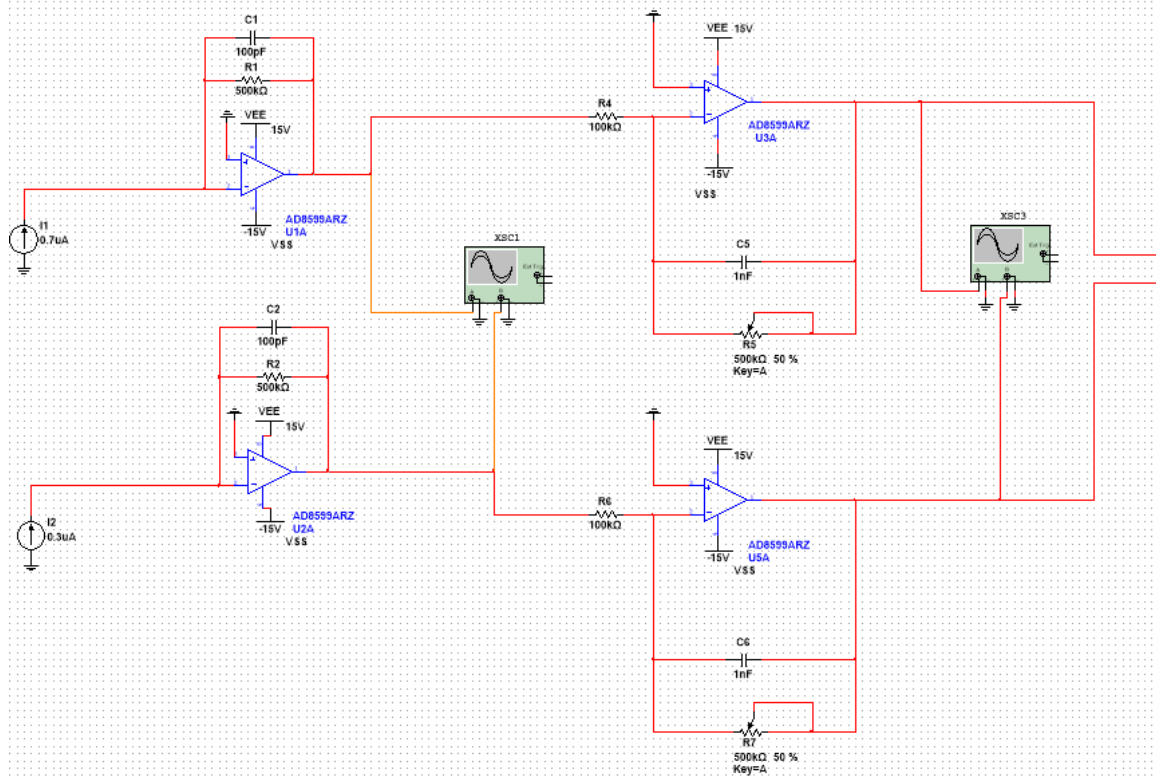


Figure 4.11: Application of the TIA with the photodetectors used in our system

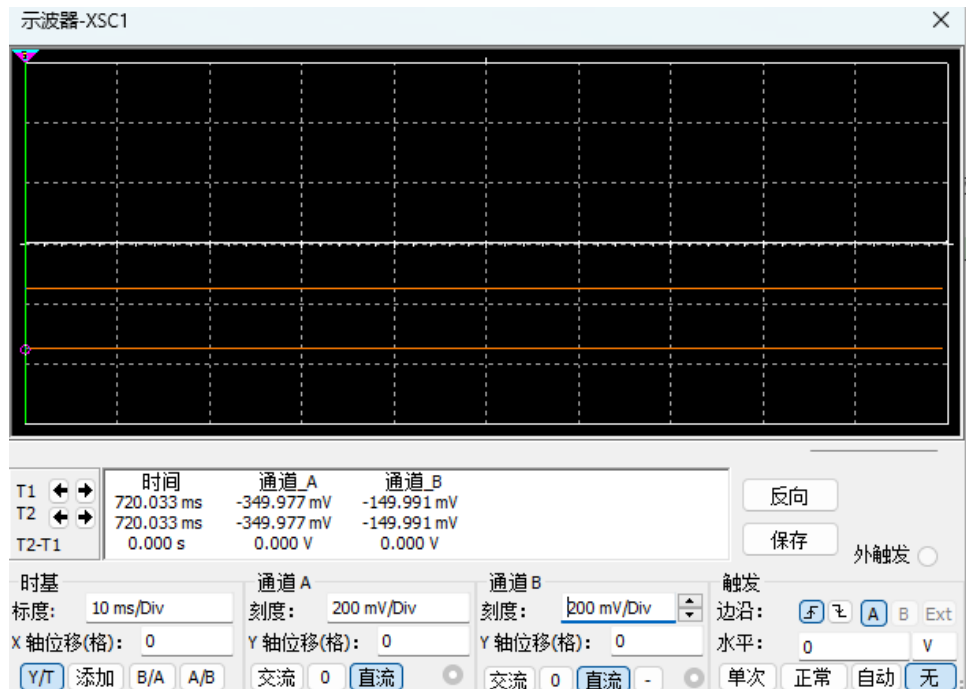


Figure 4.12: Transmission and reference TIA output

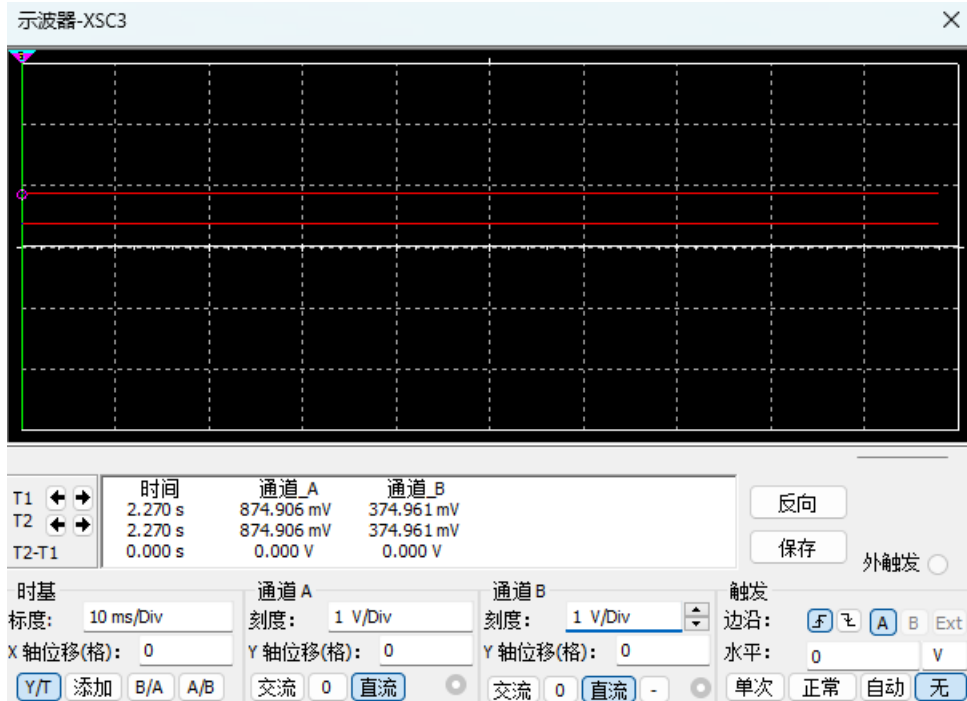


Figure 4.13: Variable gain amplification and low pass filter output

4.4.3 Differential amplifier circuit design and simulation

INA114 is a high-precision instrumentation amplifier launched by Texas Instruments, designed for low noise, high common-mode rejection and wide dynamic range applications [31]. INA114 has very low input bias voltage and temperature drift, and can achieve flexible gain adjustment through a single resistor R_G , which is very suitable for high-resolution data acquisition system applications. The Multisim simulation schematic is shown in Figure 4.14. The two signals at the transmission holder and reference holder are input into the differential amplifier after passing through the TIA circuit, the variable gain amplifier and the low-pass filter. The output waveform result is shown in Figure 4.15.

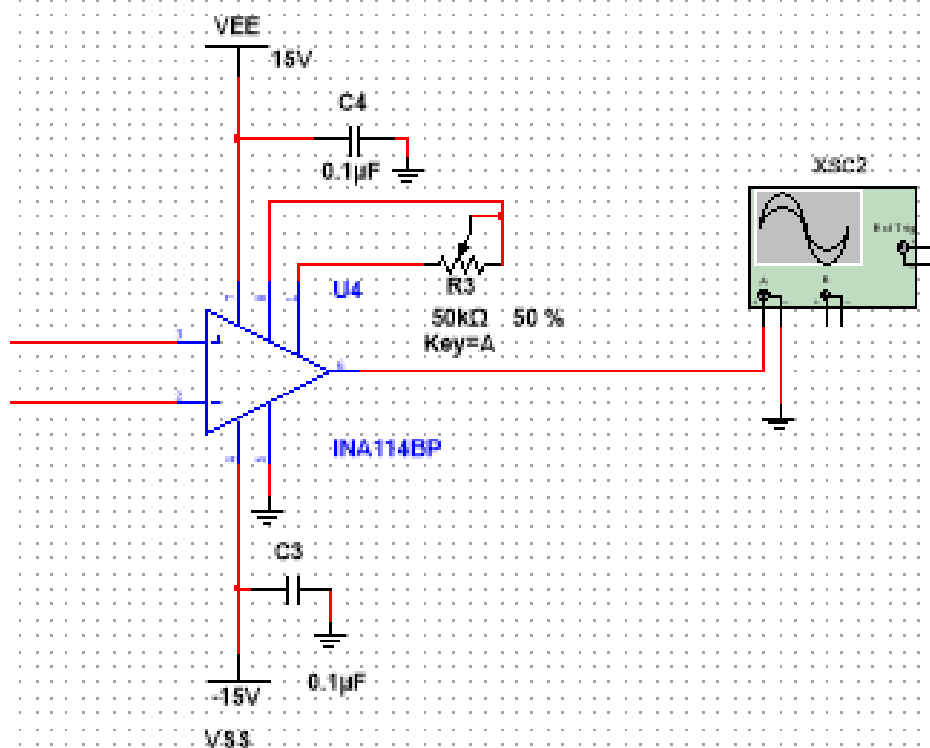


Figure 4.14: Differential amplifier

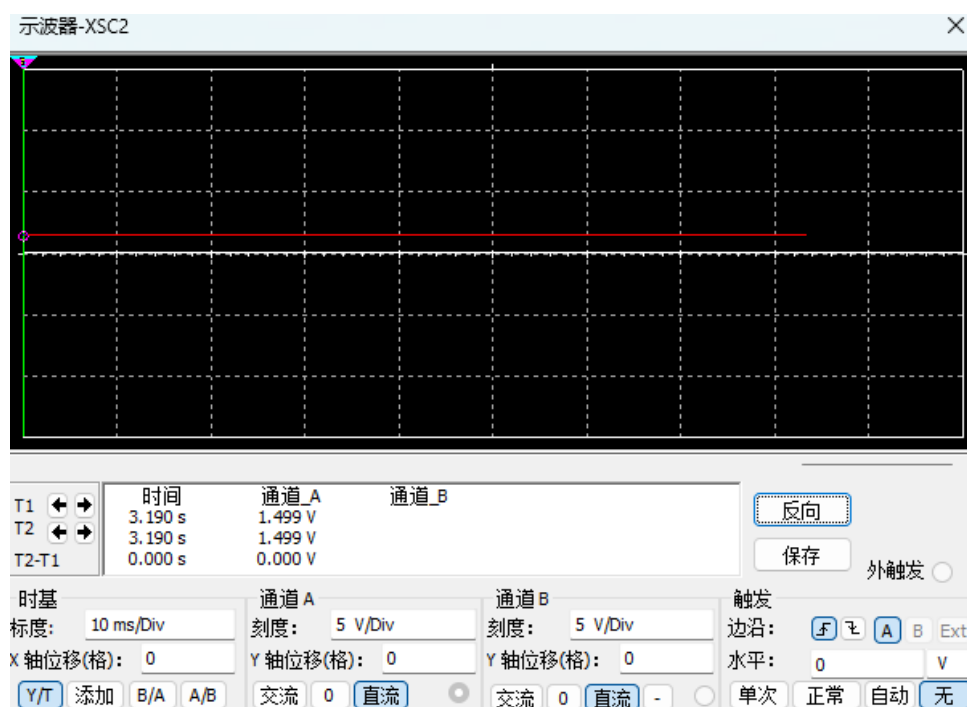


Figure 4.15: Differential amplifier result

4.4.4 LIA circuit design and simulation

The detector used in this dissertation at the PMT holder is the H11462-011 module shown in Figure 4.16. The H11462 series is an integrated photomultiplier tube module launched by Hamamatsu Photonics [36]. It combines a side window photomultiplier tube (PMT), a high voltage power supply circuit, and a low noise amplifier, and is designed for weak light signal detection. The module's built-in amplifier provides $1 \text{ V}/\mu\text{A}$ (bandwidth DC to 20 kHz) or $0.1 \text{ V}/\mu\text{A}$ (bandwidth DC to 200 kHz), which supports high-speed or high-resolution signal conditioning. Since the module can directly output voltage signals, we no longer need to design a TIA circuit to achieve current signal conversion.

This project plans to use the LIA circuit to detect weak fluorescence signals. LIA is a precision instrument that extracts weak signals from a strong noise background through synchronous demodulation technology. Its core structure usually includes the following modules: First, the input signal channel, where we directly connect the output voltage signal from the PMT module. The second is the reference signal channel.



Figure 4.16: H11462-011 module

Here we use a sinusoidal signal input with the same frequency and phase as the modulated LED. Here, we may need to perform experimental tests to adjust the reference signal phase so that it aligns with the input signal phase to maximize the demodulation efficiency. The most important part is the phase-sensitive detector. The core module of this project is AD630 as a balanced demodulator, which multiplies the input signal with the reference signal to achieve phase-sensitive detection of frequency domain signals. Finally, a gain-variable amplifier and a low-pass filter are required to output the high-frequency noise after demodulation, retain the DC or low-frequency signal components, and output a voltage proportional to the amplitude of the target signal.

AD630 is a high-precision balanced modulator/demodulator launched by Analog Devices, designed for applications requiring high dynamic range, low noise, and fast switching [37]. AD630 plays a very critical role in LIA. By synchronously demodulating the input signal and the reference signal, suppressing asynchronous noise, and extracting the target frequency component, it is very suitable for weak signal detection applications.

The simulation of the LIA circuit using Multisim is shown in Figure 4.17. The working power supply used in AD630 simulation is positive and negative power supply, positive and negative 15 V.

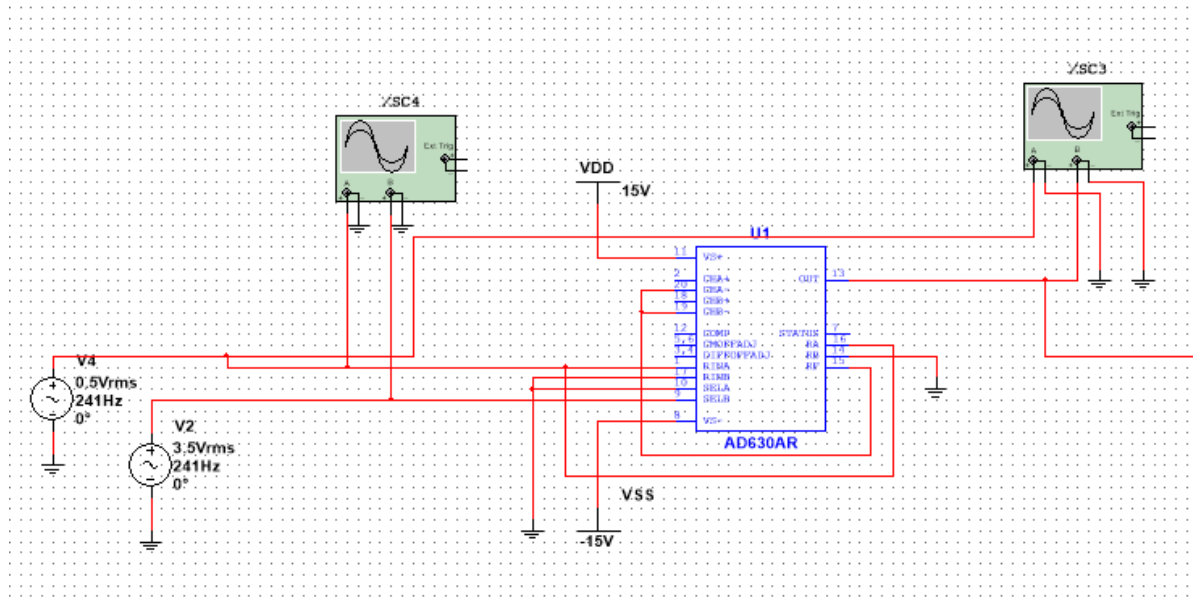


Figure 4.17: Lock-in amplifier

Set the input signal channel voltage RMS value to 0.5 V, voltage offset 2 V, and frequency 1 kHz; set the reference signal channel voltage RMS value to 3.5 V, voltage offset 5 V, and frequency 1 kHz.

The input signal waveform diagram is shown in Figure 4.18. The output waveform diagram obtained after the synchronous demodulation by AD630 is shown in Figure 4.19.

Input the waveform signal from AD630 into the gain variable amplifier and low-pass filter, set the cutoff frequency to 1 kHz, the simulation schematic diagram is shown in Figure 4.20, and the final output waveform result is shown in Figure 4.21. The output signal can be collected directly by the ADC module.

Through simulation, it is not difficult to find that the AD630 does play the role of synchronous demodulation. At the same time, due to the design of the low-pass filter, the signal below 1 kHz can pass without distortion, so the signal waveform output at the end of the circuit is still a sine wave. Here, due to the lack of experimental data, the design of the variable gain circuit also needs to be considered. By adjusting the potentiometer, we can meet the readable voltage range requirements of the ADC module.

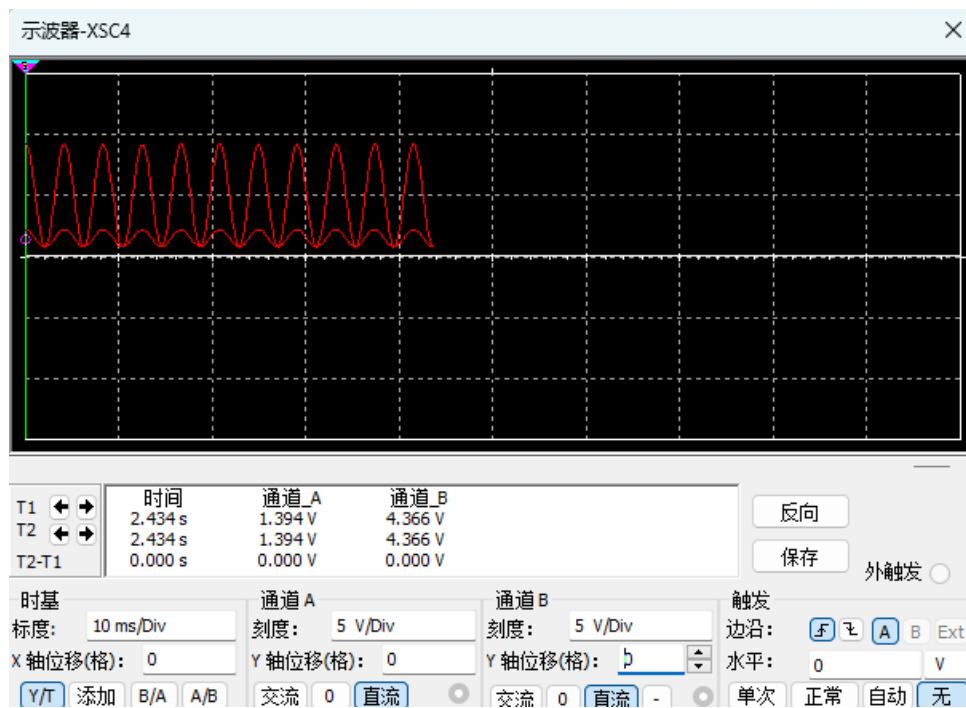


Figure 4.18: Lock-in amplifier input

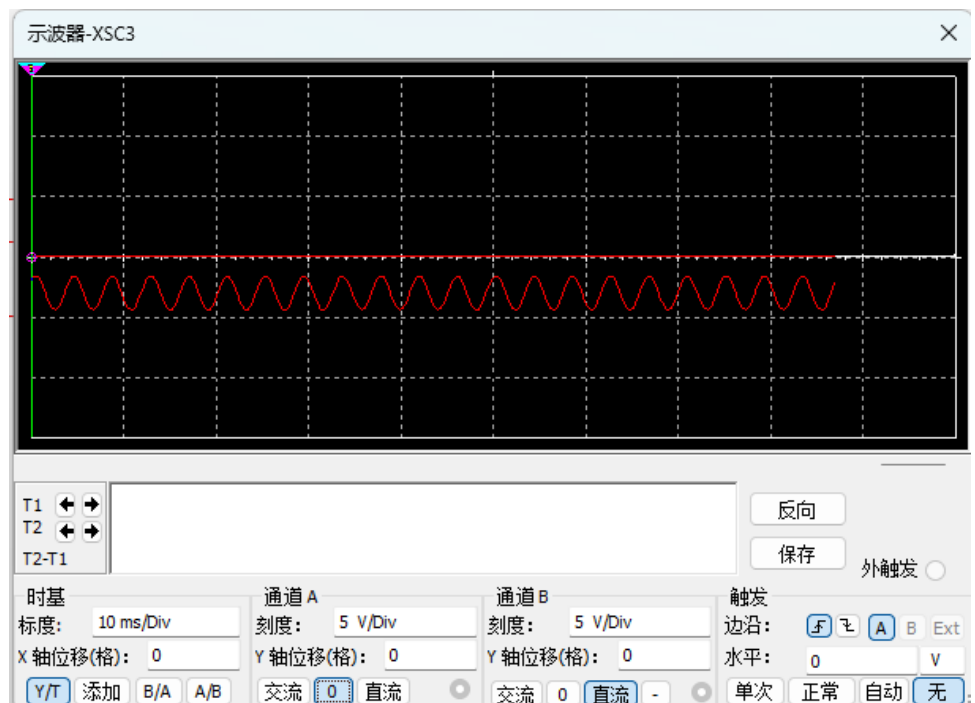


Figure 4.19: Lock-in amplifier output

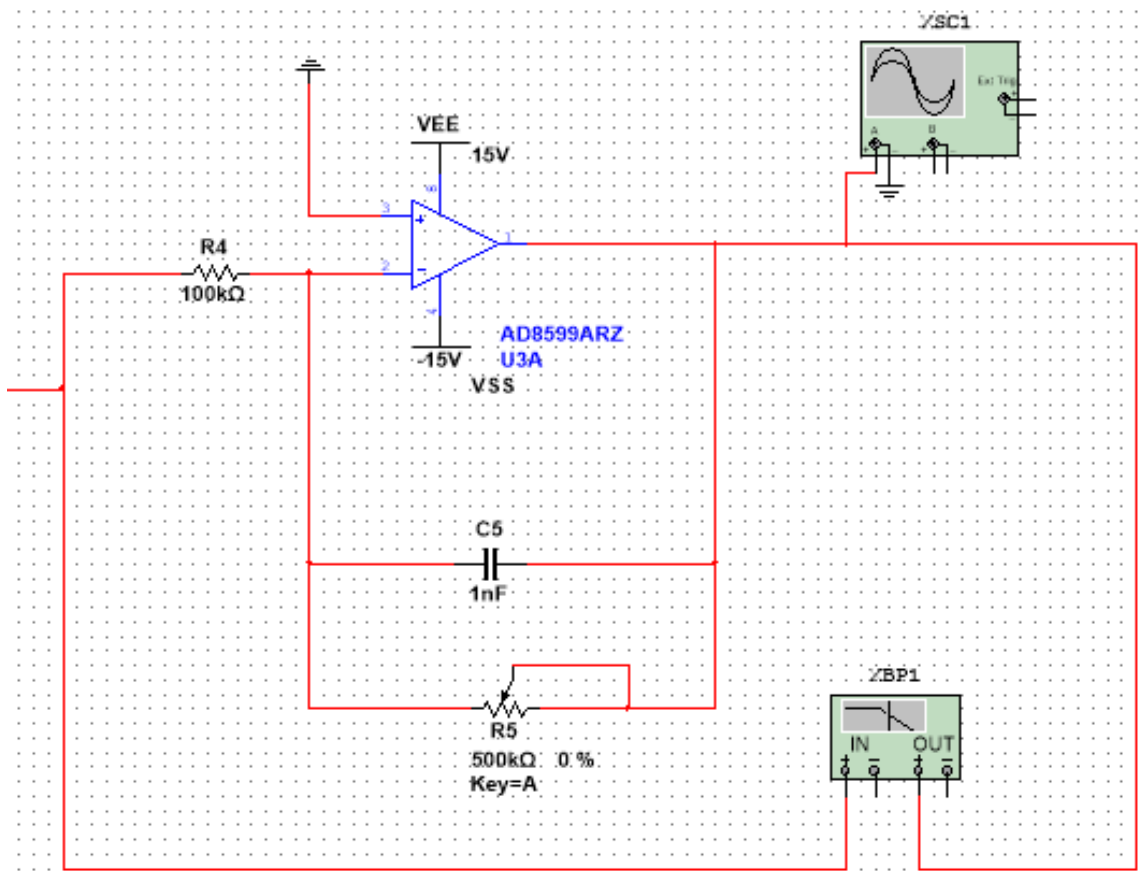


Figure 4.20: Low-pass filter

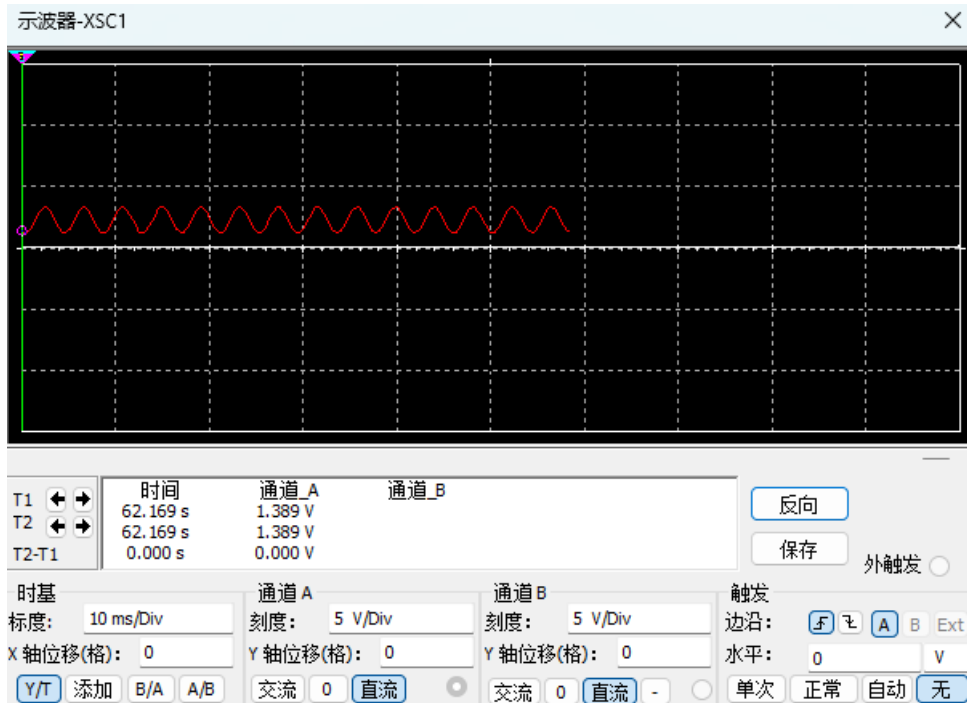


Figure 4.21: Low-pass filter output

4.5 MCU peripheral module usage

In addition to the design of the signal conditioning circuit described above, the MCU also needs to use various peripheral modules to complete the subsequent data collection and analysis work, including the ADS1115 module and the OLED display module. The framework diagram of each specific peripheral module is shown in Figure 4.22.

Among them, the ADS1115 module is used to collect the voltage signals of the three-way detectors and communicate with ESP32 through IIC; the OLED LCD screen displays the collected voltage data through the IIC protocol, and the voltage data is synchronously displayed on the mobile phone web interface through the built-in Bluetooth and WIFI modules of ESP32 in the form of waveform recording.

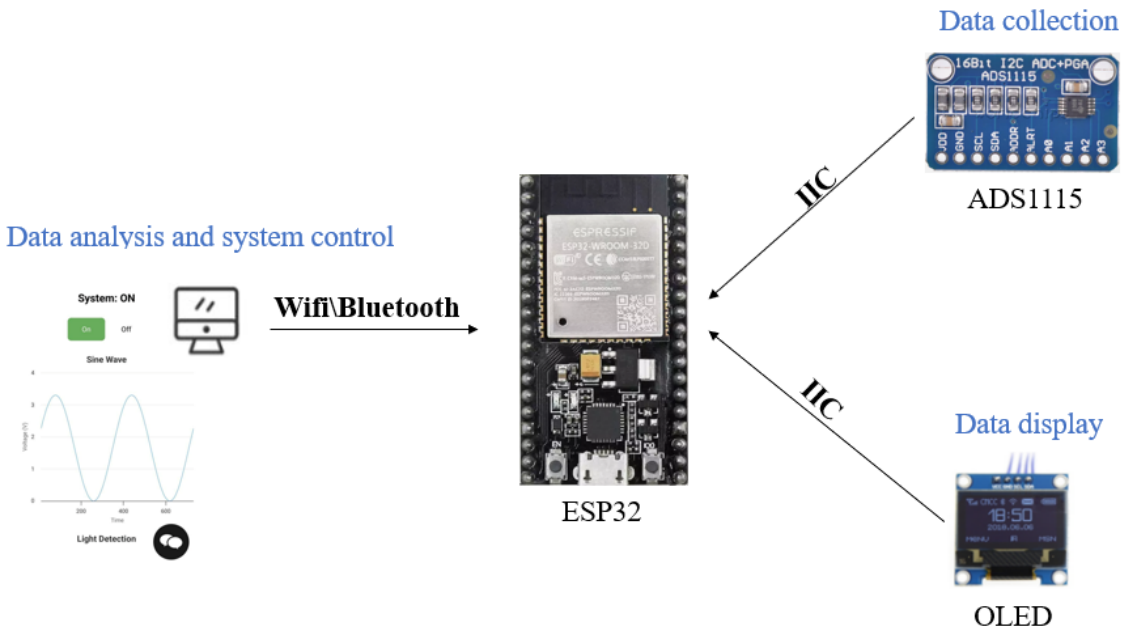


Figure 4.22: Framework diagram of each module of the microcontroller

4.6 Circuit schematic and PCB drawing

After verifying the simulation results of the designed circuit using Multisim software, the circuit schematics and PCBs of each part drawn using EDA software will be shown one by one below.

When using EDA software to draw PCB, we first need to create a project and enter the schematic editor. We can call the built-in component library or self-built package library. After completing the component placement and line connection, perform an electrical rule check (ERC) to ensure that there are no flying wires. Then enter the PCB design stage. First, draw a closed frame that matches the actual structure on the mechanical layer. Prioritize the installation of related components and layout according to functional modules. Place high-frequency components close to the corresponding circuits, sensitive analog signals and digital signals to optimize signal integrity.

The schematic of the light-emitting circuit and the PCB diagram located in the emission holder are shown in Figure 4.23. The function of this PCB is to place the LED light source.

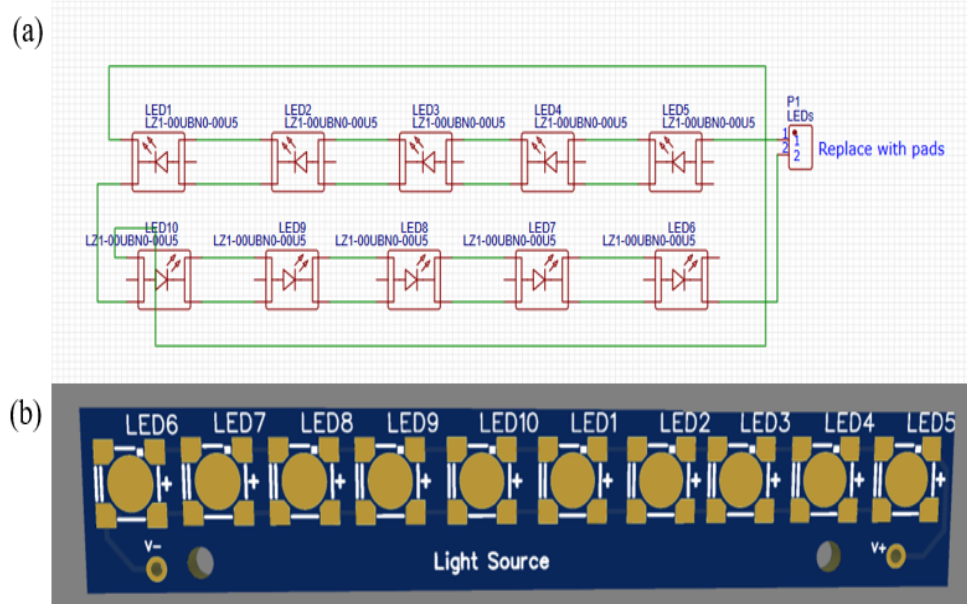


Figure 4.23: Light source ((a)circuit schematic; (b)PCB)

The schematic of the LED detector circuit and the PCB diagram located in the reference holder are shown in Figure 4.24. The function of this PCB is to place the LED detector in the reference holder.

The schematic of the LED detector circuit and the PCB diagram located in the transmission holder are shown in Figure 4.25. The function of this PCB is to place the LED detector in the transmission holder.

The TIA circuit schematic and the PCB diagram used at the reference holder are shown in Figure 4.26. The function of this PCB is to convert the current signal generated by the LED detector at the reference holder into a voltage signal.

The TIA circuit schematic and the PCB diagram used at the transmission holder are shown in Figure 4.27. The function of this PCB is to convert the current signal generated by the LED detector at the transmission holder into a voltage signal.

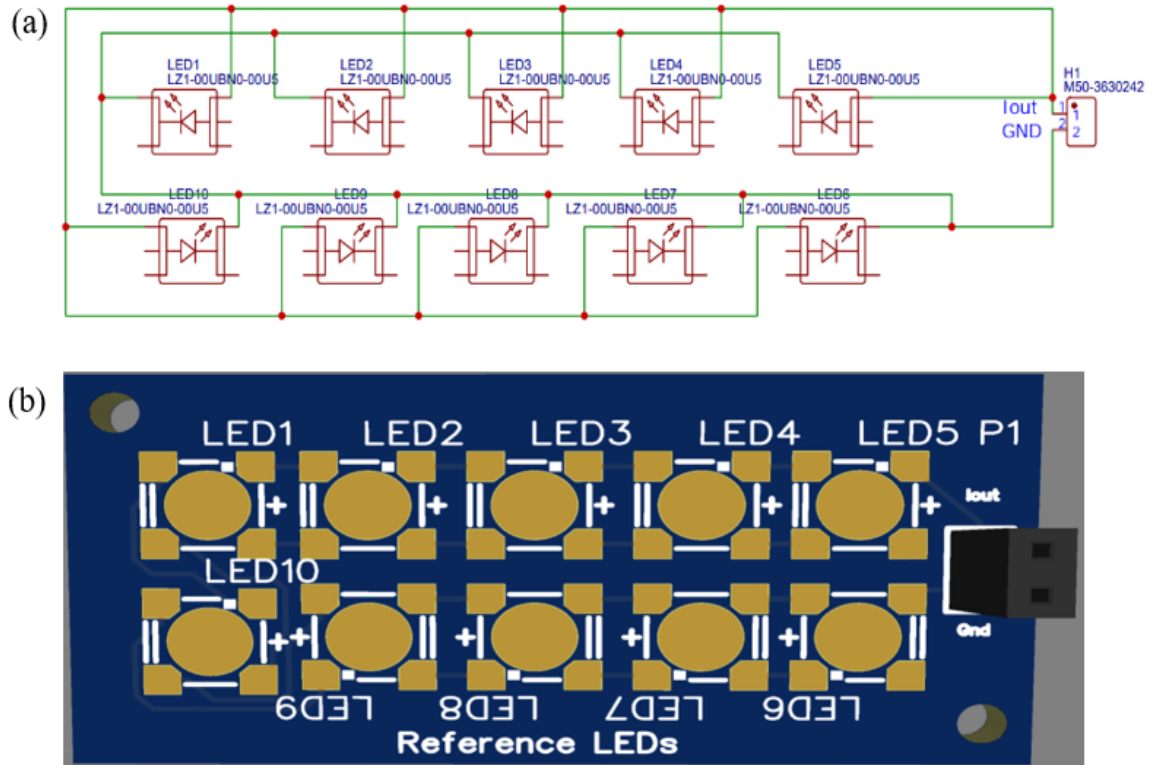


Figure 4.24: Reference holder LEDs((a)circuit schematic; (b)PCB)

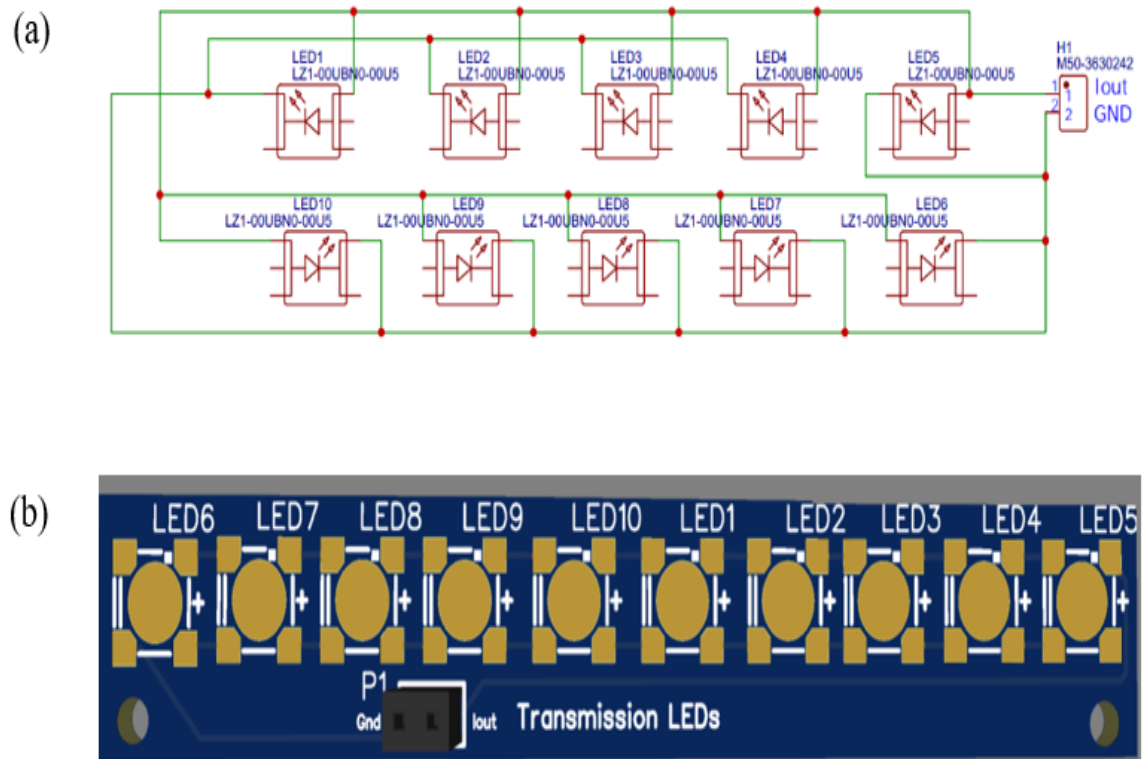


Figure 4.25: Transmission holder LEDs((a)circuit schematic; (b)PCB)

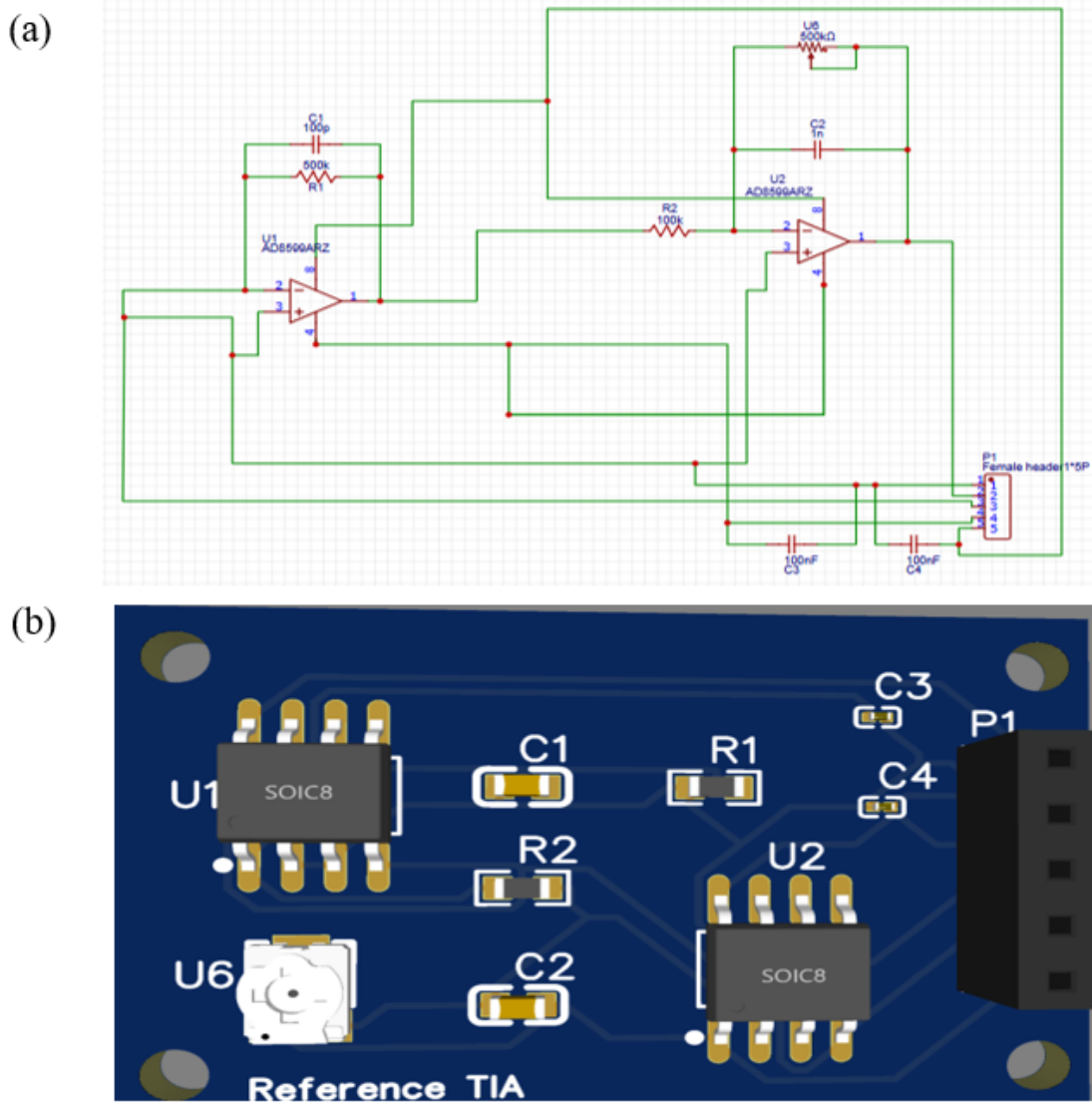


Figure 4.26: Reference TIA((a)circuit schematic; (b)PCB)

The circuit schematic and the PCB diagram for differential amplification are shown in Figure 4.28. The function of this PCB is to amplify and measure the signal difference between the photodetector at the reference holder and the transmission holder.

The LIA circuit schematic and the PCB diagram used at the PMT holder are shown in Figure 4.29. The function of this PCB is to extract weak light signals from a large amount of background light noise through the method of locked-in amplification.

The circuit schematic and the PCB diagram for adjusting the amplitude of the sine wave are shown in Figure 4.30. The function of this PCB is to transform the amplitude of the sinusoidal signal generated by the MCU to meet the input requirements of constant current source analog dimming.

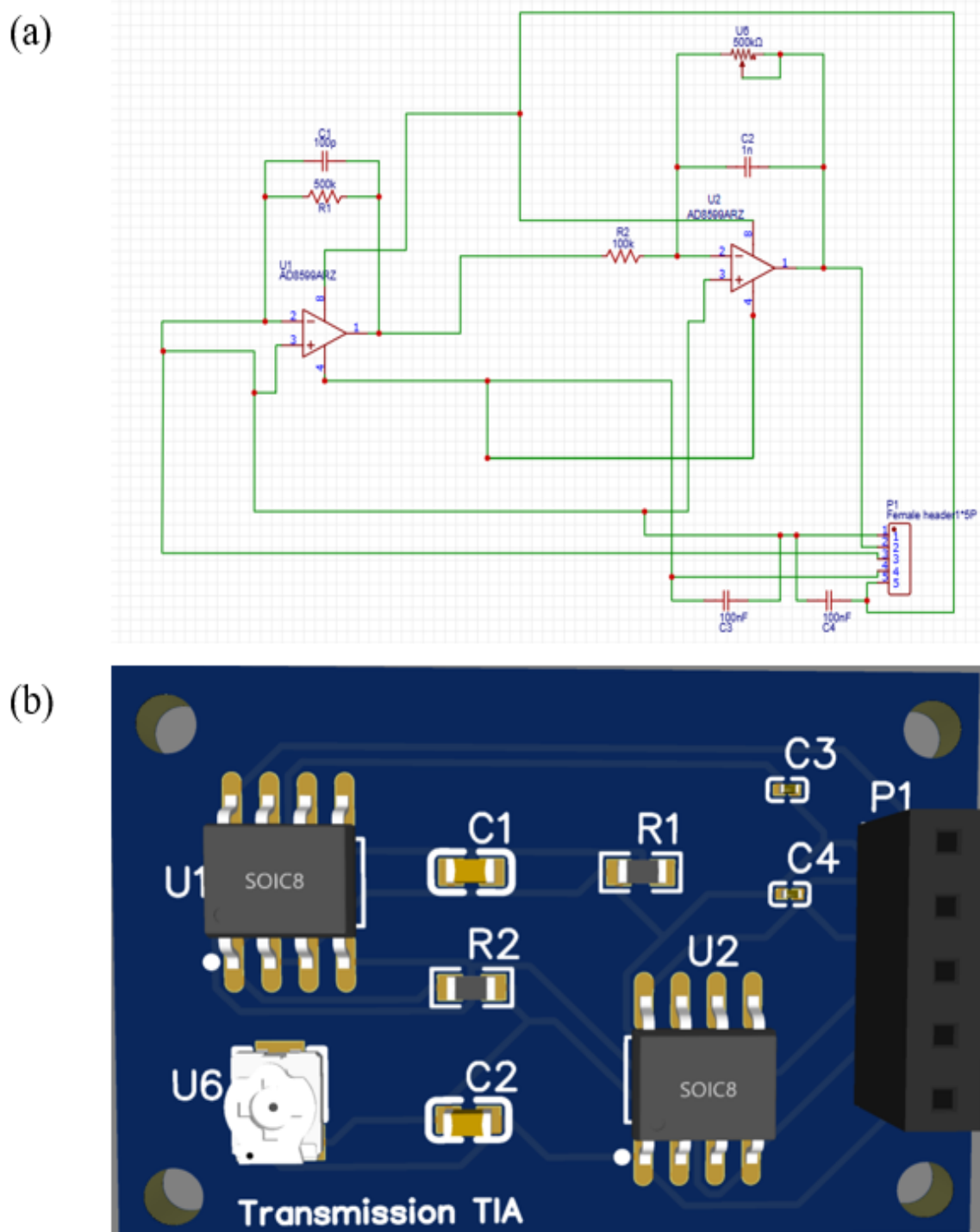


Figure 4.27: Transmission TIA((a)circuit schematic; (b)PCB)

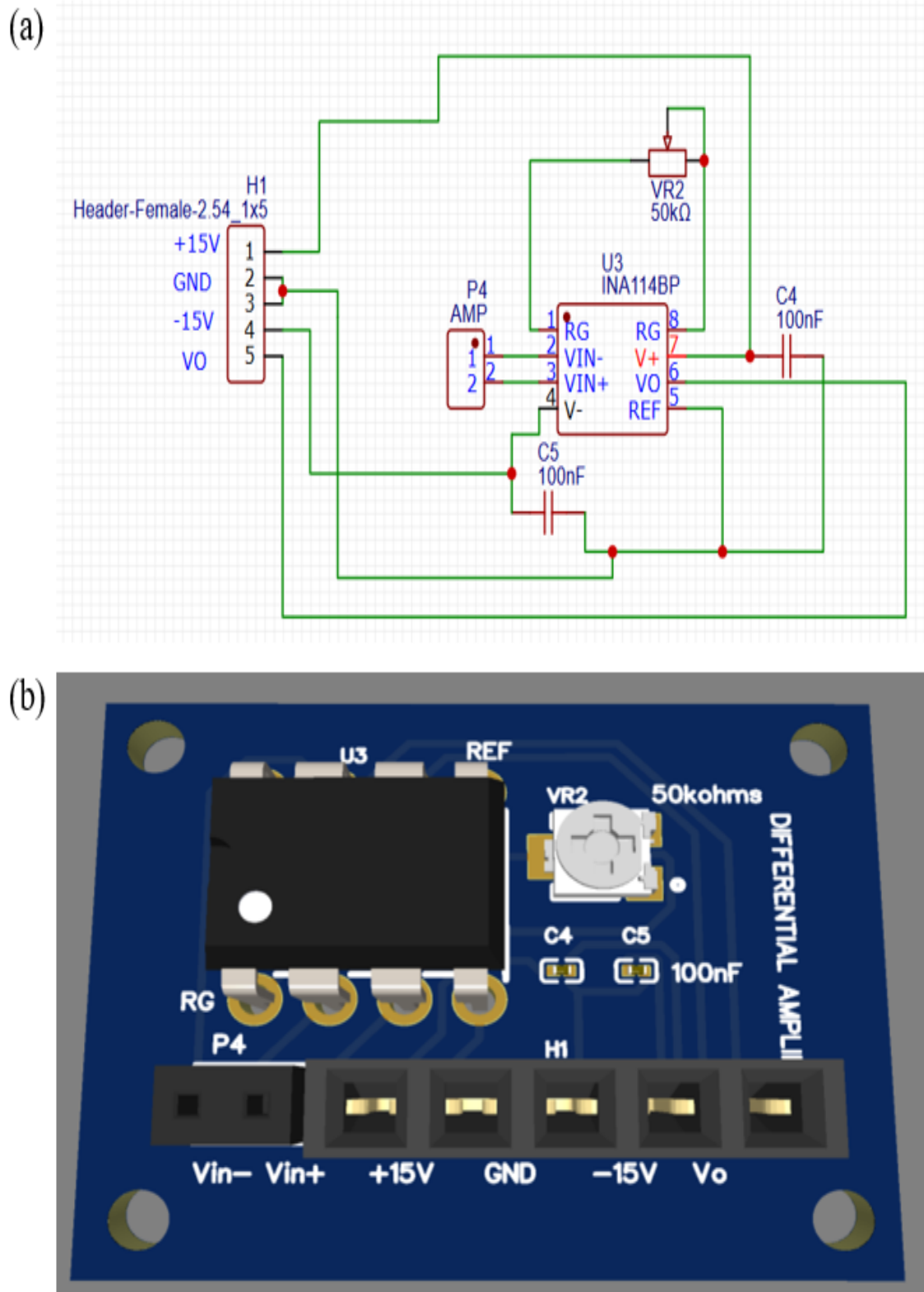


Figure 4.28: Differential amplifier((a)circuit schematic; (b)PCB)

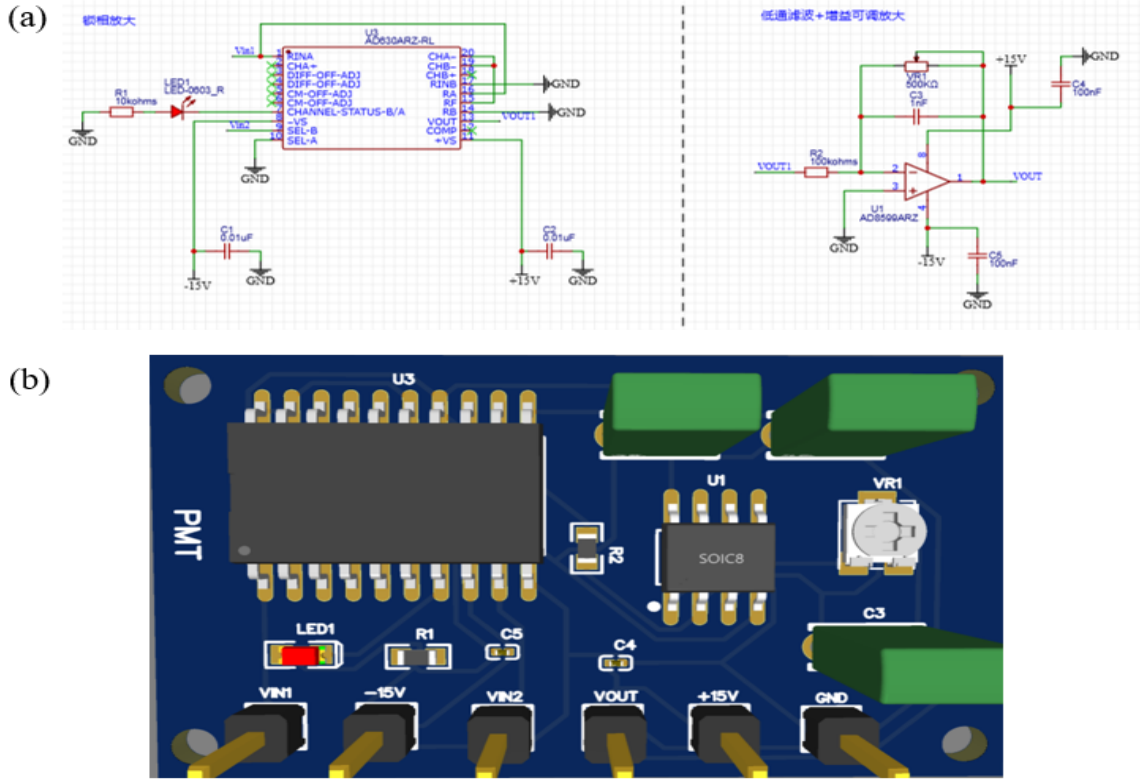


Figure 4.29: LIA((a)circuit schematic; (b)PCB)

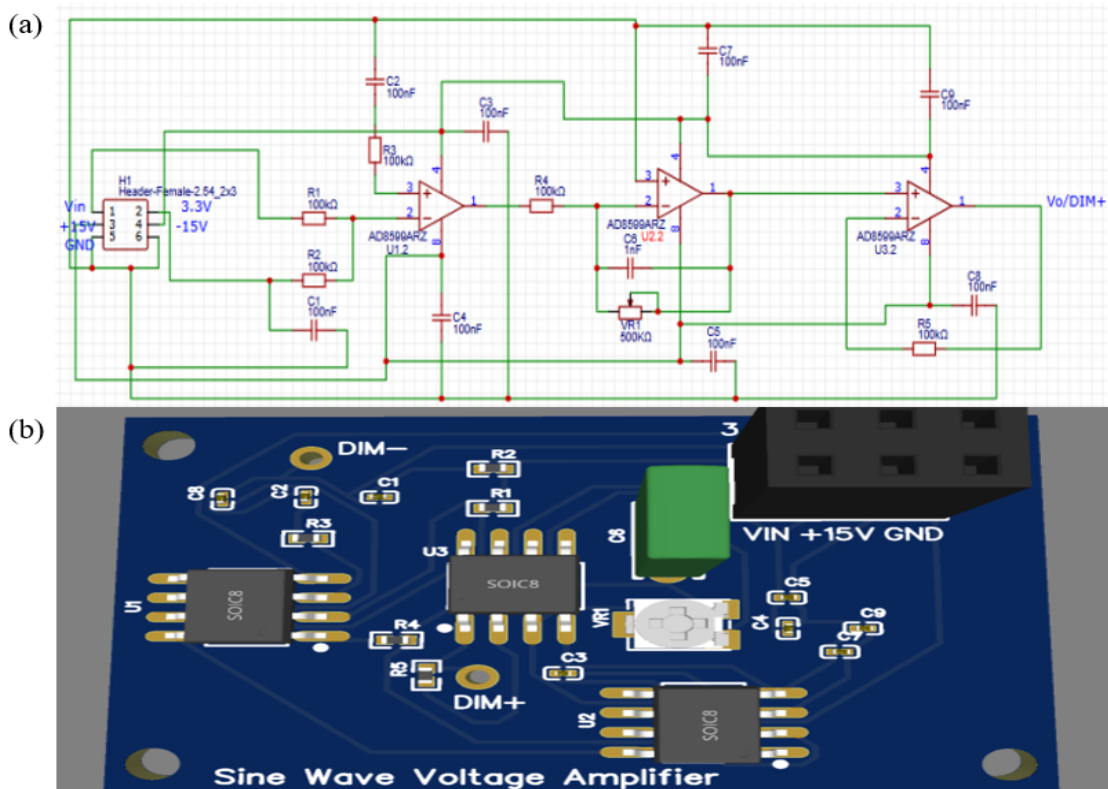


Figure 4.30: Sine wave voltage amplifier((a)circuit schematic; (b)PCB)

4.7 Conclusion

This chapter designs the hardware circuit for the low-intensity optical analysis platform and designs a signal conditioning circuit consisting of three parts: an LED constant current driver, a differential amplifier, and a lock-in amplifier. According to the calculation formula of the transimpedance amplifier and the design requirements of the circuit working bandwidth, AD8599 is selected as the operational amplifier of the circuit. Multisim is used to complete the circuit simulation of each part to verify the rationality of the design. The circuit schematic and PCB are drawn using the Jiali Chuang EDA design tool. For the microcontroller peripheral modules used, the models of each module are determined, such as the ADS1115 module and the OLED display module, and the hardware prototype is built.

Chapter 5

Key accomplishments

5.1 Development of our designed optical system

A low-intensity light detection platform based on an elliptical cylindrical reflective cavity is proposed. The water sample is placed at the first focus and the fluorescence signal is focused at the second focus, solving the problem of low light collection efficiency in the traditional integrating sphere model.

This passage simplifies the system structure and reduces the actual application cost through non-imaging focusing design. Several attempts are made using different lens combination schemes to achieve a significant increase in the ultraviolet irradiance of water samples (comparing the optical simulation data of different iterations, the collection power of the UV light flux at the water sample is increased from 2.7305 W to 5.7470 W, and the collection efficiency is increased by 110.47 %). At the same time, the focusing advantage of the elliptical cylindrical model is verified by Zemax simulation, proving its feasibility in weak light signal detection.

We use 3D printing technology to manufacture an elliptical cavity prototype (as shown in Figure 5.1). The inner wall is coated with aluminum, combined with collimation technology of cylindrical lenses to achieve efficient convergence of light signals. A modular approach was adopted when designing the system structure, and rapid assembly and disassembly through track connection was considered to solve the problems of complex integration and difficult maintenance of traditional optical systems.



Figure 5.1: System physical picture

5.2 Design of low-noise hardware circuitry

A two-stage amplification and filtering circuit based on the AD8599 operational amplifier is developed to achieve high gain and low noise conversion of weak current signals to voltage signals. At the same time, the adjustable gain circuit is combined to enable the system to adapt to different detection scenarios.

By designing a hybrid signal conditioning architecture that combines lock-in amplifier and differential amplifier technology, the background noise and light source fluctuation interference are effectively suppressed, the signal extraction accuracy is improved, and the dual parameter measurement of UVA and FLU of the system is realized.

The ESP32 microcontroller integrated control unit is used to automate signal acquisition, analog-to-digital conversion, and communication with the host computer to ensure the stability of the system in complex environments.

The web acquisition interface shown in Figure 5.2 is designed to complete the real-time detection and curve drawing of signal data, laying a solid foundation for the subsequent establishment of the relationship between fluorescence intensity and pollutant concentration through specific experiments.

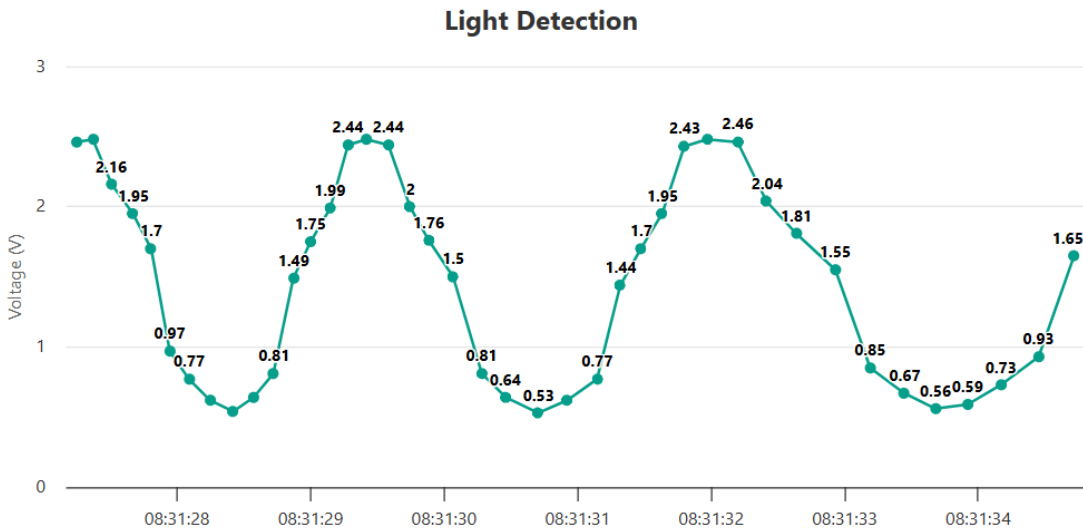


Figure 5.2: Data acquisition interface design

5.3 Cross-disciplinary contributions

The proposed system supports online water quality monitoring in Singapore's seawater desalination, enabling the synchronous detection of UV absorption and fluorescence signals to address the limitations of offline methods. Its elliptical optical design enhances light collection efficiency, while the hardware circuit minimizes noise for precise real-time analysis.

With a modular architecture and high sensitivity, this solution extends to biomedical testing, food safety, and other fields, offering interdisciplinary potential by integrating optical engineering and advanced signal processing for scalable, reliable multi-parameter monitoring.

Chapter 6

Conclusions and suggestions for future work

6.1 Conclusions

This passage focuses on the minisystem for monitoring water quality using UV absorption and fluorescence, focusing on the optical system and hardware circuit design. Chapter 1 introduces the background of fluorescence analysis and the motivation for building a water purity analysis platform through fluorescence detection. Chapter 2 reviews the basic knowledge of fluorescence, existing detection systems and weak signal processing methods, and on this basis, the main research content of this paper is developed:

1. For the design of the optical system, first, the layout of the optical components of the entire system is clearly introduced. Based on the Zemax optical simulation platform, multiple rounds of iterative optimization were completed to determine the optical path structure of UVA parameter detection. Based on the optimization results, the key parameters such as the lens curvature radius and the aperture of the transmitting mirror group and the receiving mirror group were quantitatively analyzed. At the same time, the optical path structure of FLU parameter detection was preliminarily explored, and an improvement plan was proposed based on the simulation results.
2. For the hardware circuit design, a three-stage linkage signal conditioning

system was constructed, which consists of three parts: LED constant current driver, differential amplifier and phase-locked amplifier. According to the calculation formula of the transimpedance amplifier and the design requirements of the circuit working bandwidth, AD8599 was selected as the operational amplifier of the circuit. Multisim was used to simulate the circuits of each part to verify the rationality of the design. The circuit schematic and PCB were drawn using the Jiali Chuang EDA design tool. For the use of microcontroller peripheral modules, the models of each module were determined, such as ADS1115 module, OLED display module, etc. According to the communication methods of different modules, the connection with the microcontroller was completed and the hardware prototype was built.

6.2 Future work

This dissertation proposes a design scheme for the overall system by integrating the coordinated optimization of optical and electrical systems, and builds a complete minisystem prototype for monitoring water quality using UV absorption and fluorescence. The goal is to achieve multi-modal (UVA and FLU) synchronous detection. However, there are still some problems that need to be analyzed and optimized in depth, and the research and design methods used in this paper also need to be improved. These are mainly reflected in:

1. In terms of optical system verification, although the simulation optimization of the lens group parameters has been completed, due to the processing cycle of precision optical components (about 6-8 weeks), the actual optical path alignment and efficiency test have not yet been carried out; in addition, the simulation of the fluorescence part needs to be improved, and a very excellent optical path simulation scheme has not yet been found to achieve the maximum collection efficiency of fluorescence.
2. In terms of hardware integration, the UVA and FLU parameter measure-

ment system currently built in this paper is only a preliminary prototype. Due to the limitation of PCB manufacturing cycle, it has not been tested and verified in the laboratory. Therefore, the miniaturization and integration of the whole system need to be improved.

3. In terms of detection application expansion, the quantitative mapping relationship between water quality parameters and optical characteristics has not yet been established. It is recommended that the focus of subsequent research should be on: on the one hand, constructing concentration-fluorescence intensity calibration curves based on standard substances (such as chlorophyll a, polycyclic aromatic hydrocarbons, etc.); on the other hand, developing a fluorescence spectrum recognition algorithm based on convolutional neural networks to achieve simultaneous detection of multiple pollutants.

References

- [1] J. R. Lakowicz. *Principles of Fluorescence Spectroscopy*. Springer, 2006.
- [2] Singapore Public Utilities Board. *Singapore's Water Story: Sustainability and Innovation*. PUB Singapore, 2015.
- [3] H. Michaels and J. Smith. Development of low intensity light detection for optical analysis. *Journal of Environmental Sciences*, 35:45–60, 2020.
- [4] F. Hammes and T. Egli. Fluorescence-based analytical methods for microbial cells. *Applied and Environmental Microbiology*, 71:759–768, 2005.
- [5] J. Sambrook and D. W. Russell. *Molecular Cloning: A Laboratory Manual*. Cold Spring Harbor Laboratory Press, 2001.
- [6] H.-H. Perkampus. *UV-VIS Spectroscopy and Its Applications*. Springer, 1992.
- [7] J. R. Albani. *Principles and Applications of Fluorescence Spectroscopy*. Wiley, 2007.
- [8] G. G. Guilbault. *Practical Fluorescence: Theory, Methods, and Techniques*. Marcel Dekker, 1990.
- [9] O. S. Wolfbeis. Fluorescence methods and applications: Spectroscopy, imaging, and probes. *Chemical Reviews*, 111:2361–2415, 2011.
- [10] J. N. Demas. *Excited State Lifetime Measurements*. Academic Press, 1983.
- [11] BMG LABTECH. Fluorescence intensity. <https://www.bmglabtech.com/fluorescence-intensity>, 2024. Accessed: 2024-07-12.

- [12] Joseph R. Lakowicz. *Principles of Fluorescence Spectroscopy*. Springer Science & Business Media, 2006.
- [13] Laurence M. Loew. *Spectroscopic Membrane Probes*. CRC Press, 2010.
- [14] Otto S. Wolfbeis. *Fluorescence: Basics, Methods and Applications*. Springer, 2015.
- [15] Robert F Chen. Fluorescence quantum yields of tryptophan and tyrosine. *Analytical Biochemistry*, 21(2):339–342, 1967.
- [16] Ralph Weissleder and Vasilis Ntziachristos. Shedding light onto live molecular targets. *Nature Medicine*, 9(1):123–128, 2003.
- [17] Scott Kable. *Basic principles of fluorescence*, pages 1–34. Jenny Stanford Publishing, 2019.
- [18] Bernard Valeur and Mario N. Berberan-Santos. *Molecular Fluorescence: Principles and Applications*. John Wiley & Sons, 2012.
- [19] J. R. Albani. *Principles and Applications of Fluorescence Spectroscopy*. Wiley - Blackwell, 2007.
- [20] Zheng Shi et al. Design of an in-situ sensor for chlorophyll-a in water based on dual-path fluorescence intensity method. *Chinese Journal of Sensors and Actuators*, 32(5):670–687, 2019.
- [21] Hong Ji, Yan Wu, Zhijie Duan, Fan Yang, Hongyan Yuan, and Dan Xiao. Sensitive determination of sulfonamides in environmental water by capillary electrophoresis coupled with both silvering detection window and in-capillary optical fiber light-emitting diode-induced fluorescence detector. *Electrophoresis*, 38(3–4):452–459, 2017.
- [22] Chongde Zi, Junsheng Shi, Yonghang Tai, Huan Yang, and Xicai Li. Design of portable time-resolved fluorometer. *Advances in Bioscience and Bioengineering*, 4(6):79–84, 2016.

- [23] Bingcheng Yang, Feng Tan, and Yafeng Guan. A collinear light-emitting diode-induced fluorescence detector for capillary electrophoresis. *Talanta*, 65:1303–1306, 2005.
- [24] Alan V. Oppenheim and Ronald W. Schafer. *Digital Signal Processing*. Prentice-Hall, 1975.
- [25] Graham Smith and B. T. Dent. *Scientific Measurement and Analysis*. Oxford University Press, 1997.
- [26] M. L. Meade. *Lock-in Amplifiers: Principles and Applications*. Peter Peregrinus Ltd., 1983.
- [27] Yang Liu, Shoufeng Tong, Sheng Chang, Yansong Song, Yongkang Dong, Xin Zhao, Zhenyang An, and Fei Yu. Design of a delayed XOR phase detector for an optical phase-locked loop toward high-speed coherent laser communication. *Applied Optics*, 57(14):3770–3780, 2018. ISSN: 1559-128X.
- [28] Jacob J. Lamb, Julian J. Eaton-Rye, and Martin F. Hohmann-Marriott. LED-based fluorometer for chlorophyll quantification in the laboratory and in the field. *Photosynthesis Research*, 114(1):59–68, 2012.
- [29] Yang Li, Yong Wang, Li Xiao, Qiang Bai, Xiaoyu Liu, Yang Gao, Hao Zhang, and Baoquan Jin. Phase demodulation methods for optical fiber vibration sensing system: A review. *IEEE Sensors Journal*, 22(3):1842–1866, 2022.
- [30] Xingfei Li et al. *Measurement and Control Circuits*. China Machine Press, Beijing, 5th edition, 2017.
- [31] Texas Instruments. *INA114 Precision Instrumentation Amplifier*, 2000. Revised 2024.
- [32] Espressif Systems. *ESP32-WROOM-32D & ESP32-WROOM-32U Datasheet*, 2019.
- [33] ams-OSRAM AG. *LZ1-00UBN0 High Power Ceramic LED*, n.d.

- [34] Inventronics. *EUM-075SxxxDx Programmable LED Driver*, n.d. Revision B.
- [35] Analog Devices, Inc. *AD8597/AD8599 Low Noise Op Amp*, 2017. Revision F.
- [36] Hamamatsu Photonics. *H11462 Series Photosensor Module*, n.d.
- [37] Analog Devices, Inc. *AD630 Balanced Modulator/Demodulator*, 2016. Revision G.